Studies of submarine slope failures in the North Atlantic:

Causes, timing and consequences

Dissertation

zur Erlangung des Doktorgrades

der Mathematisch-Naturwissenschaftlichen Fakultät

der Christian-Albrechts-Universität zu Kiel

vorgelegt von

Judith Elger

Kiel, 2016

Erster Gutachter:……..... Prof. Dr. Sebastian Krastel-Gudegast

Zweiter Gutachter:……..... Prof. Dr. Christian Berndt

Tag der mündlichen Prüfung:……..... 4. Juli 2016

Zum Druck genehmigt am:……..... 4. Juli 2016

Erklärung

Hiermit erkläre ich, dass ich die vorliegende Doktorarbeit selbstständig und ohne Zuhilfenahme unerlaubter Hilfsmittel angefertigt habe. Sie stellt, abgesehen von der Beratung durch meine Betreuer, nach Inhalt und Form meine eigene Arbeit dar. Weder diese noch eine ähnliche Arbeit wurde an einer anderen Abteilung oder Hochschule im Rahmen eines Prüfungsverfahrens vorgelegt, veröffentlicht oder zur Veröffentlichung vorgelegt. Ferner versichere ich, dass die Arbeit unter Einhaltung der Regeln guter wissenschaftlicher Praxis der Deutschen Forschungsgemeinschaft entstanden ist.

Kiel, den 14.Juni 2016

……

Judith Elger

Abstract

Submarine landslides are a significant geohazard to offshore infrastructure and coastal areas. They occur worldwide on the slopes of volcanic islands and continental margins. In the NE Atlantic, many large-scale Holocene and Pleistocene submarine landslides are located at the mouth of cross-shelf troughs and were probably triggered by earthquakes. Discussions on critical preconditioning processes for slope failure relate to cyclic sedimentation patterns during glacial periods, gas hydrate dissociation caused by changing pressure and temperature condition, and over-steepening due to toe erosion or uneven sedimentation patterns. However, the significant geological destabilizing processes leading to slope failure are still not fully understood and require further studies. The main objective of this thesis is to gain new insights about the initiation of submarine landslides and to identify which particular destabilizing preconditioning processes make slopes prone to failure. This aim is addressed by the reconstruction of the failure chronology of the newly discovered Fram Slide Complex, and by a numerical modeling approach that investigates a new preconditioning process related to gas hydrates.

This thesis shows that low-sedimentation-rate slopes on glacial continental margins can bear significant geohazards related to slope failure. The Fram Slide Complex covers an area of ~5500 km² at 850 to 4200 m water depth ~35 km NW off the Svalbard shelf. This distal location relative to proximal plume deposits rules out a causal relationship of the slope failure in this area to overpressure generation caused by rapidly deposited glacial sediments. Nevertheless, the Fram Slide Complex underwent repeated slope failure since 5 Ma without obvious limitation or concentration to a certain period. Spatial variation of recurrence frequencies and volume of past failures of different parts of the Fram Slide Complex are significant but do not present a simple explanation for destabilization. The absence of evidence for destabilization linked to tectonics, climate and oceanographic conditions emphasizes the impact of local destabilizing processes. The combination of toe erosion and slope shape might have caused repeated slope failure in the southern part of the study area. Another possible local destabilizing process could be related to overpressure generation by gas hydrates. Numerical modeling shows that critical overpressure from below the gas hydrate stability zone can transfer through pipe structures to inherently weak layers in the shallow subsurface. The pressure can build up laterally in the weak layer and can initiate retrogressive submarine slope failure.

The results of this thesis show that the investigated region is highly instable. Potential future slope failures are a threat to offshore infrastructure but the limited volumes of evacuated material and water depth below 1000 m of most recent landslides suggest a rather small tsunami potential. The investigation could not identify a significant reason for slope failure which demonstrates that hazard assessments for the glaciated NW European continental margins are more complex than the results of many studies suggest that analyzed major slope failures adjacent to trough mouth fans. The focus on the glacial cycles has to be reconsidered and expanded.

To further improve the understanding of slope stability and destabilizing processes in the future, a compilation of in situ and laboratory measurements and experiments could provide information on the detailed sediment composition. Theses integrated and multi-disciplinary investigations of geophysical and geotechnical data could be based on drilling and gravity cores of failed and intact sediments to reveal shear strength, environmental in situ stresses or pore pressure. These findings could contribute to a new assessment of slope stability in the North Atlantic.

Zusammenfassung

Submarine Hangrutschungen stellen ein bedeutendes Risiko für Offshore-Infrastrukturen und Küstengebiete dar. Sie sind ein weltweites Phänomen auf den Böschungen von vulkanischen Inseln und an den Kontinentalrändern. Viele großräumige Holozäne und Pleistozäne submarine Hangrutschungen im Norden des Atlantiks befinden sich an der Mündung von Ablagerungsfächern am Kontinentalhang. Sie wurden wahrscheinlich durch Erdbeben ausgelöst. Kritische Präkonditionierung beinhaltet (1) zyklische Sedimentationsmusters im Zusammenhang mit Eiszeiten, (2) Auflösung von Gashydraten auf-grund von sich ändernden Druck- und Temperaturbedingungen und (3) steile Hangneigung begünstigt durch Erosion am Fuße des Hanges oder ungleichmäßige Sedimentationsverteilungen entlang der Böschung. Welche geologischen Prozesse für die Herabsetzung der Hangstabilität ausschlaggebend sind und ihn anfällig für Rutschung machen, ist jedoch nicht vollständig bekannt. Das Hauptanliegen der vorliegenden Arbeit ist es, neue Erkenntnisse über die Entstehung von Hangrutschungen zu gewinnen und die ursächlichen Prozesse für Hangdestabilisierung zu identifizieren. Die zeitliche Rekonstruktion der Rutschung des neu entdeckten Fram Slide Komplexes dient dabei als Grundlage. Mit Hilfe einer numerischen Modellierung wird außerdem das Potential eines neuen Destabilisierungsprozesses geprüft, der im Zusammenhang mit Gashydraten steht.

Eine Hauptaussage der vorliegenden Arbeit ist, dass auch Kontinentalhänge mit niedrigen Sedimentationsraten einer ernstzunehmenden Gefährdung durch Hangrutschungen ausgesetzt sein können. Der Fram Slide Komplex umfasst eine Fläche von ca. 5500 km² in Wassertiefen zwischen 850 und 4200 m und befindet sich in einer Entfernung von etwa 35 km zum Spitzbergen Schelf. Diese Entfernung zu eiszeitlichen Ablagerungen schließt einen kausalen Zusammenhang der Hangrutschungen mit Überdrücken, die durch schnell abgelagert glazialen Ablagerungen verursacht wurden, aus. Trotzdem ist der Fram Slide Komplex seit über 5 Ma immer wieder durch Hangrutschungen verändert worden. Obwohl die Häufigkeit und das Volumen der gerutschten Hänge sich stark innerhalb des Rutschungskomplexes unterscheiden, ist es nicht möglich, ein eindeutiges kausales Muster zu identifizieren. Ein Zusammenhang mit regionalen Prozessen, verknüpft mit tektonischen, klimatischen oder ozeanographischen Bedingungen, ist nicht ersichtlich. Diese Tatsache verdeutlicht den hohen Stellenwert der lokalen destabilisierenden Prozesse für Hangstabilität. Es gibt Anzeichen, dass die Kombination aus Erosion am Fuße des Hanges und die allgemeine Hanggeometrie

ausschlaggebend für das wiederholte Hangversagen im südlichen Teil des Untersuchungsgebietes waren. Ein numerischer Modellierungsansatz zeigt außerdem, dass es einen möglichen kausalen Zusammenhang zwischen Gashydraten und Hangrutschungen gibt. Der besagte Prozess überträgt kritische Porenüberdruck von unterhalb der Gashydratsstabilitätszone durch eine vertikale Verbindung in eine von Natur aus schwache Schicht im flachen Untergrund. In dieser Schicht breitet sich der Druck lateral aus und löst retrogressives Hangversagen aus.

Das Untersuchungsgebiet weist viele Indikatoren für mögliche zukünftige Hangrutschungen auf, die eine Gefahr für auf dem Meeresboden installierte Infrastruktur darstellen. Die geringen Volumina der jüngsten Erdrutsche in Wassertiefen größer als 1000 m deuten jedoch auf ein eher geringes Tsunamipotenzial hin. Die Untersuchung konnte keinen eindeutigen Grund für die Rutschungen des Fram Slide Komplexes darlegen. Diese Erkenntnis zeigt, dass die Prozesse zur Hangstabilisierung auf von Eiszeiten überprägten Kontinentalhängen vielfältiger und komplizierter sind, als viele der großen Studien über Hangrutschungen in nächster Nähe zu eiszeitlichen Ablagerungsflächen vermuten lassen.

Um das Verständnis für Hangstabilität und destabilisierende Prozesse in der Zukunft weiter zu verbessern, könnte eine Kombination von Feld- und Labormessungen detaillierte Informationen über Sedimente liefern. Eine interdisziplinäre Messkampagne könnte geophysische und geotechnische Informationen über stabile und gerutschte Hänge aus Sedimentkernen und Bohrlöchern gewinnen und Aufschluss über Scherfestigkeiten und Umgebungs- und Porendrücke geben. Diese Parameter könnten zu einer neuen Einschätzung der Hangstabilitäten im Nordatlantik beitragen.

Contents

Chapter 1

Introduction

Submarine landslides are a widespread phenomenon on the slope of volcanic islands and continental margins. They bear a significant geohazard because they have the potential to destroy offshore infrastructure and can trigger tsunamis that affect coastal areas. The growing extend of offshore hydrocarbon exploration, wind farms development, related underwater infrastructure, and communication cables require detailed understanding of submarine slope stability.

Numerous studies identified large submarine landslides that shaped the glaciated margins in the NE Atlantic during the Holocene and Pleistocene, predominantly at the mouth of cross-shelf troughs (Laberg et al., 2000; Haflidason et al., 2004; Hjelstuen et al., 2007). The best studied slope failure is the Storegga Slide off Norway, the largest Holocene slope failure, which mobilized about 2300-3200 km³ of sediment (Haflidason et al., 2005; Kvalstad et al., 2005). It triggered a tsunami with maximum run-up heights of up to 20 m that affected coastal areas in Northern Europe (Bondevik et al., 2005b).

Previous studies agree that earthquakes, especially during isostatic rebound, are very likely to trigger slope failures (e.g. Laberg et al., 2000; Bryn et al., 2005a). However, the geological destabilizing processes that lead to slope failures are still not fully understood. Many studies conclude that submarine slope failures in the North Atlantic are related to the extent of ice sheet. They identify the cyclic sedimentation pattern during glacial and interglacial periods to be critical for slope stability (Laberg and Vorren, 2000; Haflidason et al., 2004; Lindberg et al., 2004; Hjelstuen et al., 2007; Winkelmann et al., 2007). Other studies discuss the potential of gas hydrate dissociation caused by changing pressure and temperature condition to reduce slope stability (Sultan et al., 2004; Mienert et al., 2005) but could not provide clear evidence for a causal correlation to slope failures. Further critical processes for slope stability as toe erosion or uneven sedimentation patterns lead to over-steepening. Established hypotheses raise the question, if slope failures are limited to certain environments defined by water depth,

gradient, sedimentation rates, and existence of gas hydrates or paleoclimate history (e.g. Lee, 2009; Urlaub et al., 2015).

In this thesis, a newly discovered submarine slope failure in the Fram Strait off Svalbard is introduced: the Fram Slide Complex (FSC). Compared to other submarine landslides in the North Atlantic its location is unique due to its deep water location/high water depth and distance to glacial sediment source. This thesis reconstructs the chronology of the FSC and discusses if prevailing hypotheses on slope stability can explain its occurrence. Furthermore, a new destabilization process is introduced that may link gas hydrate systems and submarine mass wasting.

1.1 Landslides

Landslides are defined as gravity-driven downward and outward movement of slope-forming materials along one or several shear failure surfaces (Eckel, 1958; Schuster and Krizek, 1978). They are a worldwide phenomenon and occur on active and passive continental margins, especially on continental slopes with high sedimentation rates, mid-ocean ridges, transform faults, and on the flanks of seamounts and volcanic islands (Mosher et al., 2010). Submarine slope failures can transport sediments over distances of several hundred kilometres. They are volumetrically one of the most important forms of submarine erosion. Failure types in the ocean are quite similar to those recognized on land, however, sediment transport dynamics can be different due to potential mixing of sediments with water. As a submarine landslide travels downslope, it may first transform into a debris flow and while further mixing with water it can evolve into a turbulent turbidity current (Hampton, 1972; Piper et al., 1999).

1.1.1 Slope failure terminology

The nomenclature of sediment transport in submarine landslides differentiates between the following types of slope failure. They are characterized by the architecture or composition of mass transport deposits.

Creep describes a long-term permanent deformation of sediment under constant load. Extremely slow downslope flowing sediments turn into folded stratified sediments above a

decollement surface. This process can induce failure on steep slopes of the creeping sediment itself or of the overlying rafted sedimentary layers (Lee and Chough, 2001).

Debris or rock falls are movements of fragmented bedrock or indurated sediment. They freely tumble down a steep slope and accumulate as isolated clasts or gravel with no matrix at the base of the slope (Blikra and Nemek, 1998).

Debris or rock avalanches involve large volumes of failed fragmented bedrock or indurated sediments. The material collides and disperses its momentum in a manner similar to that of a grain flow. This transportation process can result from mass transport on steep flanks of fjords on land or volcanic flanks (Masson et al., 2002). Deep rotational failures can also transform into debris avalanches through shearing, fragmentation, and dilation (Pollet and Schneider, 2004). The resulting mass transport deposits consist of ungraded to normally graded breccia or conglomerate (Blikra and Nemec, 1998).

Slide and slumps are defined as movements of coherent sediment masses over discrete basal shear planes. Slumps are rotational slides with a Skempton ratio (ratio of depth and length of a landslide) larger than 0.33. Slumps consist of relatively undisturbed masses that slide along curved rupture surfaces over a rather short distance. Slides have a Skempton ratio of <0.15. The sliding planes are parallel to the surface slope and the deformation of failing sediments is low to moderate (Nardin et al., 1979; Coleman and Prior, 1988). Rotational mass transports move along a concavely upward curved surface. Translational failures take place parallel to the slope along a roughly planar surface with little rotation or backward tilting translational.

Debris flows are (pseudo-)plastic, poorly sorted flows, in which clasts float in a fine-grained matrix, e.g. mud or sand (Piper et al., 2012). They occur if water incorporates into slumps or slides during downslope movement. Incorporation of only a few percent of water reduces the shear strength and increases the fluid behavior of the debris, thereby causing it to *flow* rather than *slide*. The availability of water in the marine environment suggests favorable conditions for the development of debris flows from submarine landslides (Hampton, 1972).

Turbidity currents form when the material of submarine debris flow extensively dilutes, mainly by mixing with the surrounding water. This interaction can be caused by erosion of material from the front of the flow or directly into the body of the flow. The material ejects into the overlying water and forms a dilute turbulent cloud, a so-called turbidity current (Hampton, 1972). The deposits of turbidity currents are characterized by a fining upward sequence, which is known as the Bouma Sequence (Bouma, 1962).

The architecture of submarine slope failures is closely related to their failure dynamics and to environmental conditions. Landslides leave an imprint on the sea floor morphology. An amphitheater-shaped headwall marks the upper boundary of the affected area and sidewalls define the lateral extension. An aggradation at the base of the slope contains the mass transport deposits. These chaotic slide bodies can contain rotated blocks of coherent stratified sediments. The downslope behaviour of the evacuated sediments depends on the setting and can be frontally emergent, meaning that material flows over the seabed until it terminates at a snout, or it can be frontally confined. In the latter scenario, landslides deposits show progressive frontal thrusting (Frey-Martínez et al., 2006).

Retrogressive slope failures can affect areas of several hundred square kilometres, e.g. the Storegga Slide off Norway (Bryn et al., 2005a). They initiate at the toe or on the mean slope and progress further upslope. Unloading of the bottom headwall causes strain concentrations and strength loss in the base layer (strain softening behaviour). The failure starts to propagate upslope along this base layer. The sediment body above expands and accelerates into the slide scar under gravity loading with the formation of a new headwall (Bryn et al., 2005a). Upslope retreat continues until stronger sediments are encountered. Geomechanical properties can improve due to change in sediments type, degree of consolidation or change of fluid-related overpressure. Irregular head scarps that often terminate on different shear planes form stepped seafloor morphology with multiple headwalls (Piper et al., 2012). Failure deposits can range from rotational slump blocks, especially in the upper slope, so debris flows and turbidity currents that can flow over several hundreds of kilometres (Haflidason et al., 2004).

1.1.2 Investigations of submarine landslides

Although submarine slope failures get buried by sequential sedimentation processes they can be identified in geophysical data that provide information about subsurface structures. Seismic data can reveal buried headwalls, absence of evacuated sediment packages and chaotic mass transport deposits that appear as body with no internal structure. If failure occurred in the near past, sedimentations rates are low or the induced headwalls are sufficiently high, the characteristic imprint on the sea floor morphology is still visible in bathymetric data (cp. Chapter 3).

Past slope failures were identified all over the world on passive and active margins, in the Mediterranean Sea (Camerlenghi et al., 2010), at subduction zones, e.g. off Japan (Yamada et

al., 2010), and on the flanks of volcanic islands, e.g. Canary Islands (Krastel et al., 2001) or Hawaii (Moore et al., 1989). In the North Atlantic, several submarine slope failures were investigated on the western margin off the US coast (Chaytor et al., 2009) and the Canadian coast (Piper et al., 2012) as well as on the European margin in the eastern North Atlantic (Laberg and Vorren, 2000; Lindberg et al., 2004; Haflidason et al., 2005; Hjelstuen et al., 2007; Winkelmann et al., 2007) (Fig. 1.1). As the newly discovered Fram Slide Complex (FSC) in the Fram Strait will be a major part of this thesis, the following overview focuses on previously studied slope failures on the eastern North Atlantic European margin.

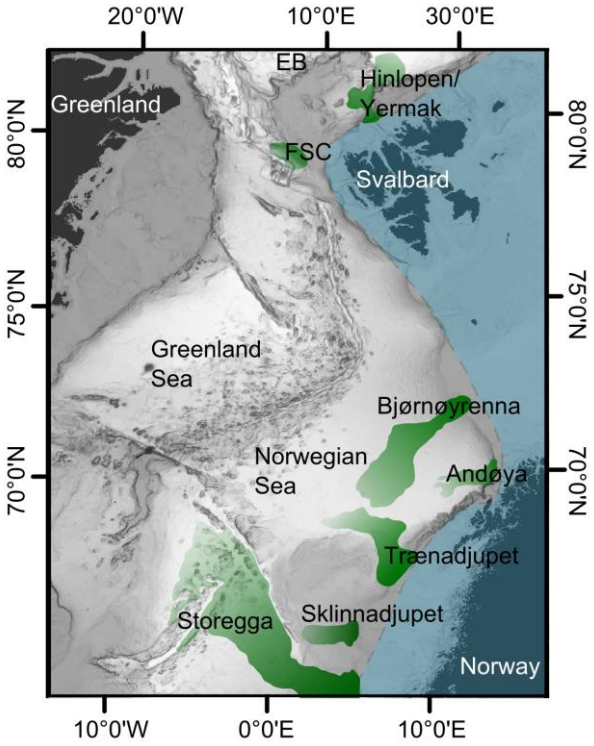

Figure 1.1: Overview map with the maximum ice extent since 100 ka (blue area) (after Ingólfsson and Landvik, 2013) and the areas affected by the Storegga, Sklinnadjupet, Trænadjupet, Andøya, Bjørnøyrenna, Fram and Hinlopen-Yermak slides (green areas from south to north) (after Vanneste et al., 2006; Haflidason et al., 2007).

In the Pleistocene, the Bjørnøya Fan Slide Complex and the Bjørnøya Slide occurred at the mouth of the Bjørnøyrenna trough mouth fan (Hjelstuen et al., 2007) and the Hinlopen-Yermak Slide evacuated about 2400 km³ of sediments at the seaward part of the Hinlopen cross-shelf trough on the northern Svalbard margin (Winkelmann et al., 2006). In the

Holocene, slope failures affected the mouth of the Andøya cross-shelf trough (Andøya Slide) (Laberg et al., 2000) and the mouth of the Trænadjuped cross-shelf trough (Trænadjuped and Nyk slides) (Laberg and Vorren, 2000; Lindberg et al., 2004) (Fig. 1.1). The largest known Holocene slide, and one of the best studied slides worldwide, is the Storegga Slide. It initiated about 8200 years ago on the Møre Margin in the northern part of the North Sea Fan and mobilized about 2400-3200 km³ of sediment (Haflidason et al., 2004; Kvalstad et al., 2005). The slide triggered a tsunami that affected the west coast of Norway, Scotland, Shetland and Faroe Islands. The observed maximal run up height exceeded 20 m in places (Bondevik et al., 2005a). Most of the slide debris was transported up to 810 km into the Norwegian Basin by gravity flows, possibly combined with hydroplaning and turbidity currents (Haflidason et al., 2004; Bryn et al., 2005a). The failure initiated on the lower slope and stepped subsequently back until the slide development finally stopped in horizontally layered over-consolidated glacial sediments behind the shelf edge (Gauer et al., 2005).

1.1.3 Trigger mechanisms

Trigger mechanisms initiate slope failure and are often suggested being earthquakes, e.g. for the Storegga Slide (Bryn et al, 2005a) and Andøya Slide (Laberg et al., 2000). Seismicity can relate to active or reactivated local tectonic settings or post glacial rebound. Earthquakes add dynamic loads and instantaneously increase the shear stress in a slope. At the same time shaking decreases frictional forces, and compacts grains of loose, saturated sediments. This process reduces the volume of voids and increases fluid pressure in the sediment (Abramson et al., 2002). Earthquakes can trigger a phenomenon in certain clays that produces effects similar to liquefaction in water-saturated sand. These extremely sensitive clays are stiff and appear to be strong under normal conditions. However, they have the tendency to transform to a liquid mass if they are disturbed (Sultan et al., 2004). Layers that contain this material can function as laterally extensive glide planes and can induce retrogressive failure (e.g. at the Storegga Slide, Bryn et al., 2005a).

1.1.4 Preconditioning

Spatial boundaries of submarine landslides indicate that some areas are prone to fail while the adjacent slope stays intact (Fig. 1.1). This phenomenon led to the conclusion that trigger mechanisms are necessary but not sufficient to initiate slope failure. Consequently, failed slopes were affected by destabilizing preconditioning. Numerous studies showed that most

Holocene and Pleistocene submarine landslides occurred directly at or down-current from trough mouth fans or ice stream outlets on the Northern Atlantic margin (Laberg and Vorren, 2000; Piper and Ingram, 2003; Lindberg et al., 2004; Haflidason et al., 2004; Piper, 2005; Hjelstuen et al., 2007; Winkelmann et al., 2007) (Fig. 1.1). These studies concluded that the main process that decreases slope stability on the glaciated North Atlantic margin is related to variations in sedimentation rate and sediment type caused by glacial periods (Bryn et al., 2005b; Kvalstad et al., 2005; Leynaud et al., 2009; Piper et al., 2012). The main deposition centre of the last glaciation in the area of the Storegga Slide was in the North Sea Fan. The load of these sediments caused compaction of thick ooze deposits below. Kvalstad et al. (2005) showed that rapid deposition led to high excess pore pressure ratios. In normal hydrostatically pressured geological formations pore water is free to escape during consolidation. Sediments are permeable and fluid can communicate through the different layers. Over-pressurized layers are under-consolidated and have weaker geomechanical properties such as low shear strength and no cohesion (Kvalstad et al., 2005). Low permeable layers or high sedimentation rates restrict fluid circulation. The overburden stress, caused by the sediment load, transfers in part from the sediment matrix to the water. This process prevents the pores from collapsing. If forces, caused by the fluid pressure, exceed the confining stress of the sediment, it will boil or become quick (Sultan et al., 2004). This scenario was proposed for the destabilization of the Storegga Slide area. Low shear strength and sediment stiffness of contourites favour the described process. They are prone to liquefaction and can operate as glide planes for submarine slope failures.

Instable slopes in distal settings relative to proximal plume deposits do not fit the characteristics described in the previous paragraph. They indicate that other processes can be critical for slope stability.

Several studies discuss the potential of gas hydrate dissociation to reduce slope stability (Sultan et al., 2004; Priest et al., 2014). These studies argue that cyclic glacial and interglacial conditions change sea level and water temperature and shift the boundaries of the gas hydrate stability zone in the subsurface. In case of sea temperature rise, hydrate dissolves at the lower edge of the gas hydrate stability zone in great water depth and could increase pore pressure below the gas hydrate stability zone (Fig. 1.2). On the upper slope, the pinch out of the gas hydrate stability zone would shift down-slope during periods of warming (Fig. 1.2). The latter process removes the hydrate cementation of sediment grains and consequently reduces the shear strength of sediments in the former gas hydrate stability zone. At the same time, pore

pressure increases due to gas expansion (Bugge et al., 1988; Kvenvolden, 1999; Sultan et al., 2004). Although circumstantial evidence indicates an effect of hydrates on slope stability (Booth et al., 1994; Micallef et al., 2009), there is no final proof that any of the large submarine landslides were triggered by gas hydrate dissociation (Paull et al., 2007).

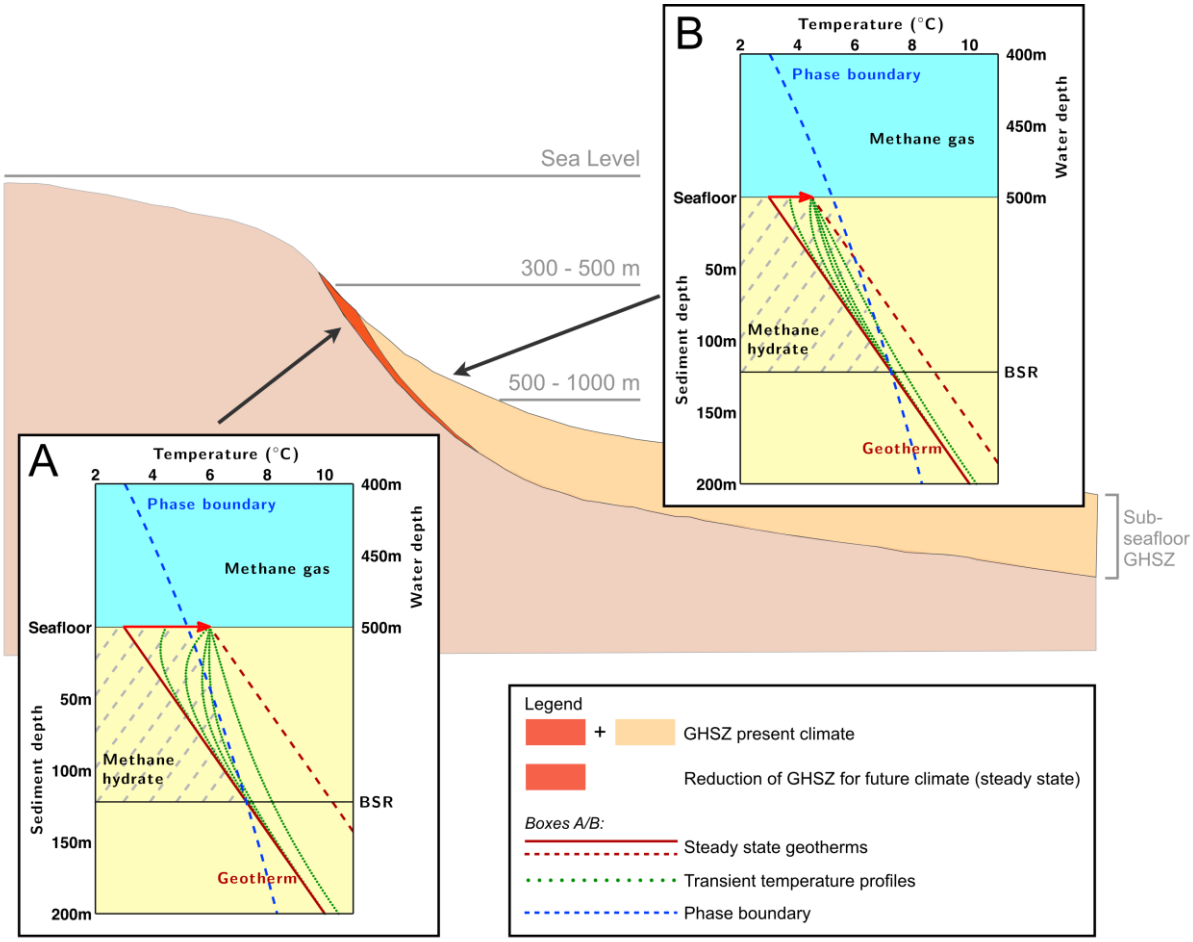

Figure 1.2: Schematic of a typical continental shelf margin depicting the present-day area of gas hydrate stability (light + dark orange). The accumulations most vulnerable to climate change are marked in dark orange. Box A and B describe in detailed how the thickness of the GHSZ may change under climate change. The solid and dashed dark red lines depict the steady state temperature profiles under present-day conditions and a warming scenario of either 3.0°C (box A) or 1.5°C (box B) (red arrows). On the upper continental slope in 300–500 m water depth, the depth of the outcrop of the GHSZ shifts down the slope, which leads to complete dissociation (box A). The lower continental slope and continental rise may face a reduction from the bottom (box B) (from Kretschmer et al. 2009).

Another preconditioning process is over-steepening that can be caused by (toe) erosion or high sedimentation rates. Gradients of 2° were sufficient to initiate past slope failures (Hühnerbach and Masson, 2004). In general, the critical gradient for slope failure equals the friction angle of the shearing sediment, assuming that cohesion is negligible (Hoek and Bray, 1981). If the gradient is smaller than the friction angle, a certain critical overpressure ratio $\lambda = p_e/(\sigma_v - p_h)$ is required for gravitational slope failure (see Fig. 1.3). Steep slopes that undergo high sedimentation are more likely to fail (Berndt et al., 2009; Urlaub and Zervos, 2011).

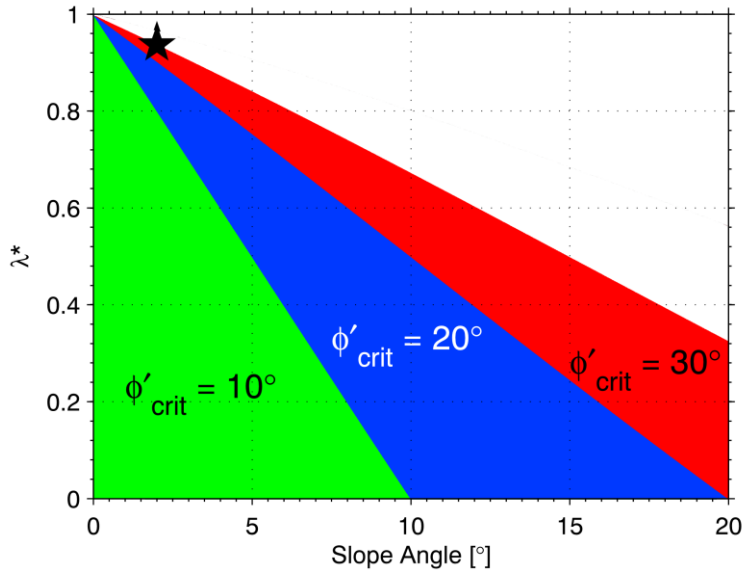

Figure 1.3: Slope stability as a function of slope angle and overpressure ratio λ^* according to infinite slope analysis. All combinations of slope angle and overpressure in the green/blue/red fields are stable for sediment that has a minimum critical friction angle, ϕ'_{crit}, of 10°/20°/30°. For example, a 2° slope made of sediment with ϕ'_{crit} = 30° is stable unless λ^* exceeds 0.94 (black star) (Urlaub et al., 2015).

Several studies classify contouritic sediments as weak layers that initially fail (e.g. Trænadjupet Slide, Sultan et al., 2004). Contourites are well sorted drift bodies formed by steady bottom currents. Their origin implements high water content and low permeability (Bryn et al., 2005b; Laberg and Camerlenghi, 2008). This combination contributes to excess pore pressure under heavy load, rapidly deposited glacial sediments or high levels of organic carbon (Berg et al., 2005). Draping and smoothing effect of the contourite deposits on inclined surfaces can lead to regional over-steepening and enable slip surfaces to form more easily within the drift deposits. High amounts of smectite further reduce the internal friction

and facilitate formation of slip planes (Bryn et al., 2005b). Mosher et al. (2004) suggest further controlling mechanisms such as salt tectonics, shelf storms and deep-seated fluid seepage. Slopes that are exposed to a combination of preconditioning processes are exceptionally unstable and can be triggered to fail in case of elevated stress conditions.

1.2 The Fram Strait – geological setting

The Fram Strait is a deep-water passage in the North Atlantic, the only deep water gateway between the Norwegian-Greenland Sea and the Arctic Ocean. It reaches down to a water depth of 5669 m and is located between Greenland and the archipelago of Svalbard, roughly between 77°N and 81°N in the vicinity of the prime meridian (Fig. 1.1).

The Formation of the Fram Strait started in the earliest Eocene, when the Eurasian and North American plates separated and formed a strike-slip fault that connected the Eurasian Basin with the Norwegian and Greenland Sea. From the earliest Oligocene, motion between Greenland and Eurasia changed from transform to divergent. The former strike-slip fault broke up into a number of spreading ridges connected by transfer faults (Talwani and Eldholm, 1977) (Fig. 1.4). The Spitsbergen Transfer Fault is the most prominent and moves in a dextral shear sense (Engen et al., 2003). It forms a narrow northwest–southeast oriented valley of ~150 km length. The Spitsbergen Transfer Fault connects the southern Lena Trough with the Molløy Ridge and reaches down to depths of up to 4450 m. An initial oceanic channel has connected the Eurasian Basin with the Norwegian-Greenland Sea since earliest Miocene (20 to 15 Ma) but the present day mode of seafloor spreading was probably delayed until late Miocene (~10 Ma) (Engen et al., 2008). The pattern of magnetic anomalies suggests comparable spreading rates in the entire Fram Strait (Engen et al., 2008) and indicates a long lasting history of seismicity along the system of transfer faults and ridges until present (cp. United States Geological Survey from 1973-2015, Fig. 1.4).

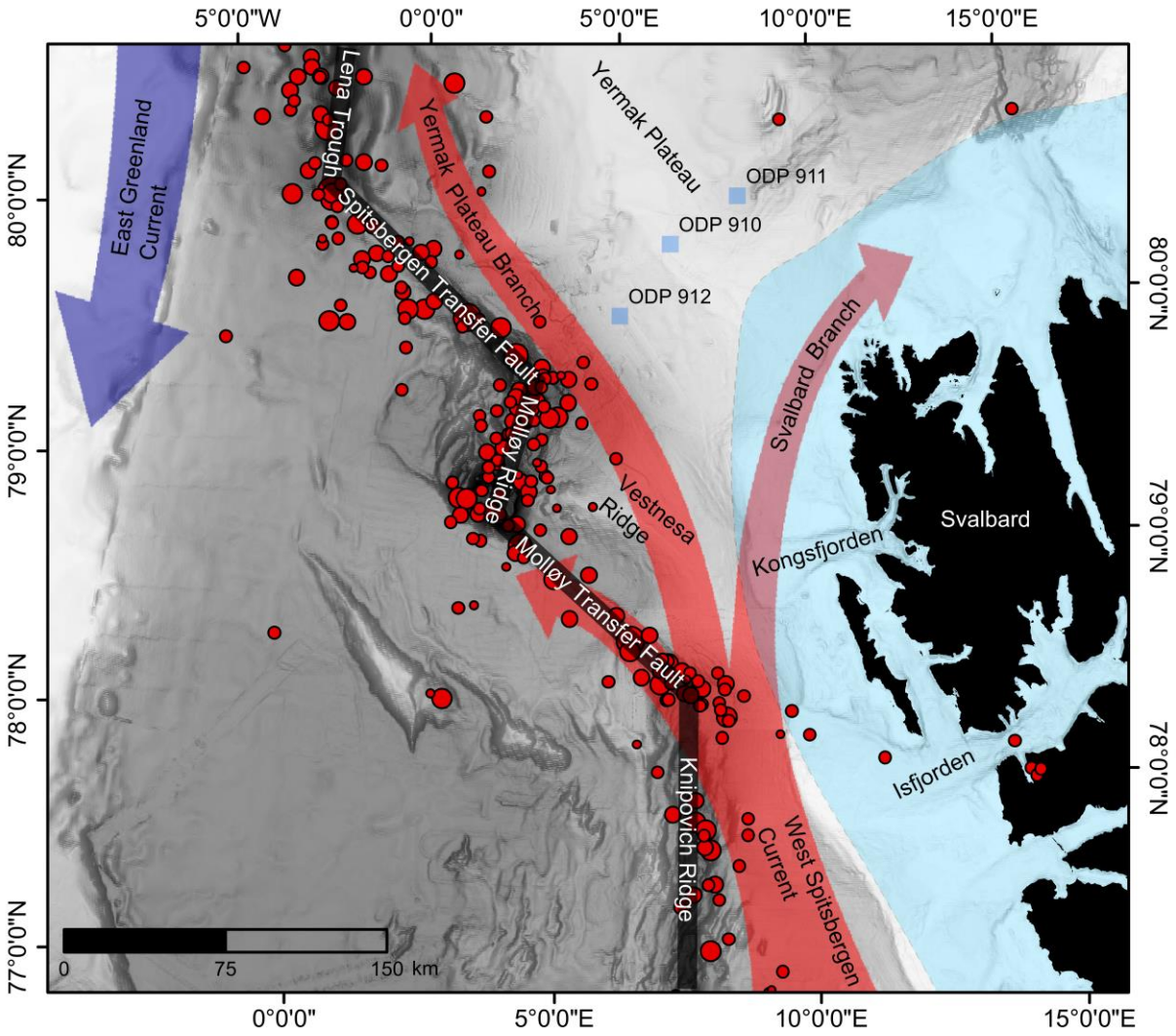

Figure 1.4: Regional bathymetry of the Fram Strait and Svalbard margin with maximum ice extent during glacial periods since 100 ka (blue shapes) (adapted from Ingólfsson and Landvik, 2013), the Lena Trough, the Spitsbergen Transfer Fault, Molløy Ridge, Molløy Transfer Fault and Knipovich Ridge, the location of the ODP bore holes 910-912, the branches of the splitting West Spitsbergen Current, and the seismicity in the area between 1973 and 2015 (US Geological Survey).

Present day oceanographic conditions in the study area are characterized by the northward inflow of the West Spitsbergen Current transporting temperate Atlantic Water into the Arctic Ocean (Manley, 1995) (Fig. 1.4). At ~79.0°N the West Spitsbergen Current splits into three branches (Quadfasel et al., 1987) (Fig. 1.4). The Svalbard Branch turns eastward directly north of the Svalbard archipelago and flows across the shallow southern Yermak Plateau (Schauer et al., 2004). The west branch flows southwards and joins the East Greenland Current (Bourke et al., 1988) that transports cold water from the Arctic Ocean into the North

Atlantic. The Yermak Plateau Branch flows northwards along the western Yermak Plateau where it enters the Arctic Ocean (Rudels et al., 2002). The initiation of the West Spitsbergen Current depends on the deep water exchange between the North Atlantic and Arctic Ocean. Temperate surface water cools on the way poleward. The dense water eventually sinks at high latitudes and flows into Ocean basins. It is unclear if the narrow ocean corridor was sufficient to initiate deep water exchange during early Miocene (Thiede et al. 1995), or if additional subsidence and widening of the Lena Trough in the late Miocene were required (as supported by Winkler et al., 2002).

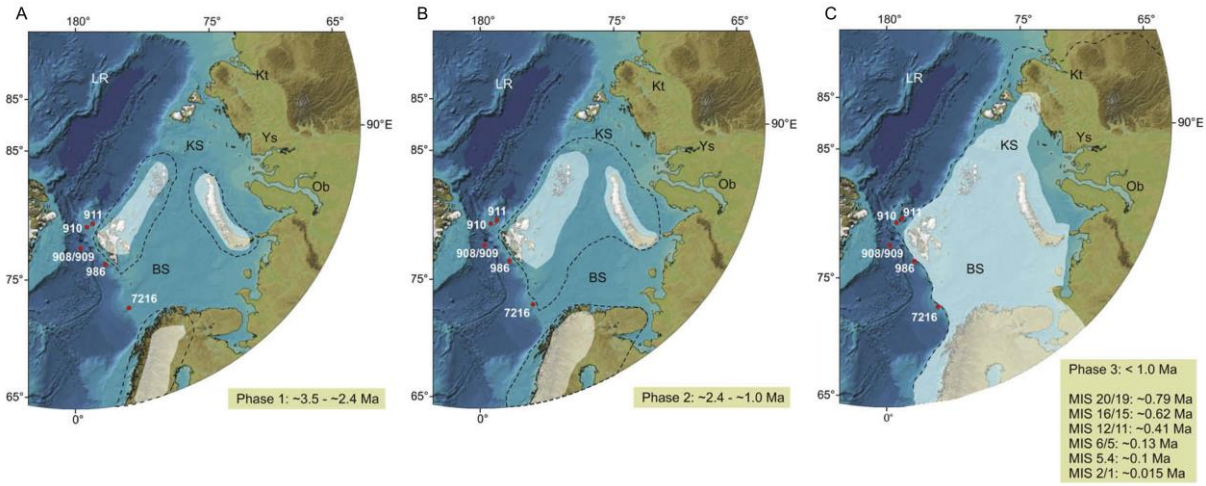

Figure 1.5: Schematic (min./max.) model of lateral ice extension in the Barents Sea region during the Late Plio-Pleistocene time period (black stippled lines = maximum; white transparent polygons = minimum): (A) The initial growth phase (~3.5–2.4 Ma), (B) transitional growth phase (~2.4–1.0 Ma), (C) final growth phase (<1.0 Ma) (Knies et al., 2009).

However, the opening of the Fram Strait had a strong impact on climate and oceanographic conditions and led to a provenance change of sediments at 11.2 Ma (cp. ODP Leg 151, Winkler et al., 2002). The opening caused gradual cooling of the northern hemisphere and ice-rafting activity (Wolf and Thiede, 1991). Three phases of Plio-Pleistocene glaciation of the Barents Sea-Svalbard region were identified by Knies et al. (2009) (Figs. 1.5A-C). The initial growth phase corresponds to the onset and termination of the Northern Hemisphere Glaciation (3.6-2.4 Ma). It is characterized by mountainous to coastal-style glaciations with a short-term glacial expansion beyond the coastline at ~2.7 Ma (Fig. 1.5A). During a transitional growth phase (~2.4-1.0 Ma) the land-based ice mass on the emergent Barents Sea shelf converted to

fully developed ice sheets with sediment transport to the shelf edge. The Barents Sea ice sheet developed to a moderate size and ice sheets on the western (Svalbard) Barents Sea margin extended to the shelf edge (Fig. 1.5B). The final growth phase started at ~1 Ma and caused large-scale intensification of glaciation in the Barents Sea and glacial expansions in the Atlantic region. Ice sheets expanded in places beyond the shelf edge and at least five or six shelf edge glaciations took place in the Barents Sea over the past 0.8 Ma (Fig. 1.5C).

Glacial periods caused isostatic sea level change due to the buildup of ice and induced seismic activity during periods of post-glacial rebound. The history of tectonic and glacial conditions created three different dispositional environments on the southern Yermak Plateau during the last 11 Ma (Mattingsdal et al., 2014). Several sediments drifts formed throughout this time (Gebhardt et al., 2014), e.g. the Vestnesa Ridge north of the Molløy Transform Fault, and the Yermak Plateau northwest of Svalbard (Fig. 1.1). From at least 11 to 2.7 Ma contourite deposition was dominant, sourced by the West Spitsbergen Current. Between 2.7 and ~1.5 Ma contourite deposition continued with a marked glacial influence. Trough mouth fans on the Svalbard shelf (e.g. at the end of the Kongsfjorden and Isfjorden) experience high sediment input of glacial material and function as sediment source. Melt water moves this glacial material down the shelf. There, the Westward Spitsbergen Current transports fine grained fraction further north where it redeposits as contourites. Contourite deposition continued after ~1.5 Ma and erosion by mega-scale tabular icebergs and/or grounded ice (Gebhardt et al., 2011) shaped the Yermak Plateau.

1.3 Motivation

Submarine landslides bear a serious geohazard for seafloor infrastructure and coastal areas. Previous studies identified several preconditioning processes that cause slope destabilization. In combination with a trigger, they can lead to slope failure. Such processes are cyclic sedimentations due to glacial periods, gas hydrate dissolution, over-steepening and contourites. Changing climate and pressure conditions can shift the gas hydrate stability zone (Kretschmer et al., 2015). Consequently, hydrate cementation is removed and can reduce the shear strength. At the same time, gas expansion increases overpressure, similar to cyclic sedimentation. These processes can transform hemipelagic layers into weak layers, vulnerable to liquefaction (e.g. Haflidason et al., 2004; Sultan et al., 2004). Contouritic sediments can amplify the effect of over-steepening and pore pressure increase (Laberg and Camerlenghi,

2008). These hypotheses imply that areas with contourites on the upper continental slope, direct or down-current from trough mouth fans, are primarily vulnerable to slope failure. But there are several slope failures in settings that do not fit these characteristics.

One example for such a setting is the Fram Slide Complex (FSC) that is introduced in this thesis. It does not fit the prevailing hypothesis of pressure build-up due to quickly accumulated glacial deposits because it is located on a low-sedimentation-rate slope between 1.3 to 3 km water depths. The closest glacial debris-flow deposits are at least 35 km away, on the Sjubrebanken Fan. This setting makes the FSC suitable to evaluate the impact of other local processes. The presence of gas hydrates and its northern latitude make the FSC exceptionally interesting for slope stability studies considering future technical and climatic developments. Predicted long-lasting bottom water warming for the 21st century (Stocker et al., 2013) will affect gas hydrate stability and possibly slope stability. At the same time climate change enhances the interest of the hydrocarbon industry to extend oil and gas exploration further north to regions that supposedly will be free of summer sea ice by the end of the 21st century. Engineering processes allow hydrocarbon exploration to expand to the deep sea and require infrastructure as well as the development of renewable offshore energy. Hence, the FSC combines multiple characteristics of slopes that will be subject of future hazard assessment. So far, the giant Hinlopen-Yermak Slide dominates the discussion about vulnerability to slope failure in the Arctic. The failure chronology of the FSC reveals spatial distribution, recurrence frequency and volume of slope failures and gives insights on potential causal relationships with climate and tectonic conditions. The impact of local preconditioning processes is assessed by the comparison of the FSC with the Vestnesa area, 120 km further southeast where no submarine landslides were reported. These findings might be transferable to other slopes and could be useful for future geohazard assessment.

A further contribution to future hazard assessment could be the newly discovered process that links gas hydrates with slope failures. Studies agree that gas hydrates influence slope stability, but no conclusive evidence has been found that links any of the major slope failures to the dissolution of hydrates. The numerical modeling approach within this thesis calculates critical overpressure below the low permeable gas hydrate stability zone for pipe formation. These structures can transfer the elevated pressure to a shallow weak layer in the subsurface and initiate slope failure. An extensive modeling approach could reveal whether this process is able to explain the spatial correlation of many large slope failures and gas hydrate systems and predict the impact of expected bottom water warming.

1.4 Study objectives

The overall aim of this thesis is to better understand the origin of submarine landslides, in particular destabilizing preconditioning of the slope that makes it prone to fail in case of a triggering event. Existing hypotheses raise the question if slope failures are limited to certain environments defined by water depth, gradient, sedimentation rates, and existence of gas hydrates or paleoclimate history. This thesis uses gravity cores and geophysical data (high-resolution 2D reflection seismic, Parasound and multibeam echosounder) of a newly discovered complex of submarine slope failure in the North Atlantic in the Fram Strait off Svalbard to discuss existing hypotheses. A numerical modeling approach investigates the feasibility of a new process that links gas hydrate systems and submarine mass wasting and may explain their spatial overlap.

Within this thesis, I seek to provide new insights for the following questions:

- How did the chronology of events that shaped the Fram Slide Complex evolve? Are recurrence frequencies of slope failures similar within the FSC equal and did they form similar morphological structures?
- Is the overpressure build-up due to quickly accumulated glacial deposits a necessary or sufficient process to cause submarine landslides on a low gradient (2-6°) slope on a passive continental margin?
- Which major processes caused the Fram Slide? Are these results transferable to assess the stability of other slopes? How do they contribute to the general discussion about slope stability?
- How high is the hazard potential of the FSC? Do failure chronology, dynamic and destabilizing processes indicate future slope failures? How high is the tsunami potential of the FSC compared to other slope failures on the eastern glaciates North Atlantic continental margin?
- Is there a causal relationship of gas hydrates and slope failures that bases on their characteristic reduction of sediment permeability? Can the accumulating gas cause critical overpressure below the gas hydrate stability zone? Can the generated hydro-fractures transfer overpressure to shallow coarser grained weak layers and trigger slope failures?

1.5 Thesis outline

This thesis consists of five Chapters. Chapter 1 gives an introduction to submarine slope failures, the study area and the aim of the thesis. The manuscripts in Chapter 2-4 discuss the various destabilizing processes and are followed by a concluding Chapter 5. The manuscripts contain an individual abstract, introduction, method, discussion, and conclusion section. They have been published by or are submitted to international peer-reviewed journals.

Chapter 2 introduces the Fram Slide; a newly discovered large landslide complex off NW Svalbard that consists of multiple, translational, retrogressive failures on several glide planes. The available 2D high-resolution seismic, Parasound, and bathymetric data rule out that this slope failure resulted from rapid glacigenic deposition which distinguishes the Fram Slide from known large slides off NW Europe. This difference is the base to discuss other potential destabilizing processes such as contour currents, tectonic faulting, and overpressure build-up related to gas hydrate systems. This chapter is published by the *Journal of the Geological Society* as *Elger, J., Berndt, C., Krastel, S., Piper, D. J. W., Gross, F., Spielhagen, R. F., and Meyer, S., 2015.The Fram Slide off Svalbard: a submarine landslide on a low-sedimentation-rate glacial continental margin. Journal of Geological Society, 172, 153-156.*

C. Berndt led the survey to acquire the data. F. Gross and S. Meyer processed the 2D high-resolution seismic and Parasound data. I processed the bathymetric data, worked on the gravity cores, interpreted the data and wrote the manuscript including all figures. All co-authors, the editor and two reviewers helped to improve and revise the manuscript.

Chapter 3 presents the results of new bathymetric and seismic studies of the Fram Slide Complex from a cruise in 2013, reconstructs its failure chronology and aims to identify causes for destabilization and uneven recurrence frequencies. Therefore, it compares the Fram Slide Complex with the tectonically similar Vestnesa area, approximately 120 km farther south, which has no history of submarine landslides. This chapter is under review under the title *Chronology of the Fram Slide complex offshore NW Svalbard and its implications for local and reginal slope stability* by Elger, J., Berndt, C., Krastel, S., Piper, D. J. W., Gross, F., and Geissler, W. H., at the journal *Marine Geology*.

W. H. Geissler led the survey to acquire the data. F. Gross and I planned and realized the data acquisition. I processed, analyzed, interpreted and discussed the data with the co-authors. I

wrote the manuscript including all figures. All co-authors contributed to write and revise the manuscript.

Chapter 4 presents a new process that may explain the spatial overlap of many submarine slope failures with gas hydrate systems. Gas hydrates reduce the permeability of sediments, seal the gas reservoir below the gas hydrate stability zone and cause accumulation of fluids. Resulting overpressure causes hydrofracturing and pipe structures could transfer the overpressure to weak layers and initiate retrogressive submarine slope failure. This chapter is submitted under the title *Pipe structure formation as a trigger for submarine slope failures* by Elger, J., Berndt, C., Rüpke, L., Krastel, S., Gross, F., and Geissler, W. H. to the journal *Geology*.

W. H. Geissler led the survey. F. Gross acquired and processed the seismic data, I interpreted them. L. Rüpke supported me to calculate the critical pore overpressure that initiates different failure patterns. L. Rüpke calculated the additional pore fluid pressure caused by sediment compaction. I wrote the manuscript and all co-authors helped to improve and revise the manuscript.

Chapter 5 summarizes the results of the manuscripts and discusses them with regards to the motivation of the thesis. It provides an outlook on potential future studies to follow-up the hypothesis and results of the presented studies.

References

Abramson, L.W., Lee, T.S., Sharma, S., Boyce, G.M., 2002. Slope stability and stabilization methods (Second Edition), Wiley, New York.

Berg, K., Solheim, A., Bryn, P., 2005. The Pleistocene to recent geological development of the Ormen Lange area. Marine and Petroleum Geology 22, 45–56. doi:10.1016/j.marpetgeo.2004.10.009

Berndt, C., Brune, S., Nisbet, E., Zschau, J., Sobolev, S.V., 2009. Tsunami modeling of a submarine landslide in the Fram Strait. Geochemistry, Geophysics, Geosystems 10. doi:10.1029/2008GC002292

Blikra, L.H., Nemec, W., 1998. Postglacial colluvium in western Norway: depositional processes, facies and palaeoclimatic record. Sedimentology 45, 909-959. doi:10.1046/j.1365-3091.1998.00200.x

Bondevik, S., Løvholt, F., Harbitz, C., Mangerud, J., Dawson, A., Svendsen, J.I., 2005a. The Storegga Slide tsunami—comparing field observations with numerical simulations. Marine and Petroleum Geology 22, 195–208. doi:10.1016/j.marpetgeo.2004.10.003

Bondevik, S., Mangerud, J., Dawson, S., Dawson, A., Lohne, Ø., 2005b. Evidence for three North Sea tsunamis at the Shetland Islands between 8000 and 1500 years ago. Quaternary Science Reviews 24, 1757–1775. doi:10.1016/j.quascirev.2004.10.018

Booth, J.S., Winters, W.J., Dillon, W.P., 1994. Circumstantial evidence of gas hydrate and slope failure associations on the United States Atlantic continental margin. Annals of the New York Academy of Sciences 714, 487–489.

Bouma, A.H., 1962. Sedimentology of some flysch deposits: a graphic approach to facies interpretation.

Bourke, R.H., Weigel, A.M., Paquette, R.G., 1988. The westward turning branch of the West Spitsbergen Current. Journal of Geophysical Research 93, 14065-14077.

Bryn, P., Berg, K., Forsberg, C.F., Solheim, A., Kvalstad, T.J., 2005a. Explaining the Storegga Slide. Marine and Petroleum Geology 22, 11 – 19. doi:http://dx.doi.org/10.1016/j.marpetgeo.2004.12.003

Bryn, P., Berg, K., Stoker, M.S., Haflidason, H., Solheim, A., 2005b. Contourites and their relevance for mass wasting along the Mid-Norwegian Margin. Marine and Petroleum Geology 22, 85 – 96. doi:http://dx.doi.org/10.1016/j.marpetgeo.2004.10.012

Bugge, T., Belderson, R., Kenyon, N.H., 1988. The Storegga Slide. Philosophical Transactions of the Royal Society of London 325, 357–388.

Camerlenghi, A., Urgeles, R., Fantoni, L., 2010. A Database on Submarine Landslides of the Mediterranean Sea. In Submarine Mass Movements and Their Consequences, Advances in Natural and Technological Hazards Research, 28. doi:10.1007/978-90-481-3071-9_41

Chaytor, D.J., ten Brink, U.S., Solow, A.R., Andrews, B.D., 2009. Size distribution of submarine landslides along the U.S. Atlantic margin. Marine Geology 264, 16-27. doi:10.1016/j.margeo.2008.08.007

Coleman, J., Prior, D.B., 1988. Mass Wasting On Continental Margins. Annual Review of Earth and Planetary Sciences 16, 101-119. doi:10.1146/annurev.earth.16.1.101

Eckel, E.B., 1958. Introduction to landslides and engineering practice. Highway Research Board Special Report 224–232.

Engen, Ø., Eldholm, O., Bungum, H., 2003. The Arctic plate boundary. Journal of Geophysical Research 108, 2075, doi:10.1029/2002JB001809, B2.

Engen, Ø., Faleide, J.I., Dyreng, T.K., 2008. Opening of the Fram Strait gateway: A review of plate tectonic constraints. Tectonophysics 450, 51-69.

Frey-Martínez, J., Cartwright, J., James, D., 2006. Frontally confined versus frontally emergent submarine landslides: A 3D seismic characterisation. Marine and Petroleum Geology 23, 585-604. doi:10.1016/j.marpetgeo.2006.04.002

Gauer, P., Kvalstad, T.J., Forsberg, C.F., Bryn, P., Berg, K., 2005. The last phase of the Storegga Slide: simulation of retrogressive slide dynamics and comparison with slide-scar morphology. Marine and Petroleum Geology 22, 171–178. doi:10.1016/j.marpetgeo.2004.10.004

Gebhardt, A.C., Jokat, W., Niessen, F., Matthiessen, J., Geissler, W.H., Schenke, H.W., 2011. Ice sheet grounding and iceberg plow marks on the northern and central Yermak Plateau revealed by geophysical data. Quaternary Science Reviews 30, 1726-1738. doi:10.1016/j.quascirev.2011.03.016

Gebhardt, A.C., Geissler, W.H., Matthiessen, J., Jokat, W., 2014. Changes in current patterns in the Fram Strait at the Pliocene/Pleistocene boundary. Quaternary Science Reviews 92, 179-189. doi:10.1016/j.quascirev.2013.07.015

Haflidason, H., Sejrup, H.P., Nygård, A., Mienert, J., Bryn, P., Lien, R., Forsberg, C.F., Berg, K., Masson, D., 2004. The Storegga Slide: architecture, geometry and slide development. Marine Geology 213, 201-234. doi:10.1016/j.margeo.2004.10.007

Haflidason, H., Lien, R., Sejrup, H.P., Forsberg, C.F., Bryn, P., 2005. The dating and morphometry of the Storegga Slide. Marine and Petroleum Geology 22, 123 – 136. doi:http://dx.doi.org/10.1016/j.marpetgeo.2004.10.008

Hampton, M.A., 1972. The role of subaqueous debris flow in generating turbidity currents. Journal of Sedimentary Research 42, 775-793.

Hjelstuen, B.O., Eldholm, O., Faleide, J.I., 2007. Recurrent Pleistocene mega-failures on the SW Barents Sea margin. Earth and Planetary Science Letters 258, 605–618. doi:10.1016/j.epsl.2007.04.025

Hoek, E., Bray, J.D., 1981. Rock slope engineering. CRC Press.

Hühnerbach, V., Masson, D.G., 2004. Landslides in the North Atlantic and its adjacent seas: an analysis of their morphology, setting and behaviour. Marine Geology 213, 343-362. doi:10.1016/j.margeo.2004.10.013

Ingólfsson, Ó., Landvik, J.Y., 2013. The Svalbard–Barents Sea ice-sheet–Historical, current and future perspectives. Quaternary Science Reviews 64, 33-60.

Knies, J., Matthiessen, J., Vogt, C., Laberg, J.S., Hjelstuen, B.O., Smelror, M., Larsen, E., Andreassen, K., Eidvin, T., Vorren, T.O., 2009. The Plio-Pleistocene glaciation of the Barents Sea–Svalbard region: a new model based on revised chronostratigraphy. Quaternary Science Reviews 28, 812-829. doi:10.1016/j.quascirev.2008.12.002

Krastel, S., Schmincke, H.-U., Jacobs, C.L., Rihm, R., Le Bas, T.P., Alibés, B., 2001. Submarine landslides around the Canary Islands. Journal of Geophysical Research: Solid Earth 106, 3977-3997. doi:10.1029/2000jb900413

Kretschmer, K., Biastoch, A., Rüpke, L., Burwicz, E., 2015. Modeling the fate of methane hydrates under global warming. Global Biogeochemical Cycles 29, 610-625.

Kvalstad, T.J., Andresen, L., Forsberg, C.F., Berg, K., Bryn, P., Wangen, M., 2005. The Storegga slide: evaluation of triggering sources and slide mechanics. Marine and Petroleum Geology 22, 245 – 256. doi:http://dx.doi.org/10.1016/j.marpetgeo.2004.10.019

Kvenvolden, K.A., 1999. Potential effects of gas hydrate on human welfare. Proceedings of the National Academy of Sciences 96, 3420-3426. doi:10.1073/pnas.96.7.3420

Laberg, J.S., Vorren, T.O., 2000. The Trænadjupet Slide, offshore Norway — morphology, evacuation and triggering mechanisms. Marine Geology 171, 95 – 114. doi:http://dx.doi.org/10.1016/S0025-3227(00)00112-2

Laberg, J.S., Vorren, T.O., Dowdeswell, J.A., Kenyon, N.H., Taylor, J., 2000. The Andøya Slide and the Andøya Canyon, north-eastern Norwegian–Greenland Sea. Marine Geology 162, 259 – 275. doi:http://dx.doi.org/10.1016/S0025-3227(99)00087-0

Laberg, J.S., Camerlenghi, A., 2008. The significance of contourites for submarine slope stability, Developments in sedimentology, 60, 537-556. doi:10.1016/s0070-4571(08)10025-5

Lee, S.H., Chough, S.K., 2001. High-resolution (2-7 kHz) acoustic and geometric characters of submarine creep deposits in the South Korea Plateau, East Sea. Sedimentology 48, 629-644. doi:10.1046/j.1365-3091.2001.00383.x

Lee, H.J., 2009. Timing of occurrence of large submarine landslides on the Atlantic Ocean margin. Marine Geology 264, 53-64. doi:10.1016/j.margeo.2008.09.009

Leynaud, D., Mienert, J., Vanneste, M., 2009. Submarine mass movements on glaciated and non-glaciated European continental margins: A review of triggering mechanisms and preconditions to failure. Marine and Petroleum Geology 26, 618-635. doi:10.1016/j.marpetgeo.2008.02.008

Lindberg, B., Laberg, J.S., Vorren, T.O., 2004. The Nyk Slide—morphology, progression, and age of a partly buried submarine slide offshore northern Norway. Marine Geology 213, 277 – 289. doi:http://dx.doi.org/10.1016/j.margeo.2004.10.010

Masson, D.G., Watts, A.B., Gee, M.J.R., Urgeles, R., Mitchell, N.C., Le Bas, T.P., Canals, M., 2002. Slope failures on the flanks of the western Canary Islands. Earth-Science Reviews 57, 1-35. doi:10.1016/s0012-8252(01)00069-1

Mattingsdal, R., Knies, J., Andreassen, K., Fabian, K., Husum, K., Grøsfjeld, K., de Schepper, S., 2014. A new 6 Myr stratigraphic framework for the Atlantic–Arctic Gateway. Quaternary Science Reviews 92, 170-178. doi:10.1016/j.quascirev.2013.08.022

Micallef, A., Masson, D.G., Berndt, C., Stow, D.A.V., Stow, D.A., 2009. Development and mass movement processes of the north-eastern Storegga Slide. Quaternary Science Reviews 28, 433–448. doi:10.1016/j.quascirev.2008.09.026

Mienert, J., Vanneste, M., Bünz, S., Andreassen, K., Haflidason, H., Sejrup, H.P., 2005. Ocean warming and gas hydrate stability on the mid-Norwegian margin at the Storegga Slide. Marine and Petroleum Geology 22, 233–244. doi:10.1016/j.marpetgeo.2004.10.018

Moore, J.G., Clague, D.A., Holcomb, R.T., Lipman, P.W., Normark, W.R., Torresan, M.E., 1989. Prodigious submarine landslides on the Hawaiian Ridge. Journal of Geophysical Research 94, 17465-17484. doi:10.1029/jb094ib12p17465

Mosher, D.C., Piper, D.J., Campbell, D.C., Jenner, K.A., 2004. Near-surface geology and sediment-failure geohazards of the central Scotian Slope. AAPG Bulletin 88, 703–723. doi:10.1306/01260403084

Mosher, D.C., Moscardelli, L., Shipp, R., al., E., 2010. Sumarine mass movements and their sonsequences: Introcuction, in: Mosher, D.C. (Ed.).

Nardin, T.R., Hein, F.J., Grosline, D.S., Edward, B.C., 1979. A review of mass movement processes and acoustic characteristics and contrasts in slope and base-of-slope systems versus canyon-fan-basin systems. Spec. Publ.-Soc. Econ. Paleontol. Mineral 27, 61-73. doi:10.2110/pec.79.27.0061

Paull, C.K., Ussler, W., Holbrook, W.S., 2007. Assessing methane release from the colossal Storegga submarine landslide. Geophysical Research Letters 34. doi:10.1029/2006gl028331

Piper, D., Cochonat, P., Morrison, M., 1999. Sidescan sonar evidence for progressive evolution of submarine failure into a turbidity current: the 1929 Grand Banks event, Sedimentology 46, 79-97.

Piper, D.J., Ingram, S., 2003. Major Quaternary sediment failures on the east Scotian Rise, eastern Canada. doi:10.4095/214209

Piper, D., 2005. Late Cenozoic evolution of the continental margin of eastern Canada. Norsk geologisk tidsskrift. Norsk geologisk tidsskrift 85, 305.

Piper, J.W.D., Mosher, D.C., Campbell, D.C., 2012. Controls on the distribution of major types of submarine landslides. doi:10.1017/cbo9780511740367.010

Pollet, N., Schneider, J.L.M., 2004. Dynamic disintegration processes accompanying transport of the Holocene Flims sturzstrom (Swiss Alps). Earth and Planetary Science Letters 221, 433-448. doi:10.1016/s0012-821x(04)00071-8

Priest, J.A., Clayton, C.R.I, Rees, E.V.L., 2014. Potential impact of gas hydrate and its dissociation on the strength of host sediment in the Krishna-Godavari Basin. Marine and Petroleum Geology 58, 186-198. doi:10.1016/j.marpetgeo.2014.05.008

Quadfasel, D., Gascard, J.-C., Koltermann, K.-P., 1987. Large-scale oceanography in Fram Strait during the 1984 Marginal Ice Zone Experiment. Journal of Geophysical Research 92, 6719-6728.

Rudels, B., Fahrbach, E., Meincke, J., Budéus, G., Eriksson, P., 2002. The East Greenland Current and ist contribution to the Denmark Strait overflow. ICES Journal of Marine Science 59, 1133-1154.

Schauer, U., Fahrbach, E., Osterhus, S., Rohardt, G., 2004. Arctic 577 warming through the Fram Strait: Oceanic heat transport from 3 years of measurements. Journal of Geophysical Research 109, C06026. doi:10.1029/2003JC001823.

Schuster, R.L., Krizek, R.J., 1978. Landslides: Analysis and Control, Transportation Research Board, National Academy of Sciences, Washington, DC, Special Report 176, 234.

Stocker, T.F., Qin, D., Plattner, G.K., Tignor, M., 2013. The physical science basis. Working Group I Contribution to the Fifth Assessment Report of the Intergovernmental Panel on Climate Change. doi:10.1017/cbo9781107415324.028

Sultan, N., Cochonat, P., Foucher, J.P., Mienert, J., 2004. Effect of gas hydrates melting on seafloor slope instability. Marine Geology 213, 379 – 401. doi:http://dx.doi.org/10.1016/j.margeo.2004.10.015

Talwani, M., Eldholm, O., 1977. Evolution of the Norwegian-Greenland Sea. Geological Society of America Bulletin 88, 969-999.

Thiede, J., Myhre, A.M., Firth, J.V. & Shipboard Scientific Party, 1995. Cenozoic Northern Hemisphere Polar and Subpolar Ocean Paleoenvironments (Summary of ODP Leg 151 Drilling Results), in: Myhre, A.M., Thiede, J., Firth, J.V., et al. (Eds.) Proceedings of the Ocean Drilling Program, Initial Reports, US College Station, Texas, 151, pp. 397–420.

Urlaub, M., Zervos, A., Talling, P.J., Masson, G.D., Clayton, I.C., 2011. How Do ~2° Slopes Fail in Areas of Slow Sedimentation? A Sensitivity Study on the Influence of Accumulation Rate and Permeability on Submarine Slope Stability, Submarine Mass Movements and Their Consequences 31, 277-287. doi:10.1007/978-94-007-2162-3_25

Urlaub, M., Talling, P.J., Zervos, A., Masson, D., 2015. What causes large submarine landslides on low gradient (<2°) continental slope with slow (~0.15m/kyr) sediment accumulation? Journal of Geophysical Research: Solid Earth 120. doi:10.1002/2015jb012347

Vanneste, M., Mienert, J., Bünz, S., 2006. The Hinlopen Slide: A giant, submarine slope failure on the northern Svalbard margin, Arctic Ocean. Earth and Planetary Science Letters 245, 373 - 388.

Winkelmann, D., Research, C.B., Jokat, W., Niessen, F., Stein, R., Winkler, A., 2006. Age and extent of the Yermak Slide north of Spitsbergen, Arctic Ocean. Geochemistry, Geophysics, Geosystems 7. doi:10.1029/2005GC001130

Winkelmann, D., Research, C.B., Stein, R., 2007. Triggering of the Hinlopen/Yermak Megaslide in relation to paleoceanography and climate history of the continental margin north of Spitsbergen. Geochemistry, Geophysics, Geosystems 8. doi:10.1029/2006GC001485

Yamada, Y., Yamashita, Y., Yamamoto, Y., 2010. Submarine landslides at subduction margins: Insights from physical models. Tectonophysics 484, 156-167. doi:10.1016/j.tecto.2009.09.007

Chapter 2

The Fram Slide off Svalbard

A submarine landslide on a low-sedimentation-rate glacial continental margin

Judith Elger [1, 2]*, Christian Berndt [1], Sebastian Krastel [2], David J. W. Piper [3], Felix Gross [1, 2], Robert F. Spielhagen [1, 4] & Sebastian Meyer [2]

[1] GEOMAR Helmholtz Centre for Ocean Research, Wischhofstrasse 1-3, 24148 Kiel, Germany

[2] Institute for Geosciences, Christian-Albrechts-Universität zu Kiel, Otto-Hahn-Platz 1, 24118 Kiel, Germany

[3] Geological Survey of Canada, Bedford Institute of Oceanography, P.O. Box 1006, Dartmouth, NS, B2Y 4A2, Canada

[4] Academy of Sciences, Humanities and Literature, Geschwister-Scholl-Strasse 2, 55131 Mainz, Germany

* Correspondence: jelger@geomar.de

Published online December 23, 2014 in Journal of the Geological Society

Received 28 May 2014; revised 24 October 2014; accepted 27 October 2014

Scientific editing by Adrian Hartley

2.1 Abstract

Submarine slope failures are a widespread, hazardous phenomenon on continental margins. The prevailing opinion links large submarine landslides along the glaciated NW European continental margins to overpressure generated by the alternation of rapidly deposited glacigenic and hemipelagic material. Here, we report a newly discovered large landslide complex off NW Svalbard. It differs from all known large slides off NW Europe, as the available data rule out that this slope failure resulted from rapid glacigenic deposition. This suggests that processes such as contour currents, tectonic faulting, and overpressure build-up related to the gas hydrate system must be considered for hazard assessment.

2.2 Introduction

Submarine slope failures occur all over the world and pose a significant natural hazard. They threaten offshore infrastructure in areas where hydrocarbon exploration is being carried out as well as underwater structures such as pipelines, rigs and communication cables. In addition, some landslides have caused destructive tsunamis endangering coastal communities.

Numerous large submarine landslides shaped the NE Atlantic glaciated margins during the Holocene and Pleistocene. The largest Holocene slide was the Storegga Slide, which initiated about 8200 years ago on the Møre Margin and mobilized c. 2400 - 3200 km³ of sediment in the northern part of the North Sea Fan (Fig. 2.1a; Haflidason et al. 2004; Kvalstad et al. 2005). The failure triggered a tsunami, which had an impact on coastal areas in Scotland, Norway, Iceland, and the Faeroe and Shetland islands; its maximum run-up height exceeded 20 m in places (Bondevik et al. 2005). Other slope failures affected the mouth of the Andøya cross-shelf trough (Andøya Slide) (Laberg et al. 2000) and the mouth of the Trænadjupet cross-shelf trough (Trænadjupet and Nyk slides) (Laberg & Vorren 2000; Lindberg et al. 2004) in the Holocene, and the mouth of the Bjørnøyrenna trough mouth fan (Bjørnøya Fan Slide Complex and Bjørnøya Slide) (Hjelstuen et al. 2007) and the seaward part of the Hinlopen cross-shelf trough on the northern Svalbard margin (Hinlopen–Yermak Slide) (Winkelmann & Stein 2007) in the Pleistocene (Fig. 2.1a).

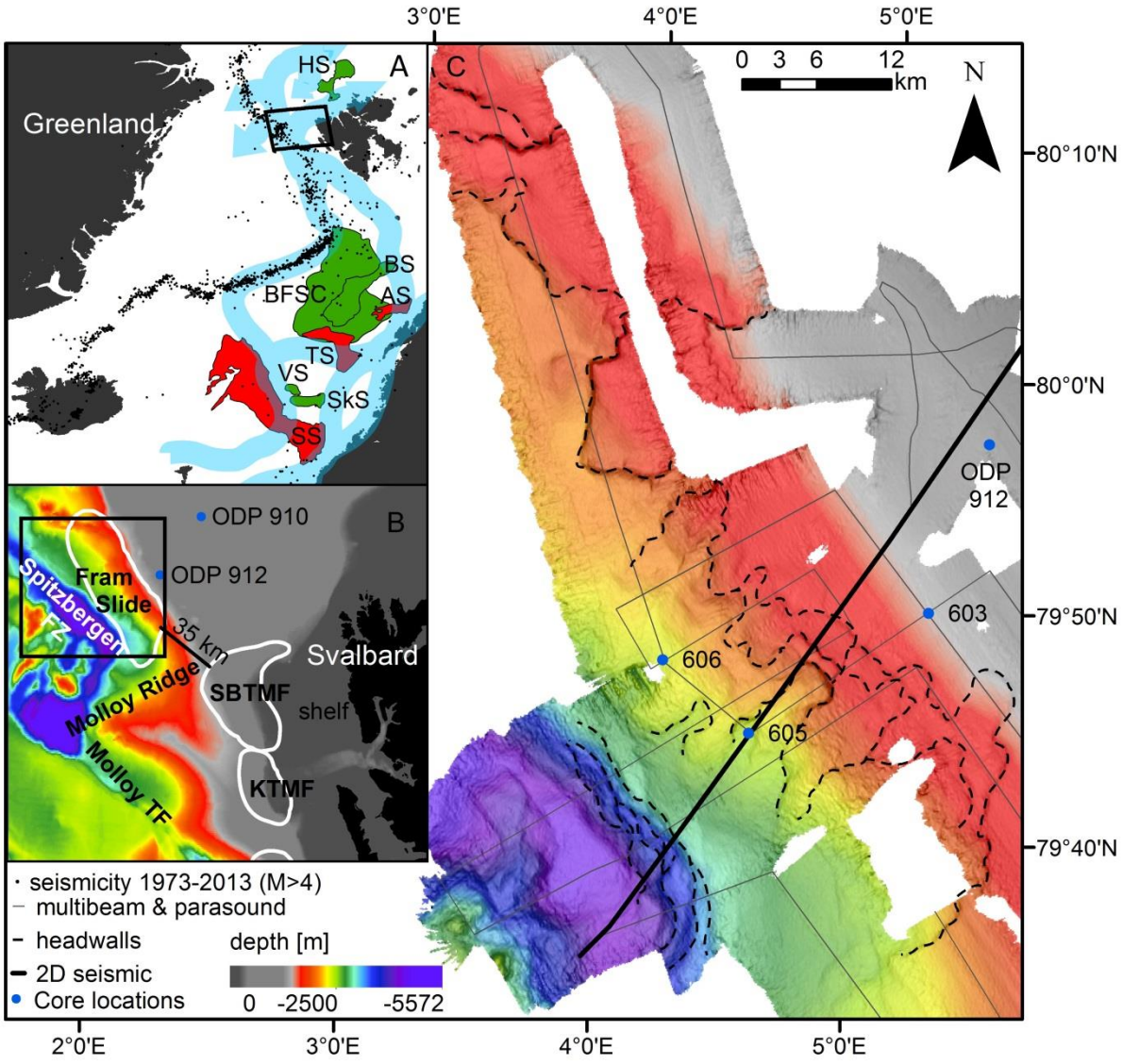

Figure 2.1: Location of the Fram Slide on the continental margin off Svalbard. (a) Overview map with seismicity in the area between 1973 and 2013 (M >4) (black dots; source: US Geological Survey), the surface water circulation in the eastern North Atlantic (blue arrows) (Haflidason et al. 2007; Vanneste et al. 2011), and the sea floor affected by the Holocene Storegga (SS), Trænadjupet (TS) and Andøya (AS) slides (coloured red), and by the Pleistocene Bjørnøya (BS), Bjørnøya Fan Slide Complex (BFSC), Sklinnadjupet (SkS), Vigid (VS) and Hinlopen–Yermak slides (HS) (coloured green) (Haflidason et al. 2007; Winkelmann & Stein 2007). (b) Local bathymetry of the Svalbard margin with the Molloy Transfer Fault (TF), the Spitsbergen Fracture Zone (FZ), glacial trough mouth fans (TMFs) and ODP Sites 910 and 912. KTMF, Kongsfjorden TMF; SBTMF, Sjubrebanken TMF. (c) Newly collected bathymetric data of the Fram Slide with Parasound profiles (grey lines), 2D high-resolution profile (black bold line), headwalls (black dashed lines) and the location of gravity cores (blue dots) acquired during expedition MSM21/4.

The geological processes that lead to submarine slope failures are still not fully understood. Numerous studies concluded that submarine slides on the glaciated European continental margins are closely related to the extent of ice sheets and the resulting variation in sedimentation rate and type owing to glacial–interglacial climate cycles in front of cross-shelf troughs (Bryn et al. 2005a; Kvalstad et al. 2005; Leynaud et al. 2009). In these areas, ice streams deposited glacigenic material rapidly during ice advances and did not allow the underlying hemipelagic sediments to dewater and consolidate normally. The resulting increase in pore pressure created potentially unstable slopes. The final trigger was possibly an earthquake (Leynaud et al. 2009) during isostatic rebound. Similar models have been proposed for several landslides at the Norwegian glaciated continental margins (Laberg & Vorren 2000; Laberg et al. 2000; Bryn et al. 2005a; Winkelmann & Stein 2007).

During a cruise to the Fram Strait in 2012, we discovered the Fram Slide, a new large submarine slide complex (Fig. 2.1). The main objective of this paper is to document that this slide is not controlled by pressure build-up owing to quickly accumulated glacial deposits. This means that other factors play an important role in slope failures; these factors will be discussed here using the Fram Slide as example.

2.3 Data

The basis of the study is a 58 km long 2D high-resolution seismic data profile (Fig. 2.1c) and about 750 km of Parasound and multibeam data that cover most of the slide over a depth range of 950–4200 m. Furthermore, we sampled near-surface sediments at three locations (Fig. 2.1c) using a gravity corer.

2.4 Results

The multibeam data reveal up to 250 m high breaks of slope extending 80 km along strike on the eastern side of the Fram Strait (dashed lines in Fig. 2.1c). These breaks of slope occur in water depths between 1260 and 3000 m, over a distance of more than 25 km in dip direction and in an amphitheater shape. The bathymetry data gridded at 100 m show that the slope breaks have gradients of up to 30° whereas the sea floor further seaward dips at 1–6°. In the toe region in water depths between 2.5 and 3 km the sea floor shows a slope angle of 1–2°. Here slope breaks are absent. Several very steep breaks of slope striking in a NW–SE

direction occur in a water depth greater than 3 km (Fig. 2.1c) at the northern edge of the trough of the Spitsbergen Fracture Zone (Fig. 2.1b).

The 2D high-resolution seismic data show a thick pile of parallel-stratified sediments in the shallow northeastern part of the profile (offset >30 km) (Fig. 2.2a). There is no seismic evidence for glacial debris-flow deposits, which are typically characterized by the absence of internal reflections and an overall wedge form (Bünz et al. 2003). Further downslope (offset 20–27.5 km), lateral thickness variations of single reflection packages indicate currentcontrolled deposition (Fig. 2.2c). A prominent 50 m high scarp at 30 km offset (Fig. 2.2d) truncates well-stratified sediments.

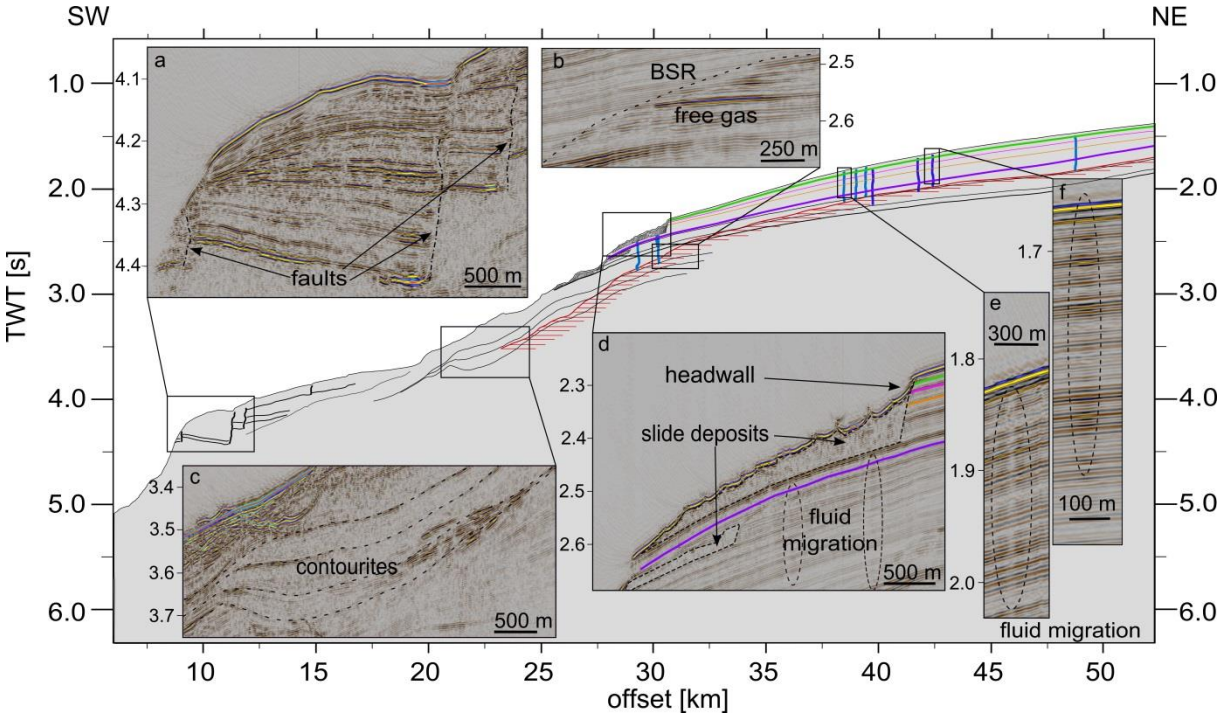

Figure 2.2: Line drawing of the 2D seismic profile showing the main features: a BSR (red) indicates free gas underneath; slide deposits are shown in dark grey; layered sediments in the shallow area with pipe structures indicate rising fluids (decreased or increased seismic amplitudes are shown in light and dark blue; respectively); location of core site 605; normal faults at about 10 km offset; the 0.78 Ma (green), 1.20 Ma (pink), 1.78 Ma (orange) and 2.58 Ma reflector (purple), implementing the seismic stratigraphy for ODP Site 912 from Mattingsdal et al. (2014). The insets show representative seismic examples for the various features: (a) faults and offsets of the prominent reflectors in about 3 km depth; (b) high amplitudes of free gas underneath the BSR; (c) undulation of single reflection packages indicating contourite deposition within a sediment drift; (d) transparent slide deposits with a hummocky surface next to the headwall and evidence for fluid migration beneath; (e) and (f) fluid migration suggested by subdued and increased amplitude, respectively.

A very prominent series of seismic high-amplitude anomalies is aligned at 300 ms two-way travel time (TWTT) beneath the seafloor reflection or c. 240 m below the sea floor (assuming a sediment sound velocity of 1600 m s−1), shoaling to the east. They terminate at a line (Fig. 2.2b) that in some places (e.g. at offset 30–32 km) forms a continuous seismic reflector. We interpret these anomalies as gas hydrate-related bottom simulating reflectors (BSR), similar to those observed along the Svalbard and mid-Norwegian margin (Berndt et al. 2004). The presence of highamplitude seismic anomalies beneath the BSR suggests the accumulation of free gas.

In addition, the seismic data show some vertical amplitude anomalies (Fig. 2.2e and f). We interpret them as pipe structures caused by upward migrating fluids. The low-amplitude anomalies indicate disruptions of the original layered sediment structure (Judd & Hovland 1992). The increased seismic amplitude anomalies within some of the pipes are possibly caused by free gas (Løseth et al. 2009).

Several steeply dipping low-amplitude anomalies interrupt the seismic reflections of the layered sediments between the offsets of 8 and 12 km (Fig. 2.2a). As they are associated with downward displacement of the seismic reflections, we interpret them as normal faults. They coincide with the breaks of slope in the bathymetry data.

Cores 605 and 606 were taken at locations with seismically transparent bodies shown by the Parasound data at a shallow depth below the sea floor (see Fig. 2.1c for location of cores), interpreted as slide deposits. This was confirmed by chaotic and sheared sediments at 270 and 210 cm depth in cores 605 and 606, respectively. Above these disturbed units, the cores consist of horizontal well layered brownish and greyish sediments with few dropstones. Radiocarbon dating of core 606 yields calculated average sedimentation rates of 46 and 36 mm ka−1, at 40–80 and 80–134 cm, respectively. Using these sedimentation rates we can estimate the onset of hemipelagic deposition following the slide event represented in the core to a minimum of c. 60 ka BP, assuming the higher sedimentation rate of 46 mm ka−1 for the 76 cm below the oldest age and the top of the slide deposit.

2.5 Discussion

Along an area of at least 2200 km2 of the continental margin NW of Svalbard, the multibeam data show numerous amphitheater-shaped slope breaks (Fig. 2.1c). We interpret the downward stepping slope-parallel scarps as headwalls of a submarine landslide complex. Adjoining pairs of slope breaks with the downthrown sides facing each other are interpreted as sidewalls. The seismic data support this interpretation. They show scarps with a truncation of the seismic reflectors upslope of the head wall, and hummocky sea-floor reflections with underlying chaotic seismic facies seaward of the headwall (Fig. 2.2). Furthermore, many of the observations point to the Fram Slide being a translational failure because it clearly cuts stratified sediments and the slide deposits are underlain by a planar surface interpreted as the glide plane (Fig. 2.2d). The limited amount of seismic data, however, does not rule out rotational movements in other parts of the slide. The multitude of nested headwalls suggests retrogressive sliding on multiple glide planes. The seismic data clearly show older buried slides (Fig. 2.2d), indicating a long history of slope failure in the region. Adopting the seismic stratigraphy from the study of Mattingsdal et al. (2014) for Ocean Drilling Program (ODP) Site 912, our data show that there have been slide events younger than 0.78 Ma and older than 2.58 Ma; the age model of core 606 suggests a minimum age of the latest slide event of c. 60 ka BP (Fig. 2.2d).

The Parasound data support this conclusion of different failure events. They show distinct morphological variation for different parts of the slide. No recent slide deposits are found downslope of some headwalls. The hummocky surface downslope of another scarp suggests that this feature was caused by a relatively recent slope failure; even the high resolution of the Parasound data does not show a drape.

The volume of mobilized slope material is between 65 and 220 km3 based on the area showing removal of sediments by the landslide and assuming a thickness of the removed sediments between 30 and 100 m, which is the height of the identified headwalls. This makes the Fram Slide smaller than most of the slides that affected the NE Atlantic margin (Hjelstuen et al. 2007) but this is a conservative estimate because of the incomplete data coverage.

With the large number of nested headwalls, translational sliding and an overall headwall length of several tens of kilometres the Fram Slide resembles other submarine landslides at glaciated margins (Laberg & Vorren 2000; Laberg et al. 2000). Therefore, similar geological processes may have controlled this slope failure. However, the continental shelf break is about

60 km SE of the slide (Ottesen & Dowdeswell 2009) and the closest observation of glacial debris-flow deposits is on the Sjubrebanken Fan, at least 35 km away (Fig. 2.1; Sarkar et al. 2011). Results from nearby ODP Site 912 (2 km off the seismic profile), the seismic data and the content of gravity cores 603, 605 and 606 (Fig. 2.1b) corroborate that the uppermost 40 m of sediments were deposited in a hemipelagic setting with some glacial influence in the form of ice-rafted debris, but with the absence of debris-flow deposits (Thiede et al. 1995), which is consistent with the glaciation model of Knies et al. (2009). Furthermore, the sedimentation rates are relatively low compared with those of areas influenced by trough mouth fans (Laberg et al. 2000; Lindberg et al. 2004; Winkelmann & Stein 2007). The absence of rapidly deposited glacigenic material rules out interlayering of hemipelagic contourite deposits and over-consolidated glacial deposits as an explanation for the Fram Slide.

We conclude that other geological processes must be responsible for generating the Fram Slide. Three processes seem most plausible, considering the geological setting. The first possibility is contour currents, which have influenced the sedimentation in large parts of the Fram Strait since the Late Miocene (Eiken & Hinz 1993; Gebhardt et al. 2014). The contourite deposits are easily distinguished in the seismic data at 20–27.5 km offset (Fig. 2.2c). There is no evidence for submarine erosion close to the slide but bottom currents may have led to repeated failure owing to over-steepening of the slope and enhanced deposition (Biscara et al. 2012). Haflidason et al. (2004) and Bryn et al. (2005b) showed that current velocities peaked for water depths in which the Storegga Slide was probably initiated. However, contourite deposits are widespread also along the Fram Strait margin farther south and slope failures have not been observed at these locations, suggesting that contourite deposition might be only a minor control on the development of the Fram Slide.

Second, faulting along the fracture zone may have resulted in toe-erosion and over-steepening of the slope. Owing to the location at the spreading ridge and the young age of the Fram Strait no abyssal plain has developed. Thus, the Fram Slide lacks a long run-out area, which is significantly different from other landslides on the glaciated margins off NW Europe. The breaks of slope observed in the bathymetric data in water depth >3 km (Fig. 2.1c) represent the surface expression of normal faults (Fig. 2.2a). These may result from tectonic activity along the Spitsbergen Fracture Zone (Fig. 2.1a and b) and probably imply vertical movements (Ritzmann & Jokat 2003; Fig. 2.2a). An alternative explanation for the presence of normal faults may be a rotational slump that developed on the steep part of the slope. Unfortunately, the data quality in this part of the profile is poor because the great water depth and the rough

topography cause seismic artefacts. However, normal faulting offsets the sea floor and thus removes the buttress for the adjacent sea floor further upslope, which could be a reason for the observed slope failures.

The third possible mechanism for slope failure in the study area is overpressure build-up owing to permeability variations in the subsurface. The BSR is conclusive evidence for gas hydrate and free gas accumulation within the main failure area (Fig. 2.2b). Gas hydrate cements the sediments and increases their shear strength (Sultan et al. 2004). This enhances the stability of the slope but also reduces the permeability (Berndt & Goswami 2007). Continuous accumulation of gas may increase pore pressure in the long term owing to buoyancy forces (Crutchley et al. 2010), which may destabilize the slope. In this scenario, pressure transfer may occur when the buoyancy force exceeds the fracture gradient of the sediments and gas blow-out pipes develop by hydro-fracturing (Bünz et al. 2003). Numerous examples of pipe structures in the seismic data (e.g. in Fig. 2.2e and f), in particular where the BSR appears brightest, imply that a large part of the slope has been affected by overpressures in the geological past. Overpressure development may have been the main destabilizing factor for the Fram Slide similar to the Ana Slide in the Western Mediterranean Sea (Berndt et al. 2012)

Mosher & Piper (2007) showed that some submarine slope failures on the Canadian glacial continental margins were caused by over-steepening owing to halokinesis. This process can be ruled out for the Fram Slide as evaporite deposits have not been reported for the Fram Strait.

Without a more robust understanding of the underlying mechanisms of the Fram Slide it is difficult to assess the associated hazard potential of slides in this area (Berndt et al. 2009), but it is likely that the combination of great water depth and multiple failures implies a low potential for destructive tsunamis (Nixon & Grozic 2006).

2.6 Conclusion

We report a new landslide complex that shapes the glacial continental margin NW off Svalbard. The Fram Slide affected the margin laterally for at least 2200 km2 at 1.3–3 km water depth with maximum headwall heights of 250 m. The estimated volume of mobilized slope material (65–220 km3) suggests the Fram Slide to be one of the smaller submarine

landslides that occurred on the NE Atlantic margin. However, this classification could be biased by the geological setting and the incomplete data coverage. The Fram Slide complex formed by multiple, translational, retrogressive failures on several glide planes. The latest event occurred c. 0.06 Ma BP, one is younger than 0.78 Ma and at least one older than 2.58 Ma.

The characteristics of the Fram Slide do not follow the prevailing explanation for failure on glacial continental margins off NW Europe, as this slide does not show any evidence for a formation history linked to the deposition of glacial deposits or salt tectonics and is therefore a very remarkable submarine landslide in the region that requires further study. It is more likely that a combination of unstable sediments owing to contourite currents, tectonic movement and/or fluid migration has played a key role in this slope failure. The potential hazard for destructive tsunamis from the Fram Slide complex is difficult to assess because of the limited database but the combination of great water depth and multiple failures suggests it is not as high as for the other major slides on the NW European margins.

2.7 Supplementary material

Data

The 2D high-resolution seismic data profile was acquired using an 88-channel Geometrics GeoEel streamer with a total length of 137.5 m and group spacing of 1.56 m. The seismic source consisted of a SERCEL GI air gun with a volume of 1.7 l which was shot in harmonic mode at 200 bar in ~2 m water depth; the main frequency was ~150 Hz. Data were sampled at 0.5 ms and sorted into common midpoint (CMP) domain with a bin spacing of 5 m. Normal move out correction was carried out with a velocity of 1500 m/s and an Ormsby bandpass filter with corner frequencies at 40, 80, 600 and 1000 Hz was applied. The data were time migrated with water velocity.

We used the hull-mounted parametric sub-bottom profiler PARASOUND P70 (Atlas Hydrographic) with a parametric frequency of 4 Hz.

Multibeam bathymetric data were recorded by the hull-mounted Kongsberg Simrad EM120 system with 191 beams per ping, an angular coverage of 150° and 12 kHz nominal frequency. The data were processed using the MB System software package. The bathymetric data was

gridded with GMT at various bin sizes. The grid shown in Fig. 2.1 has a horizontal bin size of 100 m. Seafloor attributes such as slope gradient and slope aspect were calculated with ArcGIS.

The three gravity cores were opened, described and logged (magnetic susceptibility, colour parameter) after the cruise. Planktic foraminifers were sampled at 40, 80 and 134 cm depth of core 606 and radiocarbon dated at the Leibniz-Laboratory for Radiometric Dating and Isotope Research in Kiel (Germany). Ages were calibrated to calendar years using Radiocarbon Calibration Program Calib REV7.0.1 with the Marine13 calibration curve (Reimer et al., 2013) including a reservoir correction of 405 14C years.

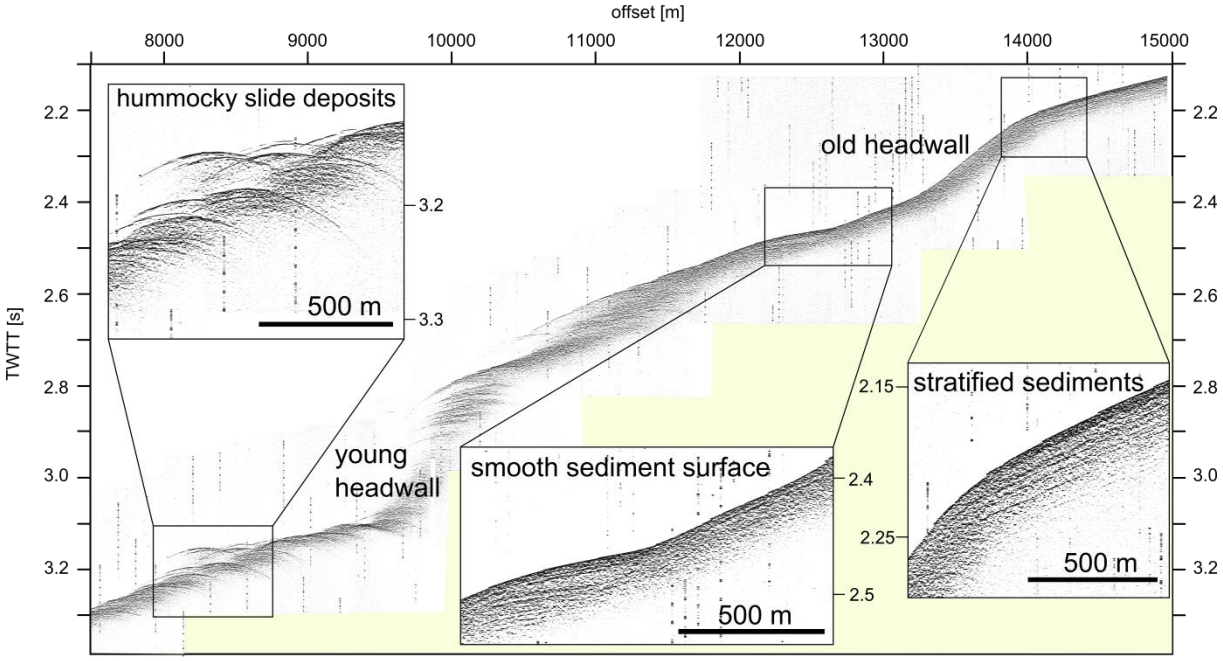

Figure 2.S1: Comparison of the characteristics of old and buried headwalls and probably relatively young headwalls as shown by the Parasound sub bottom profiler data.

Table 2.S1: Results of radiocarbon dating.

Depth [cm]	Laboratory Code	14C age [yr BP]	Standard deviation [14C yr]	Calendar age (Calib 7.0.1) using Marine13 data set and 405 yr reservoir correction	
				Mean [yr BP]	Standard deviation [yr]
40	KIA49391	15630	90	18492	109
80	KIA49392	23240	205	27194	226
134	KIA49393	38600	1345	42323	1077

Table 2.S2: Location of the gravity cores.

Core number	Latitude	Longitude
603	79°49.87' N	5°14.98' E
605	79°44.14' N	4°33.25' E
606	79°47.02' N	4°10.92' E

Figure 2.S2: Photograph of gravity core 606, every part of one meter length. The upper layer (0 to 210 cm) are well stratified, underneath there is chaotic sediments that we interpret as slide deposits.

Acknowledgements and Funding

We thank the master of R.V. Marian S. Merian and his crew for their splendid support during the cruise. Ship time was provided by the DFG Senatskommission für Ozeanographie. Financial support for the cruise came from the Centre of Excellence Future Ocean. J.E. was funded through the Helmholtz graduate school HOSST. Cruise-related data can be found on PANGAEA at: http://www. pangaea.de/search?q=campaign%3A“MSM21/4”.

References

Berndt, C. & Goswami, B. 2007. Gas hydrate-related sedimentary pore pressure changes offshore Angola. In: Yang, F. (ed.) Proceedings of the International Conference on Gas Hydrates: Energy, Climate and Environment, Taipei, Taiwan, October 4–5, 2007. National Taiwan University, Taipei, 156–161.

Berndt, C., Bünz, S., Clayton, T., Mienert, J. & Saunders, M. 2004. Seismic character of bottom simulating reflectors: Examples from the mid- Norwegian margin. Marine and Petroleum Geology, 21, 723–733.

Berndt, C., Brune, S., Nisbet, E., Zschau, J. & Sobolev, S.V. 2009. Tsunami modeling of a submarine landslide in the Fram Strait. Geochemistry, Geophysics, Geosystems, 10, http://dx.doi.org/10.1029/2008GC002292.

Berndt, C., Costa, S., Canals, M., Camerlenghi, A., de Mol, B. & Saunders, M. 2012. Repeated slope failure linked to fluid migration: The Ana submarine landslide complex, Eivissa Channel, Western Mediterranean Sea. Earth and Planetary Science Letters, 319–320, 65–74.

Biscara, L., Hanquiez, V., et al. 2012. Submarine slide initiation and evolution offshore Pointe Odden, Gabon—Analysis from annual bathymetric data (2004–2009). Marine Geology, 299–302, 43–50.

Bondevik, S., Mangerud, J., Dawson, S., Dawson, A. & Lohne, Ø. 2005. Evidence for three North Sea tsunamis at the Shetland Islands between 8000 and 1500 years ago. Quaternary Science Reviews, 24, 1757–1775.

Bryn, P., Berg, K., Forsberg, C.F., Solheim, A. & Kvalstad, T.J. 2005a. Explaining the Storegga Slide. Marine and Petroleum Geology, 22, 11–19.

Bryn, P., Berg, K., Stoker, M.S., Haflidason, H. & Solheim, A. 2005b. Contourites and their relevance for mass wasting along the Mid-Norwegian Margin. Marine and Petroleum Geology, 22, 85–96.

Bünz, S., Mienert, J. & Berndt, C. 2003. Geological controls on the Storegga gas-hydrate system of the mid-Norwegian continental margin. Earth and Planetary Science Letters, 209, 291–307.

Crutchley, G.J., Pecher, I.A., Gorman, A.R., Henrys, S.A. & Greinert, J. 2010. Seismic imaging of gas conduits beneath seafloor seep sites in a shallow marine gas hydrate province, Hikurangi Margin, New Zealand. Marine Geology, 272, 114–126.

Eiken, O. & Hinz, K. 1993. Contourites in the Fram Strait. Sedimentary Geology, 82, 15–32.

Gebhardt, A.C., Geissler, W.H., Matthiessen, J. & Jokat, W. 2014. Changes in current patterns in the Fram Strait at the Pliocene/Pleistocene boundary. Quaternary Science Reviews, 92, 179–189.

Haflidason, H., Sejrup, H.P., et al. 2004. The Storegga Slide: Architecture, geometry and slide development. Marine Geology, 213, 201–234.

Haflidason, H., de Alvaro, M.M., Nygard, A., Sejrup, H.P. & Laberg, J.S. 2007. Holocene sedimentary processes in the Andøya Canyon system, north Norway. Marine Geology, 246, 86–104.

Hjelstuen, B.O., Eldholm, O. & Faleide, J.I. 2007. Recurrent Pleistocene megafailures on the SW Barents Sea margin. Earth and Planetary Science Letters, 258, 605–618.

Judd, A.G. & Hovland, M. 1992. The evidence of shallow gas in marine sediments. Continental Shelf Research, 12, 1081–1095.

Knies, J., Matthiessen, J., et al. 2009. The Plio-Pleistocene glaciations of the Barents Sea–Svalbard region: A new model based on revised chronostratigraphy. Quaternary Science Reviews, 28, 812–829.

Kvalstad, T.J., Andresen, L., Forsberg, C.F., Berg, K., Bryn, P. & Wangen, M. 2005. The Storegga slide: Evaluation of triggering sources and slide mechanics. Marine and Petroleum Geology, 22, 245–256.

Laberg, J.S. & Vorren, T.O. 2000. The Trænadjupet Slide, offshore Norway—morphology, evacuation and triggering mechanisms. Marine Geology, 171, 95–114.

Laberg, J.S., Vorren, T.O., Dowdeswell, J.A., Kenyon, N.H. & Taylor, J. 2000. The Andøya Slide and the Andøya Canyon, north-eastern Norwegian–Greenland Sea. Marine Geology, 162, 259–275.

Leynaud, D., Mienert, J. & Vanneste, M. 2009. Submarine mass movements on glaciated and non-glaciated European continental margins: A review of triggering mechanisms and preconditions to failure. Marine and Petroleum Geology, 26, 618–632.

Lindberg, B., Laberg, J.S. & Vorren, T.O. 2004. The Nyk Slide—morphology, progression, and age of a partly buried submarine slide offshore northern Norway. Marine Geology, 213, 277–289.

Løseth, H., Gading, M. & Wensaas, L. 2009. Hydrocarbon leakage interpreted on seismic data. Marine and Petroleum Geology, 26, 1304–1319.

Mattingsdal, R., Knies, J., Andreassen, K., Fabian, K., Husum, K., Grøsfjeld, K. & De Depper, S. 2014. A new 6 Myr stratigraphic framework for the Atlantic–Arctic Gateway. Quaternary Science Reviews, 92, 170–178.

Mosher, D.C. & Piper, D.J.W. 2007. Analysis of multibeam seafloor imagery of the Laurentian fan and the 1929 Grand Banks landslide area. In: Lykousis, V., Sakellariou, D. & Locat, J. (eds) Submarine Mass Movements and their Consequences. Advances in Natural and Technological Hazards Research, 27, 77–88.

Nixon, M.F. & Grozic, J.L.H. 2006. A simple model for submarine slope stability analysis with gas hydrates. Norwegian Journal of Geological, 86, 309–316.

Ottesen, D. & Dowdeswell, J.A. 2009. An inter-ice-stream glaciated margin: Submarine landforms and a geomorphic model based on marine-geophysical data from Svalbard. Geological Society of America Bulletin, 121, 1647–1665.

Ritzmann, O. & Jokat, W. 2003. Crustal structure of northwestern Svalbard and the adjacent Yermak Plateau: Evidence for Oligocene detachment tectonics and non-volcanic breakup. Geophysical Journal International, 152, 139–159.

Reimer, P., Bard, E., Bayliss, A., and Beck, J., 2013, IntCal13 and Marine13 radiocarbon age calibration curves 0–50,000 years cal BP: Radiocarbon, v. 5

Sarkar, S., Berndt, C., Chabert, A., Masson, D.G., Minshull, T.A. & Westbrook, G.K. 2011. Switching of a paleo-ice stream in northwest Svalbard. Quaternary Science Reviews, 30, 1710–1725.

Sultan, N., Cochonat, P., Foucher, J.-P. & Mienert, J. 2004. Effect of gas hydrates melting on seafloor slope instability. Marine Geology, 213, 379–401.

Thiede, J., Myhre, A.M., Firth, J.V. & Shipboard Scientific Party. 1995. Cenozoic Northern Hemisphere Polar and Subpolar Ocean Paleoenvironments (Summary of ODP Leg 151 Drilling Results). In: Myhre, A.M., Thiede, J., Firth, J.V., et al. (eds) Proceedings of the Ocean Drilling Program, Initial Reports, 151, 397–420.

Vanneste, M., Harbitz, C.B., de Blasio, F.V., Glimsdal, S., Mienert, J. & Elverhøi, A. 2011. The Hinlopen–Yermak landslide, Arctic Ocean—geomorphology, landslide dynamics and tsunami simulations. In: Shipp, R.C., Weimer, P. & Posamentier, H.W. (eds) Mass-transport deposits in deepwater settings. SEPM Society for Sedimentary Geology, Special Publications, 95, 509–527.

Winkelmann, D. & Stein, R. 2007. Triggering of the Hinlopen/Yermak Megaslide in relation to paleoceanography and climate history of the continental margin north of Spitsbergen. Geochemistry, Geophysics, Geosystems, 8, 1525–2027.

Chapter 3

Chronology of the Fram Slide Complex offshore NW Svalbard and its implications for local and regional slope stability

Judith Elger [1,2], Christian Berndt [1], Sebastian Krastel [2], David J.W. Piper [3], Felix Gross [2], Wolfram H. Geissler [4]

[1] GEOMAR Helmholtz Centre for Ocean Research Kiel, Germany

[2] Institut für Geowissenschaften, Christian-Albrechts-Universität zu Kiel, Germany

[3] Geological Survey of Canada, Bedford Institute of Oceanography, Dartmouth, NS, Canada

[4] Alfred-Wegener-Institut Helmholtz-Zentrum für Polar- und Meeresforschung, Bremerhaven, Germany

This is a version of the manuscript that is under review at the journal *Marine Geology*

3.1 Abstract

The best known submarine landslides on the glaciated NW European continental margins are those at the front of cross-shelf troughs, where the alternation of rapidly deposited glacigenic and hemipelagic material generates sedimentary overpressure. Here, we investigate landslides in two areas built of contourite drifts bounded seaward by a ridge-transform junction. Seismic and bathymetric data of the Fram Slide Complex are compared with the tectonically similar Vestnesa area ~120 km to the south, to analyse the influence of local and regional processes on slope stability. These processes include tectonic activity, changes of climate and oceanography, gas hydrates and fluid migration systems, slope gradient, toe erosion and style of contourite deposition. The comparison demonstrates the strong impact of variation in the local controls on slope stability. Two areas within the Fram Slide Complex underwent different phases of slope failures, whereas there is no evidence at all for major slope failures in the Vestnesa area. These different failure chronologies suggest that slope shape, which influences contour currents and the resulting sedimentation pattern, toe erosion, which is dependent on the throw of normal faults, and the different thickness and geometry of contourite deposits exert pronounced effects on slope stability. These results highlight the limitations of regional hazard assessments and the need for multi-disciplinary investigations as small differences in local controlling factors led to substantially different slope failure histories.

Keywords

Fram Strait; Svalbard continental margin; submarine landslides; slope stability; pre-conditioning; trigger mechanisms; gas hydrates

Highlights

- The Fram Slide Complex has been active from late Miocene to late Pleistocene.
- Local processes were most significant for slope stability in the Fram Strait area.
- Toe erosion caused by normal faulting may have led to retrogressive failure.
- Low gradient geometries of contouritic sedimentation might stabilize submarine slopes.
- Based on historic slope failure pattern the tsunami potential of the Fram Slide Complex region is small.

3.2 Introduction

Submarine slope failures are a worldwide phenomenon and represent a significant natural hazard. They can destroy offshore infrastructure and generate destructive tsunamis which endanger coastal communities. Numerous studies show that submarine landslides occurred in the Holocene and Pleistocene on the NE Atlantic glaciated margin (Fig. 3.1A) and concluded that the cyclic sedimentation pattern related to glacial/interglacial conditions critically influences slope stability (Laberg and Vorren, 2000; Haflidason et al., 2004; Lindberg et al., 2004; Hjelstuen et al., 2007; Winkelmann and Stein, 2007). This hypothesis fits well for slopes with failures at the edge of the ice extent of past glaciers where the deposition of trough mouth fans led to very high sedimentation rates during glacial melting. It does not explain the occurrence of submarine slope failures in other geological settings.

Future climate models predict that the Arctic will be mostly free of summer sea ice by the end of the 21st century (Stocker et al., 2013) and forecast a long-lasting bottom water warming. This trend may have an effect on gas hydrate stability while at the same time enhances the interest of the hydrocarbon industry to extend oil and gas exploration further north. Hence, it is necessary to improve our knowledge about the processes and settings that favour slope instability in order to assess hazards in the Arctic and to minimize the impact of seafloor stability on hydrocarbon exploitation.

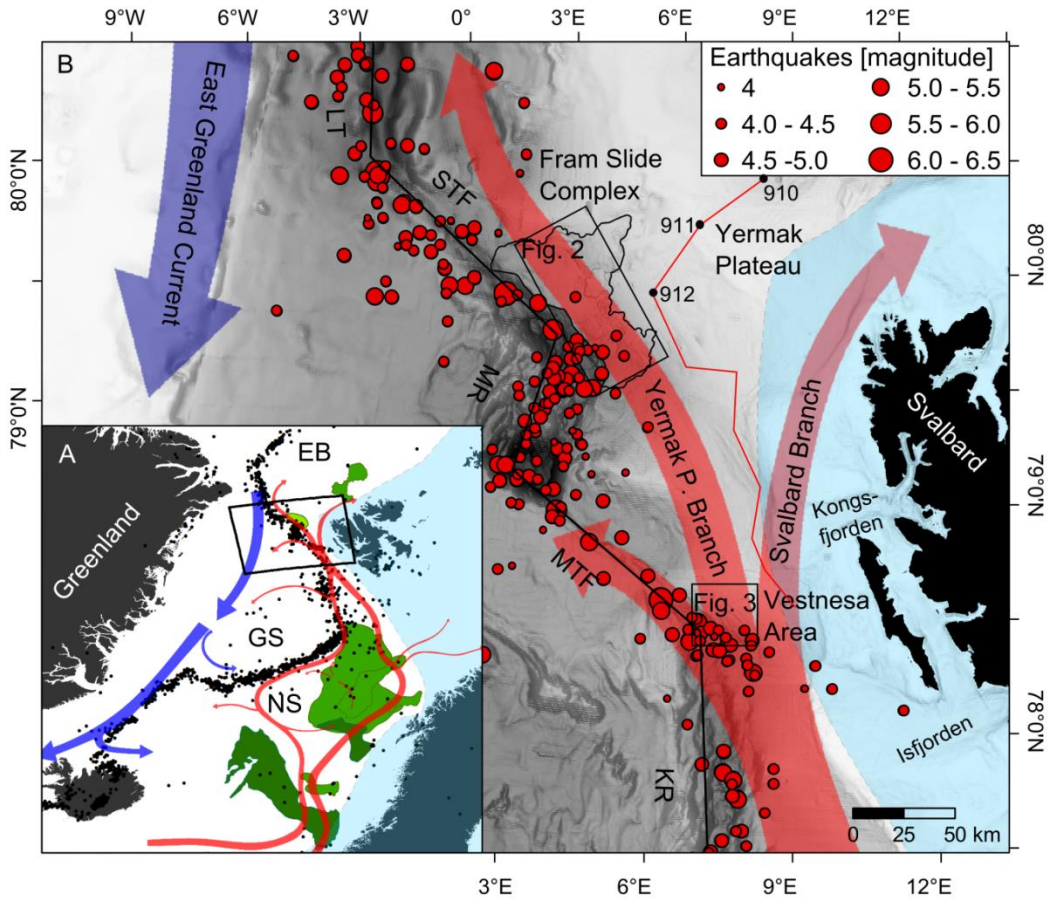

Fig. 3.1: Location of the Fram Slide Complex on the continental margin off Svalbard: (A) overview map with the maximum ice extent during glacial periods since 100 ka (blue shapes) (adapted from Ingólfsson and Landvik, 2013), seismicity in the area between 1973 and 2015 (M >4) (black dots; source: US Geological Survey), the location of the Norwegian and Greenland Sea (NS and GS), the Eurasian Basin (EB), the surface water circulation in the eastern North Atlantic including the East Greenland Current and the West Spitsbergen Current (red arrows) (adapted from Beszczynska-Möller et al., 2012), the sea floor affected by the Holocene Andøya, Trænadjupet and Storegga slides (light green, north to south), and by the Pleistocene Hinlopen–Yermak, Vigid, Sklinnadjupet, Bjørnøya Fan Slide Complex and Bjørnøya slides (dark green, north to south) (Haflidason et al., 2007; Winkelmann and Stein, 2007) and the location of the FSC (outlined in black) (map projection: azimuthal equidistant). (B) Regional bathymetry of the Fram Strait and Svalbard margin with the Lena Trough (LT), the Spitsbergen Transfer Fault (STF), Molløy Ridge (MR), Molløy Transfer Fault (MTF) and Knipovich Ridge (KR), the location of the ODP bore holes 910-912, the seismic profiles from which the stratigraphy of Mattingsdal et al. (2014) was extrapolated, the branches of the splitting West Spitsbergen Current, the northern and southern part of the FSC (NP and SP), the seismicity in the area between 1973 and 2015 (US Geological Survey) and the location of Figs. 3.2- 4 (map projection: WGS 1984 UTM Zone 32N).

There are not many submarine landslides known and studied in the European Arctic apart from the Hinlopen/Yermak slide complex (Winkelmann and Stein, 2007) and the Fram Slide (Elger et al., 2015). Elger et al. (2015) reported on the extent of the Fram Slide and compared it with the typical characteristics of slope failures on the NE Atlantic glaciated margin. That study confirmed that submarine slope failure in the NE Atlantic is not necessarily tied to areas close to the edge of the ice extent where interglacial/glacial sedimentation patterns are presumed to lead to overpressure build-up in the sediment pore space. Rather, the Fram Slide Complex (FSC) is developed in a contourite drift, near the tectonically active intersection of the Spitsbergen Transfer Fault and the Molløy Ridge (Fig. 3.1B). An analogous tectonic setting is found 120 km southeast, in the Vestnesa area on the Svalbard continental margin, in contourite drifts near the intersection of the Knipovich Ridge and the Molløy Transfer Fault. No submarine landslides have been reported there previously.

The purpose of this paper is to constrain the chronology of events that shaped the Fram Slide Complex (FSC) based on a new seismic and bathymetric data set. A second objective is to evaluate the role of regional and local geological processes that pre-condition and trigger submarine landslides, by comparing the internal variability in morphology and recurrence interval of landslides in the FSC and the Vestnesa area. Tectonic activity, influence of climate and oceanography, and contourite deposition are considered processes that shape the slope and can lead to toe erosion and over-steepening, whereas gas hydrates and basinal fluids are relevant for buoyancy-related overpressure. In addition, we assess the hazard of the FSC by comparing its features with other slope failures on the eastern glaciated North Atlantic continental margin and their estimated hazard.

3.3 Regional setting

The FSC is located at the intersection of the Spitsbergen Transfer Fault and the Molløy Ridge in the Fram Strait that connects the Eurasian Basin with the Norwegian and Greenland Sea (Fig. 3.1A). When the Eurasian and North American plates separated in the earliest Eocene, the two basins were connected by a strike-slip fault. From the earliest Oligocene, motion between Greenland and Eurasia changed from transform to divergent and the sheared margin was rifted and broken into ridges connected by transfer faults (Talwani and Eldholm, 1977). The Spitsbergen Transfer Fault is the most prominent of several transfer faults that connect the adjacent spreading ridges and move in a dextral shear sense (Engen et al., 2003) (Fig.

3.1B). It forms a narrow northwest–southeast oriented valley with a length of ~150 km connecting the southern Lena Trough in the north with the 60-km-long Molløy Ridge in the south. The Molløy Ridge is bounded to the southeast by the Molløy Transfer Fault, which intersects with the Knipovich Ridge in the Vestnesa area.

An initial oceanic channel connected the Eurasian Basin with the Norwegian-Greenland Sea since earliest Miocene (Thiede et al., 1995) but the present day mode of seafloor spreading was probably delayed until late Miocene (Engen et al., 2008). A major provenance change of sediments at 11.2 Ma documented in sediment cores of ODP Leg 151 (Winkler et al., 2002) supports this tectonic change. The connection of the two basins led to gradual cooling of the northern hemisphere, as evidenced by ice-rafting activity from 5.7 to 3.2 Ma (Wolf and Thiede, 1991). Long-lasting moderate glacial conditions from 2.6 to 1.0 Ma were followed by increased glacial/interglacial environmental conditions until 0.6 Ma. These climate conditions were associated with the transition to characteristic glacial and interglacial shifts in deep water properties. From 0.6 Ma to present, large differences in glacial/interglacial environmental conditions with a maximum contrast in surface water regimes led to different modes of deep water production and exchange rates with the North Atlantic (Henrich and Baumann, 1994; Henrich, 1998). Present day oceanographic conditions are characterized by the northward inflow of the West Spitsbergen Current carrying warm Atlantic Water into the Arctic Ocean (Manley, 1995) (Fig. 3.1A). At ~79.0°N the West Spitsbergen Current splits into three branches (Quadfasel et al., 1987) (Fig. 3.1B). The Svalbard Branch turns eastward directly north of the Svalbard archipelago and flows across the shallow southern Yermak Plateau (Schauer et al., 2004). The west branch flows southwards and joins the East Greenland Current (Bourke et al., 1988) and the Yermak Plateau Branch transports water northwards along the western Yermak Plateau where it enters the Arctic Ocean (Rudels et al., 2002).

In both the FSC and the Vestnesa area, plastered sediment drifts with large-scale sediment waves have developed on the Svalbard continental margin. The Vestnesa Ridge, a NW-SE elongated sediment drift north of the Molløy Transform Fault, indicates the great influence of contour currents in the Vestnesa area that led to high sedimentation rates. Gas hydrate and free gas within the drift form gas seeps and have been subject of several studies (Hustoft et al., 2009; Petersen et al., 2010).

3.4 Materials and methods

This study uses multibeam data of the FSC and Vestnesa area that were acquired during cruises MSM31 (FSC only) and MSM21/4 with the hull-mounted Kongsberg EM122 and EM120 system, respectively (Figs. 2A, 3A). Both systems operate with an angular coverage of 150° and a nominal transducer frequency of 12 kHz. We used the open source MB System software for processing, GMT for gridding at various bin sizes and ArcGIS for the calculation of slope angles. The illustrated grids have a horizontal bin size of 50 m.

2D high-resolution reflection seismic data acquired during cruises MSM21-4 and MSM31 cross the slope in different parts of the FSC (location in Fig. 3.2A, coordinates in the supplementary material Table 3.S1). Seismic data were collected with an 88-channel Geometrics GeoEel streamer of a total length of 137.5 m and a group spacing of 1.5625 m. The signal was generated by a 1.7 l GI-Gun, shot at 200 bar at ~2 m tow depth. We used the VISTA package (Schlumberger) for seismic processing. Data were binned at 3.125 m. Normal move out correction was carried out with a constant velocity of 1500 m/s and an Ormsby band pass filter with corner frequencies at 40, 80, 600 and 1000 Hz was applied. Finite difference time migration was performed with a constant velocity of 1500 m/s. A shot interval of 7 s and a recording length of 6 s were chosen at a cruise speed of ~ 4.5 knots to obtain an average CMP (Common-Mid-Point) fold of ~15 by applying a bin size of 3.125 m. The wavelet of the reflections in the water column shows peak energy at frequency ~100 Hz. Assuming a constant sound speed of 1500 m/s, the vertical resolution is ~3.75 m. Seismic data from the Vestnesa area were filtered in the shot gather domain by a τ-p filter to suppress surface-generated water noise. A zero-phase band-pass filter was applied, using corner frequencies of 60 Hz and 360 Hz. For normal move out correction an interpolated and extrapolated 3D velocity model based on regional velocity information from MCS data (Sarkar et al., 2012) was used. Common midpoint (CMP) profiles were generated through crooked-line binning with a CMP spacing of 1.5625 before applying an amplitude preserving Kirchhoff post-stack time migration (Dumke et al., 2016).

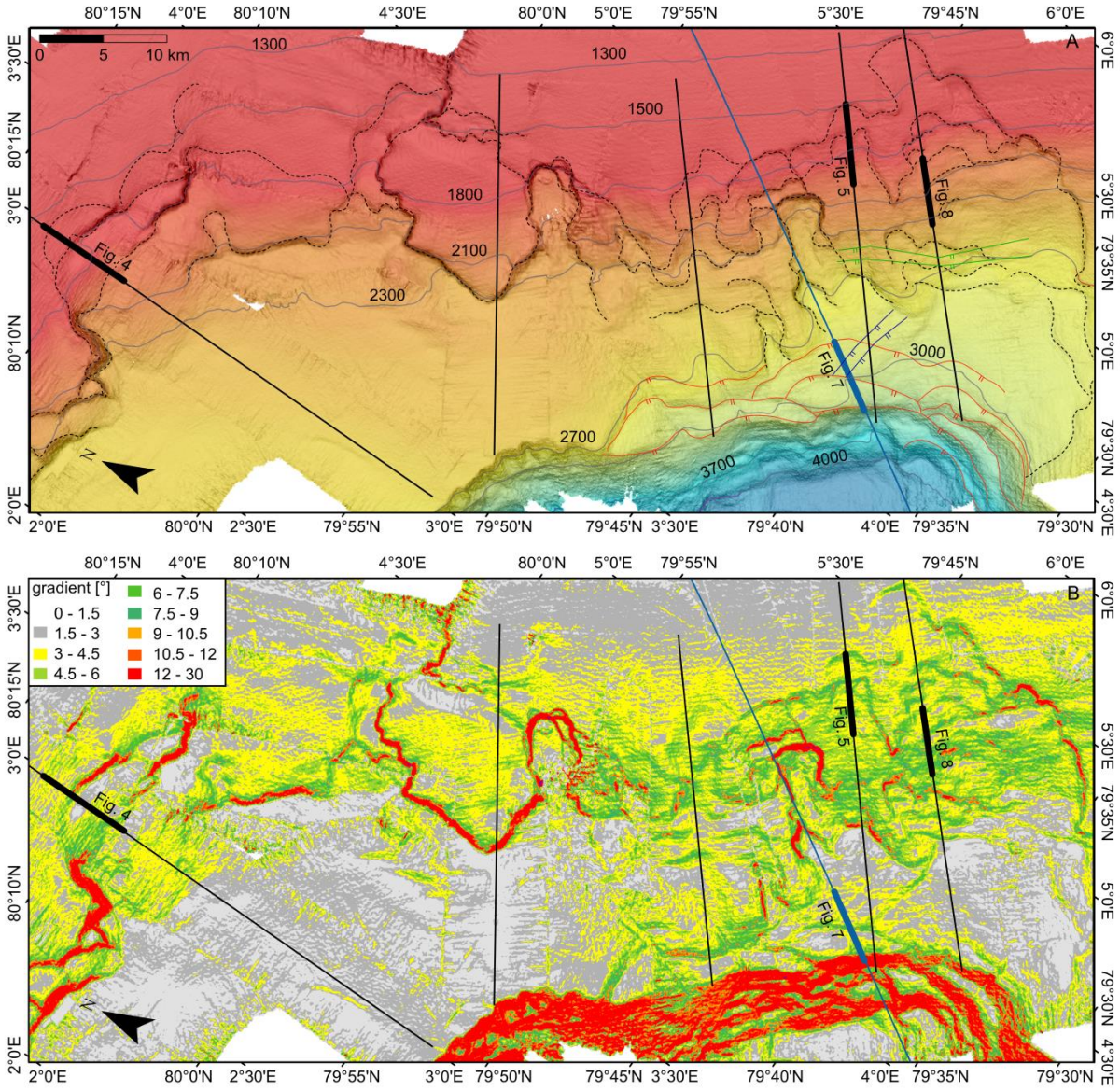

Fig. 3.2: Maps (map projection: WGS 1984 UTM Zone 32N)of the FSC (A) of local bathymetric data with contour lines (gray lines in meters), the 2D high-resolution profiles from MSM31 (black lines) and MSM21-4 (blue line), head- and sidewalls (black dashed lines), location of Figs. 5, 6, 8, and 9 (bold lines) and normal curved faults that trace the shape of the deep water pathway (red lines), faults with a strike direction of ~55° dip towards the southwest (green line) and faults that strikes ~10° and dips south-southwest (blue lines); (B) of the slope gradient of the FSC with the reflection seismic profiles from MSM31 (black lines) and MSM21-4 (blue line) and the location of Figs. 5, 6, 8 and 9 (bold lines).

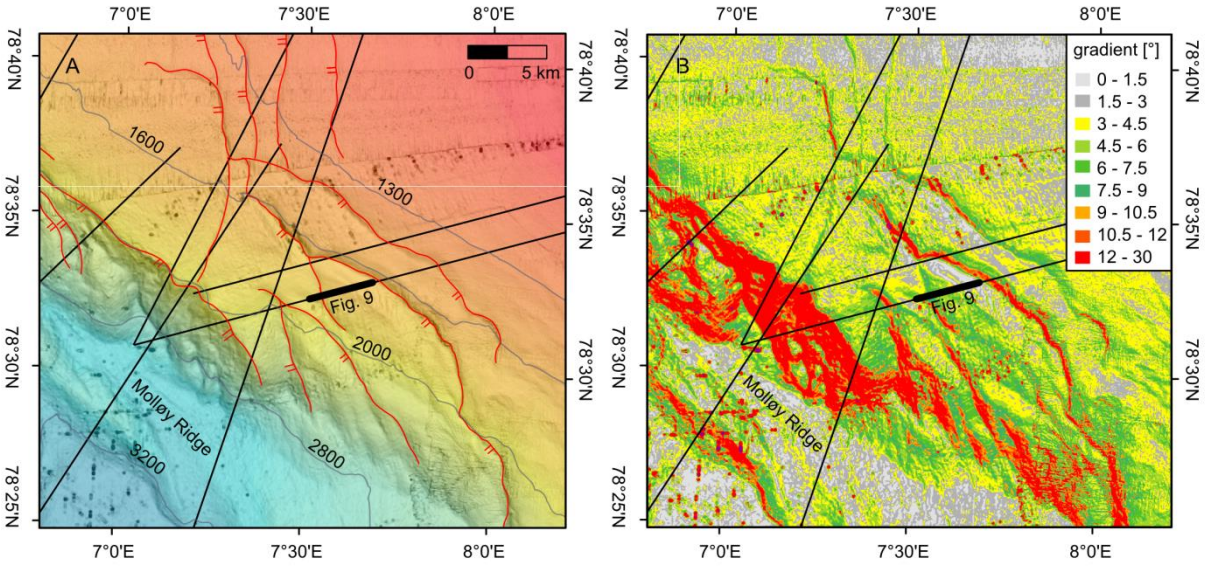

Fig. 3.3: Maps (projection: WGS 1984 UTM Zone 32N) of the Vestnesa area of (A) local bathymetric data with contour lines (gray lines in meters), the reflection seismic profiles from MSM21-4 (black lines), location of Fig. 3.10 (bold black line) and normal faults (red lines) (B) slope gradient with the reflection seismic profiles from MSM 21-4 (black lines) and the location of Fig. 3.10 (bold black line).

In order to estimate the minimal age of the landsliding, we applied the seismic stratigraphy from Mattingsdal et al. (2014). Mattingsdal et al. (2014) used paleomagnetic and biostratigraphic samples in combination with high-resolution seismic data connecting ODP holes to establish a comprehensive stratigraphic framework for the Fram Strait for the last 6 Ma (location in Fig. 3.2A). Although our seismic profiles do not intersect the lines used for that stratigraphy (Fig. 3.1B), typical reflection patterns in the seismic profiles of undisturbed sediments at the top of the slope were correlated confidently and allow ages to be assigned to particular seismic horizons. We estimate the uncertainty for the ages of old slope failures (~5 Ma) to be on the order of 1 Ma, and for the recent slope failures to be on the order of 100 ka. Headwalls and sidewalls that occur at the same stratigraphic level and are connected by one surface expression in the bathymetry were combined to one slope failure. We calculated the maximum evacuated volume of the events by multiplying the affected area derived from the bathymetry (from the headwall down to the slope break in ~3 km water depth) with the maximum height of the headwall. This approach to volume estimation contains large uncertainty but it is the best procedure possible considering the data base.

3.5 Results

3.5.1 Seafloor morphology of the FSC

Based on new bathymetric data, the FSC covers an area of 5500 km² east of the Spitsbergen Transfer Fault in water depths between 850 m to 4200 m (Figs. 1B and 2A). This is more than twice the area previously estimated (Elger et al., 2015). The gradient map in Fig. 3.2B shows that the slope is divided into areas of maximal 2.7 ° dip mostly at the top of the slope, minor steep parts (3 to 8°) in the upper part of the slope and very steep parts of up to 22° at the very bottom of the slope. In the northern part, the minor steep slope (3 to 8 °) is up to 25 km distant from the surface expression of the Spitsbergen Transfer Fault, separated by a gently sloping area (< 2.7°). In the southern part of the FSC, a narrow stretch of margin of only 10 km links the upper part of the slope with the depression of the Molløy Ridge and Spitsbergen Transfer Fault (Fig. 3.2B). The bathymetric and gradient maps show a large number of morphological steps on the upper part of the slope that illustrate the characteristic amphitheatric shape of headwalls and sidewalls of submarine landslides (Figs. 2A and 2B).

North of 79°55'N (northern part of the FSC), a displacement of up to 270 m height and 100 km length is the most prominent morphological feature of the seafloor (Fig. 3.2A). Seismic data show a buried scarp that truncates in total ~600 m thick well-stratified sediments (Fig. 3.4). Hence, this structure originates from a buried, large-scale slope failure with different glide planes in the very northern part of the FSC. This interpretation is similar to the composite set of escarpments and multiple buried slip surfaces of the Hinlopen Yermak slide with its >1000 m high headwall (Vanneste et al., 2006). Other minor scarps on the seafloor close to the buried large-scale headwall (Figs. 2A and 2B) are identified as buried headwalls based on seismic interpretation (Fig. 3.4).

Numerous smooth and sharp steps of heights from 30 to 200 m on the seafloor (Fig. 3.2A) characterize the morphology south of 79°55'N (southern part of the FSC). The seismic data do not cover the entire area but reveal a minimum of 16 headwalls of heights of up to 120 m that are covered by sediments of different thickness (Fig. 3.5). The seafloor morphology of this part of the slide complex is not dominated by one structure but consists of a variety of diverse headwalls (compare Figs. 2A and 2B).

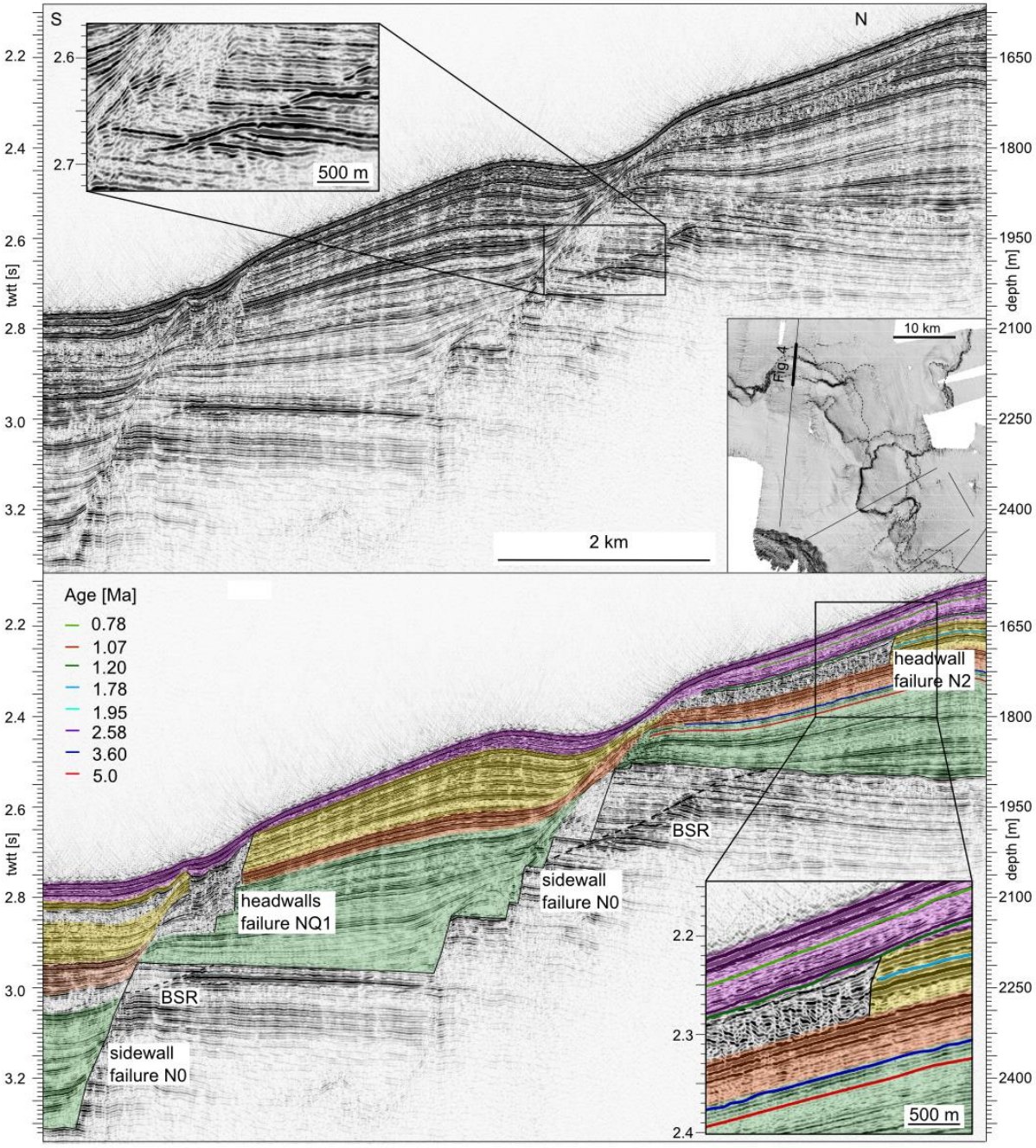

Fig. 3.4: An extract of the reflection seismic profile MSM31-P385 (top) with a zoom to truncated well-stratified sediments in the northern part of the FSC and its interpretation (bottom) showing the major ancient sidewall of the slope failure N0, the BSR (dashed line) visible in the pre failure sediments, more recent failures (N2 and NQ1) in the vicinity of the old sidewall and the extrapolated stratigraphy from Mattingsdal et al. (2014) (colored lines) that we used to estimate the age. The colored intervals of reflections indicate characteristic sediment units with distinctive architecture.

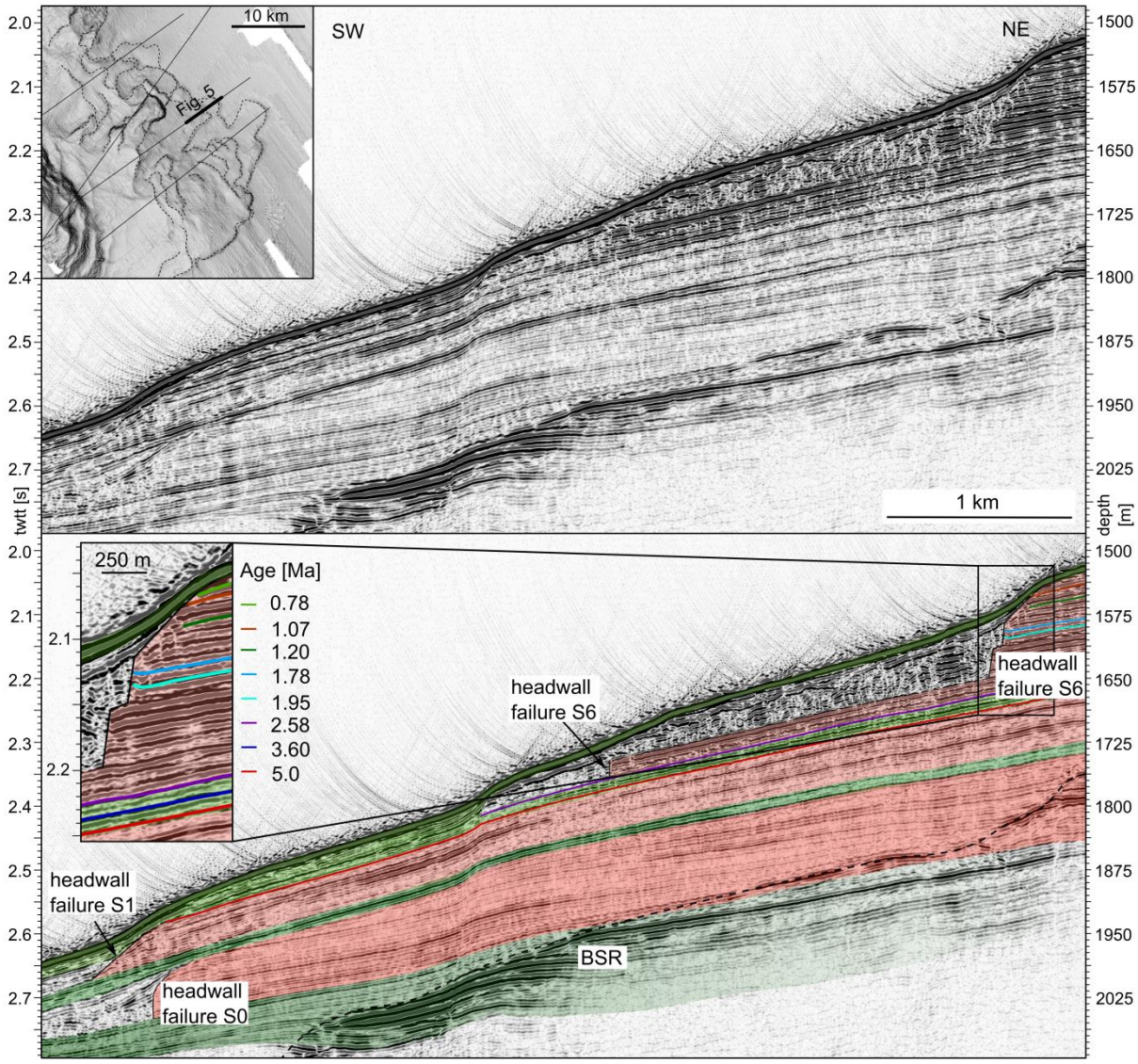

Fig. 3.5: An extract of the reflection seismic profile MSM31-P370 (top) in the southern part of the FSC and its interpretation (bottom) showing the buried headwalls of multiple failures (S0, S1 and S6), a continuous BSR in ~300 ms twtt parallel to the sea floor reflection and a detailed zoom to the headwall of the slope failure S6 with the seismic stratigraphy adapted from Mattingsdal et al. (2014). The colored intervals of reflections indicate characteristic sediment units with distinctive architecture.

3.5.2 Chronology and volume of failures of the FSC

The slope failures that caused the headwalls occurred before more than 5 Ma to about 0.68 Ma applying the seismic stratigraphy from Mattingsdal et al. (2014) (Table 3.1 and Fig. 3.6). Before 5 Ma a submarine slope failure formed major headwalls and sidewalls in the northern part and evacuated ~1160 km³ of sediment. Minor slope failures in the vicinity of this structure created scarps of 23 to105 m height and occurred less than 2.58 to 0.78 Ma ago

(Table 3.1 and Fig. 3.6). Heights of the headwalls and corresponding volumes decrease over time, with the smallest features being the youngest. The chronology of the events in the southern part of the FSC shows a much more even distribution of slope failures in the time period of >5 to 0.68 Ma (Table 3.1 and Fig. 3.6). There is no distinct correlation between age, water depth or height of the headwalls. The estimated volumes of failed sediment range from 3 to 62 km³. The slope failures that caused maximum headwall heights of 120 m originated at about 0.78 Ma (Table 3.1).

Table 3.1: Identified slope failures in the FSC with their minimal estimated age of origin based on the extrapolation of the seismic stratigraphy of Mattingsdal et al. (2014), height and water depth of the head or sidewalls and the estimated evacuated volume.

mass failure	age [Ma]	height [m]	volume [km³]	water depth [m]
S0	>5	60	20.4	1820
N0	>5	600-300	1161.1	1020
S1	5	60-23	37.6	1820
S2	2,58	15	5.2	1650
S3	2,58	53	19.4	1660
S4	1.95-2.58	30	10.3	1750
N1	1.95-2.58	105	13.1	1500
N2	1.2-1.78	38	1.7	1350
S5	1.2	98	32.8	1660
S6	0.78	120	62.3	1290
N3	0.78	23	1.7	1380
S7	0,68	23	3.3	1650
S8	<0.78	180	26.6	1640
SQ1	-	120	23.8	2550
SQ2	-	98	17.1	2470
SQ3	-	90	19.5	2240
NQ1	-	90	13.4	1670

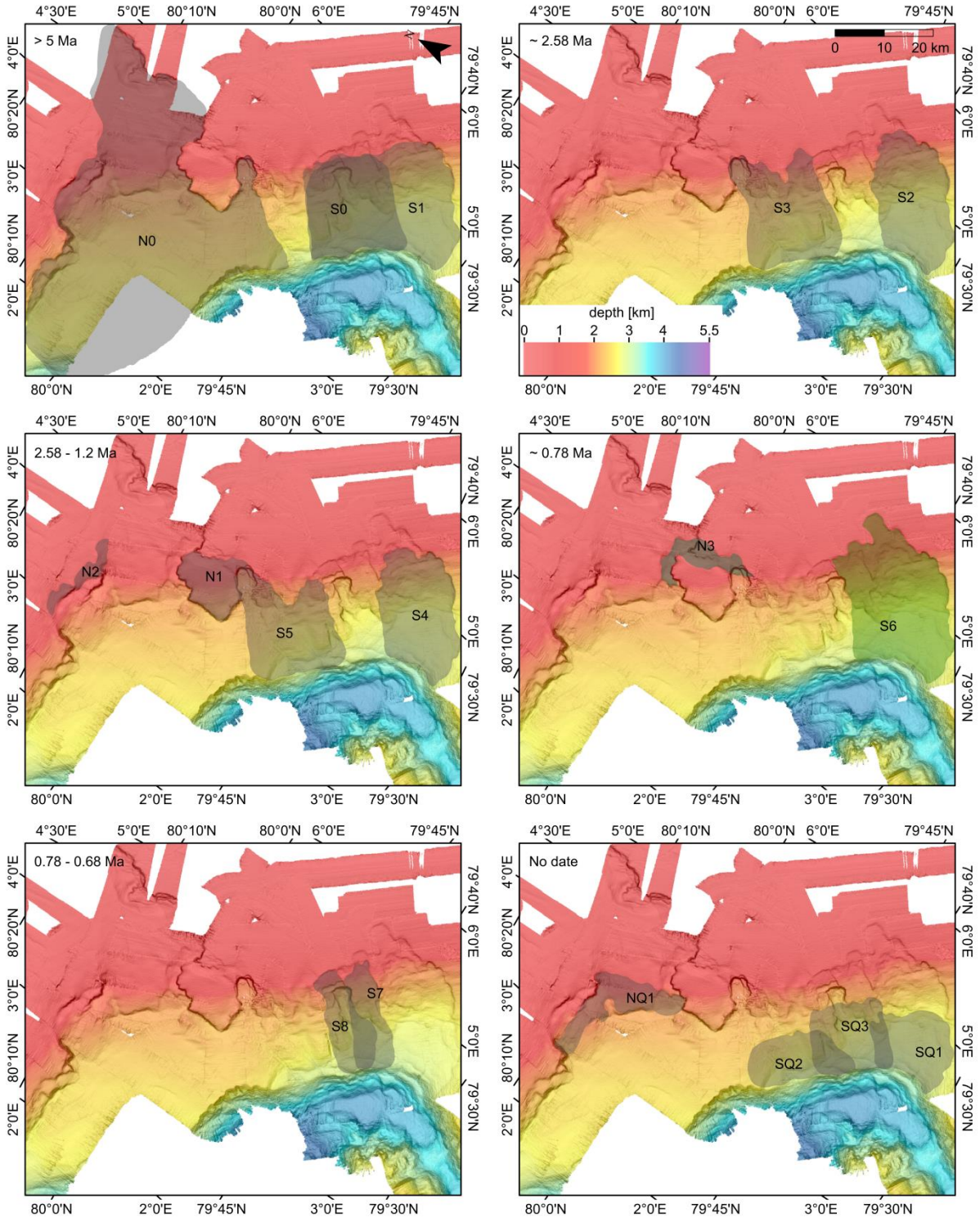

Fig. 3.6: Bathymetric maps with the history of slope failures of the FSC show the extent of the slope failures (in grey) listed in Table 3.1 over five time intervals, and those with no age estimate. Ages are based on the extrapolation of the seismic stratigraphy of Mattingsdal et al. (2014).

3.5.3 Subsurface features of the FSC

Seismic data image a series of seismic high-amplitude anomalies running parallel to the seafloor. They cut the sediment layers at ~300 ms two-way travel time (twtt) or ~225 m below the sea floor (assuming a sediment sound velocity of 1500 m s^{-1}). The anomalies terminate in this depth and in some places (e.g. Fig. 3.5) they form a continuous seismic reflection. We interpret these anomalies as a bottom simulating reflection (BSR), similar to those observed elsewhere along the Svalbard and mid-Norwegian margin (Berndt et al., 2004). The BSR marks the base of the gas hydrate stability zone. Free gas accumulating underneath the gas hydrate stability zone appears as areas of enhanced negative phase amplitudes.

Generally, we identify a coherent BSR in the upper part of the slope but further downslope there are only local high-amplitude reflections at the expected depth of the BSR. Shedd et al. (2009) termed this series of bright spots a 'segmented' BSR. The two southern seismic profiles (Fig. 3.2A) image the BSR well on the entire slope down to 2900 m water depth (Fig. 3.5). At the sidewall in the northern part of the FSC, the BSR is visible from the top down to the bottom of the sidewall (Fig. 3.4). It cuts the stratigraphy of the pre-failure sediments but not the sediments that accumulated afterwards. Gas is trapped underneath the uppermost layer that did not fail. This phenomenon appears at several locations and may represent sealing sediments that trap gas and may create buoyancy-related overpressure.

Several steeply dipping low-amplitude anomalies interrupt seismic reflections of layered sediments with changing dip (Fig. 3.7) in the southern part of the complex and correspond to bathymetric escarpments (Fig. 3.2A). As they are associated with rotational downward displacement of the seismic reflections, we interpret them as normal faults of up to 120 m throw (average 41 m using a velocity of 1500 ms^{-1}). There are three types of faults. Curved faults trace the shape of the deep water pathway built by the depressions of the Molløy Ridge and Spitsbergen Transfer Fault and terminate at the slope in ~3 km water depth. Further upslope, in the lower part of the slide area (2300-3000 m water depth), faults with a strike direction of ~055° dip towards the southwest. Another set of faults strikes ~010° and dips south-southwest (Fig. 3.2A).

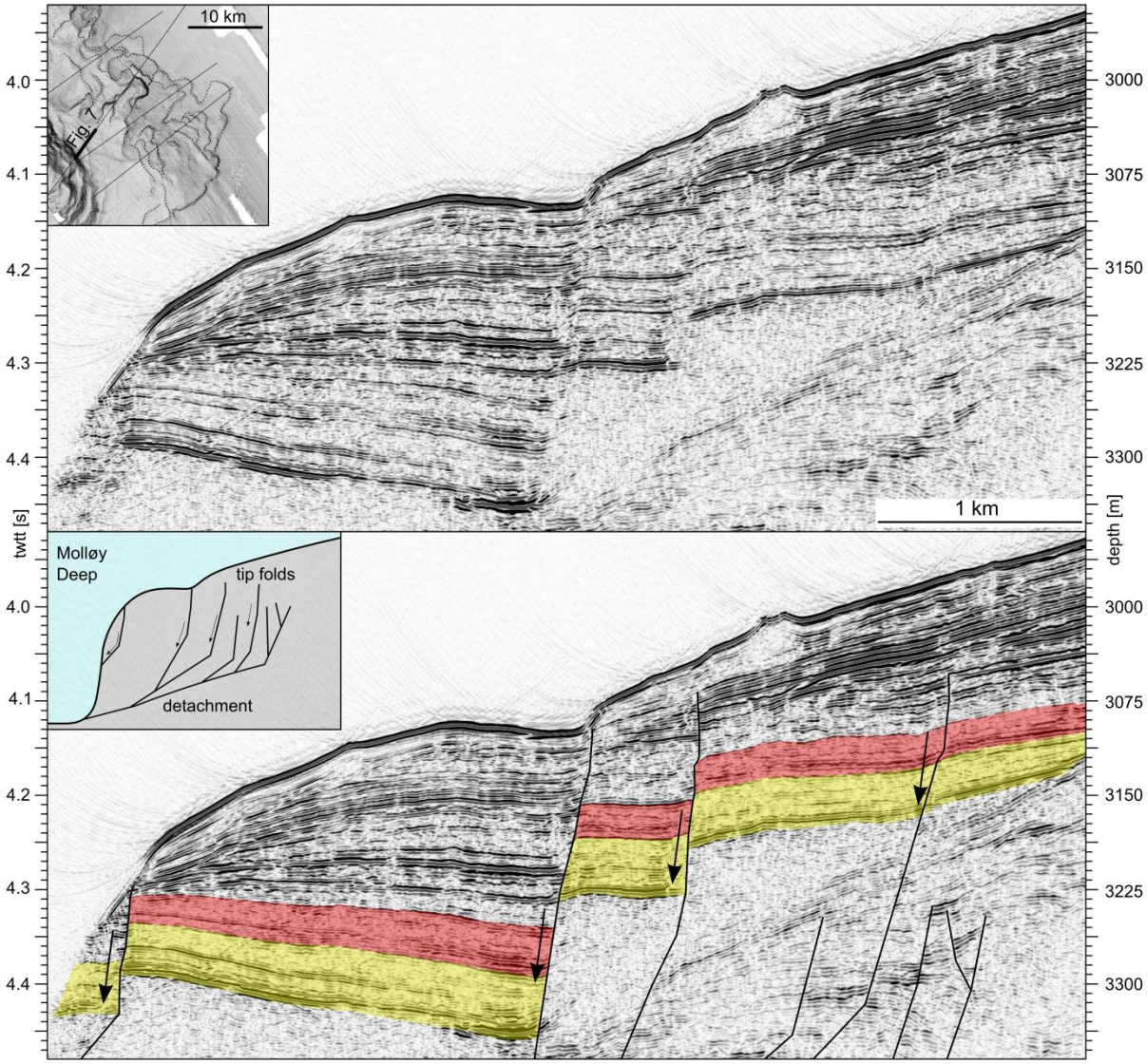

Fig. 3.7: An extract of the reflection seismic profile MSM21_4-P500 (top) in the southern part of the FSC and its interpretation (bottom) showing normal faults in ~3 km water depth with different offset and of different age and a line draw of the lower slope in the southern part of the FSC next to the Molløy Deep. The colored groups of reflections indicate characteristic sediment units.

Seismic data in the southern part of the FSC image lateral thickness variations of reflection packages as well as unconformities that form wavy layers (Fig. 3.8). These characteristics indicate current-controlled deposition which we interpret as sediments waves, discordances and moats. These sediment structures document the spatial and temporal variation of contour currents in water depths between 1700 and 2800 m and their influence on the sedimentation process on the slope.

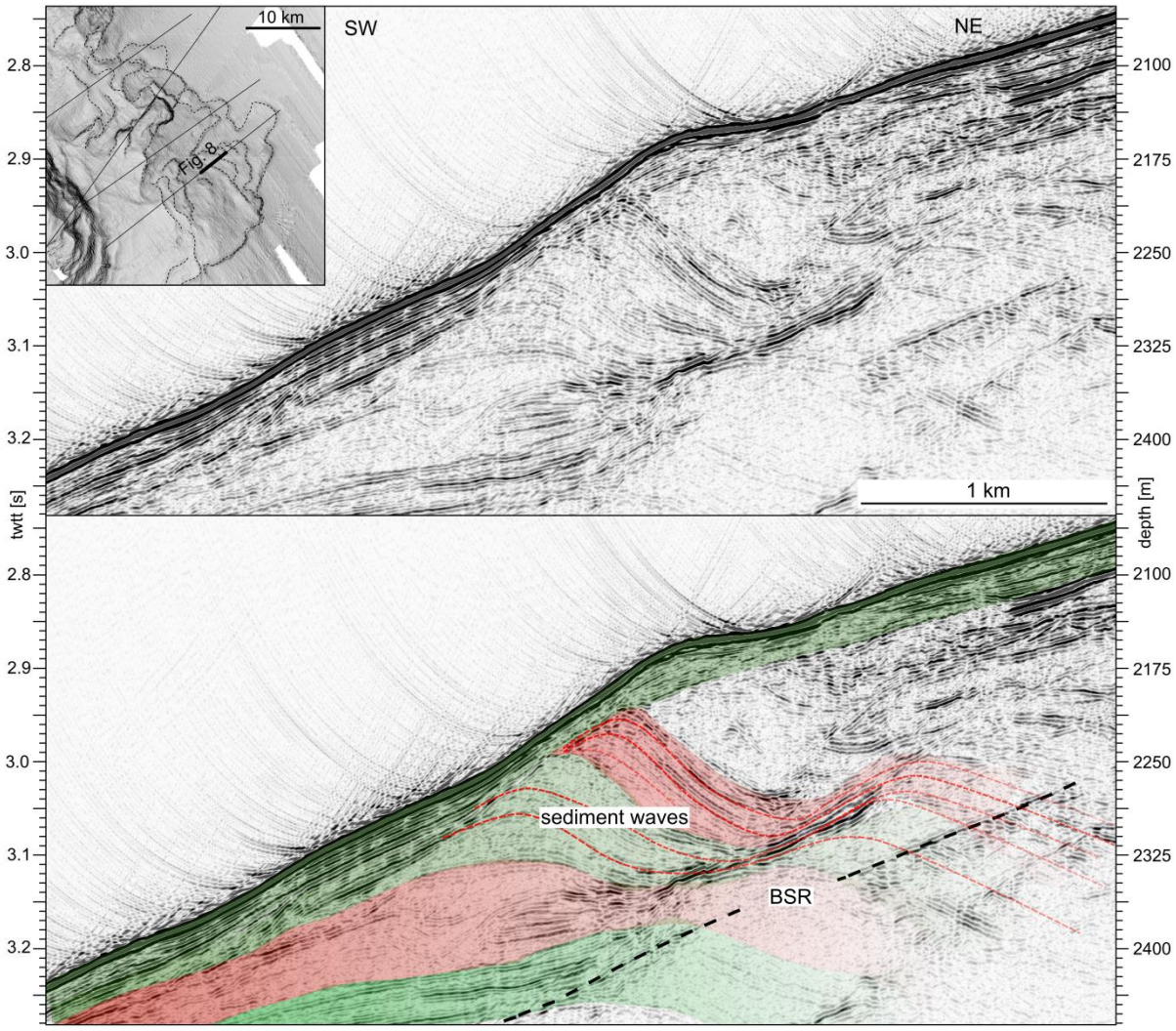

Fig. 3.8: An extract of the reflection seismic profile MSM31-P365 (top) in the southern part of the FSC and its interpretation (bottom) showing sediments waves and a patchy BSR. The colored groups of reflections indicate characteristic sediment units, not stratigraphic layers.

3.5.4 Characteristics of the Vestnesa area

Based on bathymetric data (Fig. 3.3A), the slope in the Vestnesa area (Fig. 3.3B) is divided into a region with a maximum gradient of 2.7° at the top of the slope, minor steep parts (2.7 to 11°) and a steep region with gradients of up to 20° at the bottom of the slope. The bathymetric map shows a few morphological steps (Fig. 3.3A) but the seismic data illustrate no evidence for buried or recent slope failures at a scale clearly resolved in seismic data. It reveals high-amplitude anomalies parallel to the seafloor that transect through sediment layers at ~250 ms twtt beneath the sea floor reflection (Fig. 3.9). This 'segmented' BSR (cf. Shedd et al., 2009)

marks the base of the gas hydrate stability zone and implies free gas underneath (Vanneste et al., 2005). This interpretation corresponds to several studies that showed active gas venting in the gas hydrate system in this region (e.g. Hustoft et al., 2009). The seismic data also show normal faulting (Fig. 3.9) with throws of up to 37 m (average 12 m). The lateral thickness of the sediments is mostly constant. Only on the very eastern profiles lateral thickness variations and wave-like patterns clearly indicate current controlled deposition (Fig. 3.9).

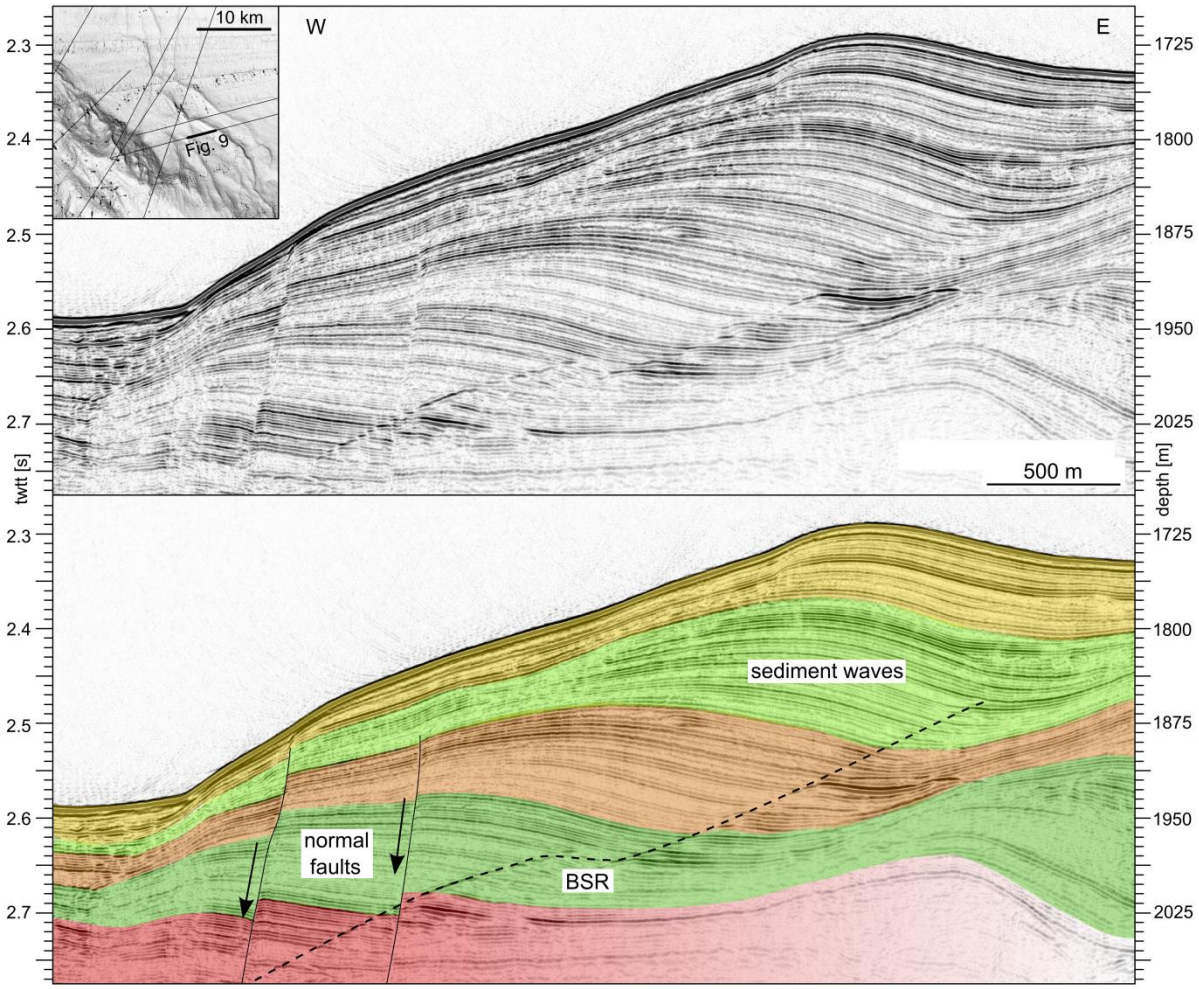

Fig. 3.9: An extract of the reflection seismic profile MSM21_4-P100 (top) in Vestnesa area and its interpretation (bottom) showing sediments waves, the BSR and normal faults. The colored groups of reflections indicate characteristic sediment units.

3.6 Discussion

3.6.1 Timing and evolution of the Fram Slide Complex

The entire FSC has been active from the late Miocene until the late Pleistocene (at least 60 ka BP) (Fig. 3.6 and Table 3.1). Slope failures in the FSC occurred since the formation of the present day configuration of the Fram Strait as an oceanic gateway (Engen et al., 2008). There is no obvious limitation or concentration of events to a certain period regarding the entire area of the FSC. Therefore, the FSC stands out from most other studied large-scale slope failures on the glaciated Northeast Atlantic margin which are primarily dated to the Holocene and Pleistocene (Hjelstuen et al., 2007). On the other hand, it resembles the pattern of slope failures known from the lower latitude glaciated margin off Nova Scotia (Campbell et al., 2004), in the Northwest Atlantic.

A detailed spatial analysis of slope failures (Fig. 3.6) shows that the northern part of the FSC is primarily shaped by one major slope failure that occurred more than 5 Ma ago (slope failure N0 in Table 3.1). It stands out from all other events because the headwall is overall ~600 m high and the calculated volume of failed material (~1160 km³) is about 60 times larger than of most of the other failures. Sediments that deposited before this slope failure are horizontally layered and there is no evidence in the seismic data that they are underlain by an older headwall (Fig. 3.4). These characteristics suggest that it is the initial slope failure in the northern part of the FSC. Younger and much smaller slope failures in that area seem to be related to over-steepening, as they are restricted to the vicinity of this old headwall (Figs. 2A and 4). The history of slope failures in the southern part of the FSC started in the late Miocene, approximately at the same time as in the northern part, but involving smaller volumes (2-3% of the volume that failed during N0) (Table 3.1). Since this time, the reflection seismic data document repeated slope failures until the late Pleistocene, with volumes of 2 to 62 km³ along the entire slope between 1290 and 2440 m water depth (Fig. 3.6). Thus, slope failure evolution in the northern part and the southern part of the FSC clearly differ in size, age and recurrence interval.

3.6.2 Regional controlling mechanisms

Most slope failures in the North Atlantic on the European margin are located directly at or down-current from trough mouth fans or ice stream outlets (Fig. 3.1A). This fact leads to the

conclusion that the main driving processes which decrease slope stability on the glaciated North Atlantic margin are related to glacial sediment deposition and seismicity due to rapid glacial unloading caused by the glacial cycles (Bryn et al., 2005; Kvalstad et al., 2005; Leynaud et al., 2009; Piper et al., 2012). Build-up of extensive overpressure reduces the effective stress and makes slopes prone to slope failure, especially if they contain particularly unstable clayey hemipelagic layers. A trigger, e.g. an earthquake, can activate a preconditioned system through a further increase of pore pressure or deformation of sediments and lead to liquefaction. The location of the FSC in a more distal setting relative to proximal plume deposits, ~35 km to the Sjubrebanken trough mouth fan and ~85 km down-current from of the Kongsfjorden cross-shelf trough (Fig. 3.1B), does not match such typical characteristics . Its location indicates that there are probably different processes that are critical for slope stability in distal settings. For example, on the glaciated Scotian margin distant from trough-mouth fans, Mosher et al. (2004) suggested processes such as salt tectonics, erosional over-steepening in canyons by turbidity currents, lateral spreading failure (creep), the influence on pore pressure of hydrocarbon gas or other deep-seated fluid seepage all preconditioned glacial plume deposits for failure. In order to identify regional processes that were important for the slope stability in the Fram Strait, we concentrate on the significantly different evolution of slope failure history in the northern and southern part of the FSC. We compare them with the Vestnesa area (Fig. 3.1), where previous studies (Sarkar et al., 2012; Plaza-Faverola et al., 2015) and our seismic interpretation show no evidence for slope failures in the seismically imaged section.

3.6.3 Tectonics

The history of slope failures in the FSC is restricted to the time when the region was tectonically active with the present day mode of seafloor spreading (Engen et al., 2008). Previous studies identified the seismicity and steep slopes linked the fault and ridge systems as destabilization factors that potentially represent an environment vulnerable to slope failure (Schwab et al., 1991, Gardner et al., 1999). The magnetic anomaly identified by Engen et al. (2008) suggests comparable spreading rates in the Fram Strait and Vestnesa area and indicates a similar history of seismicity. Recent seismicity along the transfer faults and the ridges is documented by the United States Geological Survey (1973-2015) and show no obvious difference regarding either recurrence frequency or amplitude (Fig. 3.1B). Based on available data we interpret all three locations to be equally influenced by large-scale tectonic activity

and earthquakes that may serve as a trigger mechanism for submarine landslides. The tectonic setting does not explain the local differences in slope stability and failure recurrence frequency.

3.6.4 Climate and Oceanography

At the beginning of the slope failure history of the FSC in the late Miocene, the climate and oceanographic setting of the region was predominantly linked to the opening of the Fram Strait. Equal spreading rates in the FSC and Vestnesa area (Engen et al., 2008) indicate that regional changes of climate and oceanographic conditions as well as the eustatic changes in sea level probably developed similarly along the entire area between the Lena Trough and the Knipovich Ridge. During the remaining development of the FSC, the cyclic changes due to glacial and interglacial conditions were the main influence on regional oceanographic characteristics. The resulting changes in deep water production, water temperature and current velocity (Henrich and Baumann, 1994; Henrich, 1998) likely had the same impact on the entire area. Isostatic sea level change due to the buildup of ice and the influence of post-glacial rebound might have had slightly different impact on the FSC and the Vestnesa area, as the latter is closer to the edge of the maximal ice extent during glacial periods of the last 100 ka (Fig. 3.1). These local effects do not appear to have been significant, as recent slope failures are absent in the Vestnesa area. They cannot explain the local differences in slope stability within the FSC.

3.6.5 Gas hydrates and fluid migration

The third regional process that could be considered to influence the slope stability in the three locations is the existence of gas hydrates and fluid migration. Seismic data show a BSR as an indicator for the presence of gas hydrates above free gas in the northern area only close to the ancient headwall (Fig. 3.4), but almost continuously in the southern part (Fig. 3.5).This spatial correlation could be biased by the limited data coverage (Fig. 3.2A). A BSR is also widespread in the Vestnesa area (Dumke et al., 2016) (Fig. 3.9).

Several studies have discussed the potential of gas hydrate dissociation due to changing temperate and pressure conditions to reduce slope stability (e.g. Sultan et al., 2004) but there is no clear evidence that this process is a main driver for slope failure. There have been periods of increased bottom water temperatures of up to 6°C in the past (MCO, ~17–15 Ma)

(Zachos et al., 2001) in the Fram Strait that would increase the depth of the gas hydrate stability zone. Water depth affected by this process, 550 m in the Arctic and as little as 380 m off Norway according to Kretschmer et al. (2015), is much shallower than all three locations studied, which have water depths greater than 1300 m (Figs. 2A and 3A). Warming would rather slowly elevate the base of the gas hydrate stability zone by conductive heat transport at these water depths. Pressure conditions might have changed due to sea level rise, for example during the Paleocene-Eocene Thermal maximum (Harding et al. (2011). However, Hunter et al. (2013) showed that even rapid sea level change (> 15 mm yr^{-1}) cannot significantly counteract the thermal effects on gas hydrate stability, particularly at great water depth (Mienert et al., 2005). We conclude that the water depths of the three locations exclude gas hydrate dissociation as a direct driver for slope failures.

A relationship of the major slope failure in the northern part of the FSC to gas hydrate-related processes is particularly unlikely, as the sidewall is higher than the expected gas hydrate stability zone. For the southern part of the FSC and the Vestnesa area we cannot exclude that the presence of gas hydrates could influence slope stability as a result of fluid migration. The volume of free gas underneath the BSR probably varied temporally and may have led to buoyancy-related overpressures that may have destabilized the slopes. Fluid migration structures that are revealed in the seismic data in the southern area (Elger et al., 2015) and the active gas venting in the Vestnesa area (Bünz et al., 2012) could be indications for preconditioning due to elevated overpressures (Karstens and Berndt, 2015). In combination with an earthquake this elevated pore pressure could drive failure on low-angle slopes (Stigall and Dugan, 2010).

3.6.6 Local controlling factors

We did not find any evidence that regional processes for the formation of potentially unstable sedimentary successions nor seismicity as trigger mechanisms can explain the different pattern of slope failures in the three regions. We conclude, therefore, that local processes are crucial factors for slope stability. In the following, we discuss (1) the slope gradient, (2) toe erosion induced by rotational slumps, and (3) the distribution and architecture of contourites as significant factors for the different pattern of slope failure in the Vestnesa area and the two parts of the FSC.

3.6.6.1 Slope gradient

The seafloor morphology in the three areas (Figs. 2A and 3A) is predominantly controlled by the tectonic setting of transfer faults and slow spreading ridges (Fig. 3.1B), which are expressed on the seafloor as ~1 km deep depressions. The headwalls and sidewalls in the entire FSC are located in the upper part of the slope where the gradient ranges between 3 and 8° (Fig. 3.2B). In the Vestnesa area the gradient of the upper slope is 2.7 to 11° (Fig. 3.3B). Hühnerbach et al. (2004) showed that most source areas of slope failures in the eastern North Atlantic have gradients of 2-6°. Neither the value nor distinct regional differences of the gradient of the upper slope explain the different failure pattern in the three regions.

The lower part of the slopes is similarly steep in all three areas and reaches maximum gradients of 22° (Figs. 2B and 3B). The distinct difference consists in the connection of the upper and lower slope. In the northern area of the FSC, they are separated by up to 25 km and connected by a gently dipping area (gradient < 2.7°) (Fig. 3.2B). In the southern part of the FSC, a corresponding narrower stretch (~10 km) of low gradient slope (gradient ≤ 6°) separates the upper part of the slope from the depression of the Molløy Ridge and Spitsbergen Transfer Fault (Fig. 3.2B). In the Vestnesa area, there is no break of slope and the seafloor dips almost continuously towards the Molløy Transfer Fault (Fig. 3.3B).

The slope gradient does not seem to be a discrete reason for slope failure in the considered areas, neither in the upper slope where the headwalls are located nor in the lower part at the toe of the slope. Within the FSC, repeated slope failure occurs only where the upper and lower parts of the slope are connected by a narrow mid gradient slope. Here, the entire slope reaches the critical gradient for proceeding retrogressive failure of at least 2° gradient as proposed by Hühnerbach et al. (2004). This observation indicates that over-steepening and toe erosion are potential processes that lead to retrogressive slope failure in the FSC. The overall equally dipping steep slope in the Vestnesa area in combination with absence of evidence for slope failures support this theory. Given that gradients at the top of the slope in all compared areas are nearly equal, we consider processes and structures at the toe of the slope to be the determining factor for the differences in slope stability.

3.6.6.2 Toe erosion

Seismic data in the southern part of the FSC reveal normal faults down to 250 m below sea floor at the top of the lower slope in ~3 km water depth (Fig. 3.7). Tectonically induced strike-slip faults would typically strike linear and parallel to the slope and the strike of the Spitsbergen Transfer Fault (Reches, 1987). Due to the curved, amphitheater-like expression of the faults in the bathymetric data, we hypothesize that they are predominantly gravity faults with listric detachment planes that were induced by the gravitational stress next to the depression of the Spitsbergen Transfer Fault and Molløy Ridge (Figs. 2A and 7). This interpretation implies rotational block movements along the gravity faults, which potentially causes toe erosion and could have destabilized the slope from the bottom upwards and led to retrogressive slope failures in the upper part of the slope. This failure dynamics corresponds to the results of Elger et al. (2015) and could be the reason for repeated slope failure in the southern FSC documented by multiple normal faults (average offset of 41 m) and headwalls of different age (Fig. 3.5). However, seismic profiles do not cover the top of the lower slope in the northern part (Fig. 3.2A). Based on limited bathymetric data and the similar setting, we expect that normal faults formed there as well. The distance between the upper and lower slope of ~25 km on a gradient of < 3° would have prevented this process from affecting slope stability in the northern part of the FSC.

The equally dipping slope in the Vestnesa area is also characterized by a steep lower slope (Fig. 3.3B). At its top, seismic data reveal normal faults (Fig. 3.9) with average offsets of only 12 m which form linear rather than amphitheater-like expressions on the sea floor (Fig. 3.3A). Due to this characteristic, we consider that they are predominantly tectonically induced faults. However, no slope failures have been reported in the Vestnesa area. This phenomenon might be related to the small offset of the faults that is about 3 times less on average than in the southern part of the FSC.

3.6.6.3 Contouritic sedimentation

2D high-resolution seismic data show typical hemipelagic sedimentation patterns without major thickness variations in the northern part of the FSC (Fig. 3.4). Sediments deposited before the major slope failure more than 5 Ma ago are nearly horizontal with constant thickness. The southern part is characterized by sediment waves and varying thicknesses of sediment layers downslope (Fig. 3.8). This pattern indicates that contour currents, enhanced

sedimentation and erosion influenced sedimentation only in the southern part of the FSC and varied over time. This interpretation agrees with studies that explain varying sedimentation rates in the Fram Strait with enhanced erosion and fluvial input along the pathway of the West Spitsbergen Current caused by changing currents during different climate conditions (e.g. Gebhardt et al., 2014). The impact of this process might weaken northward as sedimentation rates should decrease down-current and with greater distance from trough mouth fans on the Svalbard margin. This argument is supported by sedimentation rates during the mid to late Weichselian of up to 105 cm per 1000 ^{14}C years in the Vestnesa area and only 10-44 cm per 1000 ^{14}C years on the Yermak Plateau (Howe et al., 2008). Results from ODP core 912, which most resembles the FSC, do not give very detailed information about sedimentation rates (~30 cm/1000 years in the last 1 Ma) but support the hypothesis of less sediment deposition in the FSC.

Spatially and temporally variable contourite sedimentation (Fig. 3.8) causes an uneven shape of the slope in the southern part of the FSC. The resulting vulnerably to over-steepening can be a preconditioning factor for slope failure. The geotechnical characteristics of contourites also lower the factor of safety. Silty sediments have low shear strength and are prone to liquefaction, especially if they over-steepen or are exposed to overburden stress. In combination with toe erosion by rotational slumps these processes may have triggered slope failures. We conclude that contourites are in general a preconditioning factor for slope failures, especially in areas with cyclic varying sedimentation rates.

Despite its similar tectonic setting, sediments in the area between Vestnesa and the termination of the Knipovich Ridge did not fail. High contouritic sedimentation rates led to the formation of thick drift bodies (Fig. 3.10), e.g. the Vestnesa Ridge drift. Previous studies linked high sedimentation rates to the generation of overpressure and over-steepening of the margin, which led to the conclusion that the area is inherently unstable (Berndt et al., 2009). Comparison with the FSC suggests that the rather even margin of the Vestnesa slope in combination with the 20-30% smaller throw of the faults in the Vestnesa area is not as vulnerable to slope failure. In contrast to sediment gravity flows on continental margins, which seek the deepest path and may produce erosion, contourites in general will deposit an irregular blanket of sediment that can smooth out steep slopes resulting from faulting (Fig. 3.3B). In Vestnesa, the rate of smoothing of the tectonically-controlled topography by contourites is greater than in the FSC, where faults appear to be more active and favour greater toe erosion.

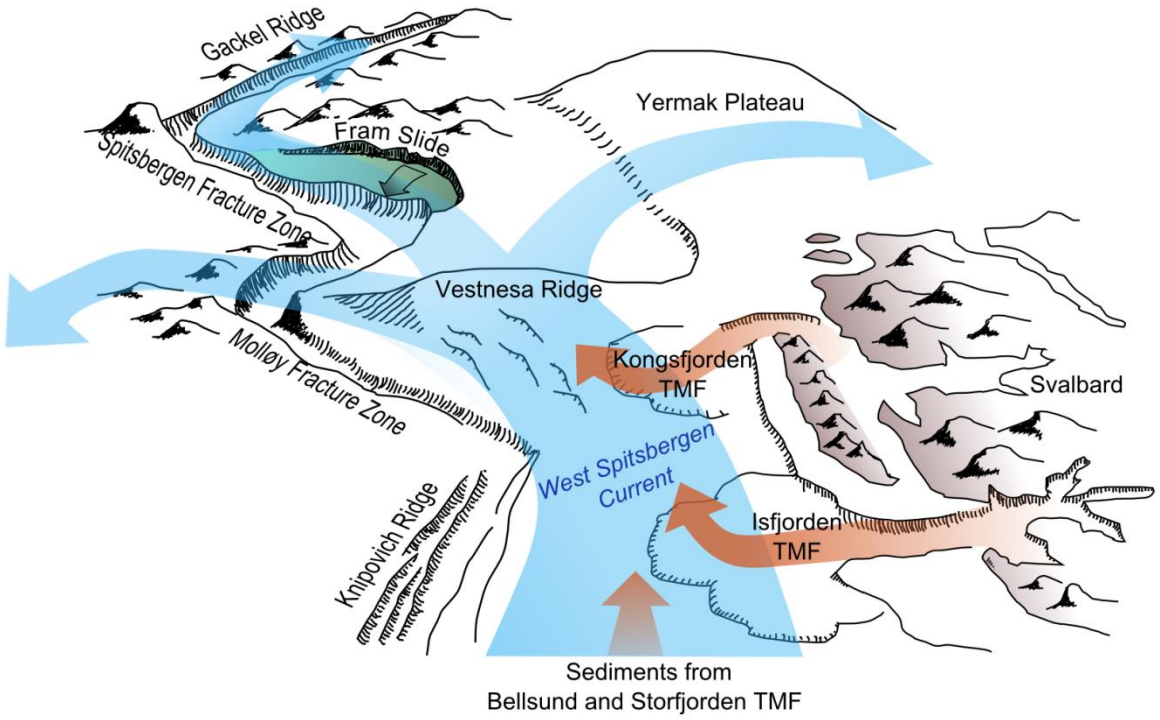

Fig. 3.10: Schematic diagram of the Fram Strait region showing the main current patterns and sediment sources with respect to the tectonic elements. The West Spitsbergen Current (blue arrow) transports the sediment (orange arrows) from the main ice streams northwards. Sedimentation rates are highest at Vestnesa Ridge where the West Spitsbergen Current splits into different branches. While all other factors (climate, sea level change, seismicity, sedimentary fluid migration systems, and sediment type) are similar we infer that it is the smoothing of topography in this high sedimentation environment that prevents toe erosion and undercutting of steep slopes that might lead to slope failures on Vestnesa Ridge. Farther north in the region of the Fram Slide steep morphology due to tectonic forces and previous slope failures is preserved much longer and makes it susceptible to further mass wasting.

In the future, integrated and multi-disciplinary investigation of geophysical and geotechnical data, in situ and from laboratory, should be considered to further analyze the difference between the two slides (cf. Vanneste et al, 2014). 3D-information about the subsurface geometry in Vestnesa and FSC in combination with in situ information about shear strength could be used for slope stability calculation. A model could reveal the reason for the different slope failure histories and test all discussed destabilization processes and scenarios. This approach could reveal soil softening behavior and give insights about the suggested retrogressive failure dynamic. The relationship between hydrate saturation and pore pressure could be measured in situ to reveal possible differences and to model the resulting pore pressure. These models might be able to provide the factor of safety of the Vestnesa area and verify the probability of a future slope failure.

3.6.7 Potential hazards of the FSC in relation to other slope failures on the eastern glaciated North Atlantic continental margin

The volume of sediment that failed during past slope failures ranges from ~2 to 1200 km³ (Table 3.1); but most of the failure deposits have a volume of less than 70 km³. The headwalls are in 1020 to 2700 m water depth (Fig. 3.2A) and there is an upslope migration of the headwalls over time in the southern part of the FSC. Compared to characteristics of other large-scale slope failures on the eastern glaciated margin of the North Atlantic the history of the FSC is much older (cf. Hjelstuen et al., 2007). The volume of most individual events in the FSC is relatively small (< 70 km^3) except for the event in the late Miocene in the northern part of the FSC (N0 in Table 3.1). Its volume of ~1200 km^3 is comparable to the Tampen, Trænadjupet, Møre and Bjørnøya slides. Berndt et al. (2009) based on numerical models showed that slope failures with volumes of >1000 km³ have to be considered for hazard assessment in the Fram Strait, as they may cause maximum wave heights of up to 6 m along the shores of the North Atlantic if they originate in ~800 m water depth or less.

There is the potential for future slope failures within the FSC, but the hazard for tsunamis posed by these slope failures is small considering the relatively small-volume and great water depth of slope failures that occurred in the past. In addition, the recurrence time of slope failures seems to be very long. The general trend that recent slides have occurred higher up on the slope indicates that the past headwall depth as the limiting factor for the tsunami hazard might not apply to future events. The similarity of geological factors controlling slope stability in the FSC and further south in the area between Vestnesa and Knipovich Ridge might suggest an increased probability of future slope failure there.

On the other hand, this study indicates an unexpected impact of contourite sedimentation rates on slope stability. Areas with high sedimentation rates were usually associated with high potential for slope failure since many past slope failures are located at the end or down-current of trough mouth fans. The high sedimentation rates cause overpressures and make the slope prone to failure. Comparisons made in this study suggest however, that high sedimentation rates of contourites can smooth seabed topography and might reduce the chance of slope failures.

3.7 Conclusions

The FSC covers an area of ~5500 km² in 850 to 4200 m water depth. Repeated slope failures occurred in the entire FSC since earlier than 5 Ma and evacuated sediments of up to 1160 km³ volume during individual events. The recurrence frequency and volume of the landslides are different in the northern part from the southern part. In the north, one major landslide occurred in the late Miocene. The southern part experienced more frequent, but smaller, slope failures between the late Miocene and late Pleistocene. Analysis of new geophysical data and their comparison with previously published research do not provide any evidence that differences in seismicity as trigger mechanism play an important role nor do regional processes linked to tectonics, climate and oceanography explain the locally different failure patterns. We conclude that local processes are the crucial factors for slope stability in this region.

We cannot identify a distinct reason for the late Miocene major slope failure of ~1160 km³ in the northern part of the survey area. Repeated slope failures in the southern part were most likely due to a combination of toe erosion and slope shape. The distance between upper and lower slope that is characterized by lower gradient, rather than the precise magnitude of the gradient, influenced retrogressive failures. We suggest that rotational block movement along gravity-driven faults must have destabilized the slope from the bottom and may have led to retrogressive slope failure. Over-steepening and uneven sediment loading along the slope due to patchy sedimentation favored this process. This slope geometry and the smaller throw of the faults at the toe seem to be the main differences when comparing the FSC to the intersection of the Molløy Transfer Fault with the Knipovich Ridge. In the latter area, high contouritic sedimentation rates led to the formation of thick drift bodies, e.g. the Vestnesa Ridge drift, and smoothed the tectonically controlled margin shape. We rule out dissociation of gas hydrate due to changes in temperature and pressure conditions as the determining factor for slope destabilization because the area was always within the hydrate stability zone. However, overpressure caused by free gas underneath the BSR may have influenced slope stability in the southern part of the FSC. We suggest a future multidisciplinary investigation that combines geophysical and various geotechnical information in a joined model to test the discussed processes.

Due to the relatively small volumes of the recent slides (up to 62 km³) in the southern part of the FSC and the relatively great water depth, the tsunami potential of the FSC seems to be

small. Only if future slope failures in the region cut further back onto the Yermak Plateau or mobilize much larger portions of the slope, could the system generate sizeable tsunamis.

3.8 Supplementary material

Table 3.S1: Location of the seismic profiles from cruise MSM31 that were used for the study.

Profile	**Start**		**End**	
	Latitude	Longitude	Latitude	Longitude
MSM31-P365	79°35.647'N	4°28.021'E	79°47.037'N	5°38.362'E
MSM31-P370	79°49.277'N	5°29.111'E	79°38.635'N	4°16.319'E
MSM31-P375	79°43.995'N	3°51.670'E	79°53.857'N	4°57.913'E
MSM31-P380	80°00.335'N	4°34.748'E	79°51.232'N	3°17.292'E
MSM31-P385	79°52.334'N	3°00.433'E	80°15.897'N	2°58.482'E

Acknowledgements

We thank the captain of R.V. Maria S. Merian and his crew for their excellent support at sea. Ship time for cruise MSM31 was provided by the DFG Senatskomission für Ozeanographie. J.E. was financed by the Helmholtz graduate school HOSST. Cruise related data are available on PANGEA.

References

Berndt, C., Brune, S., Nisbet, E., Zschau, J., Sobolev, S.V., 2009. Tsunami modeling of a submarine landslide in the Fram Strait. Geochemistry, Geophysics, Geosystems 10. Q04009, doi:10.1029/2008GC002292

Berndt, C., Bünz, S., Clayton, T., Mienert, J., Saunders, M., 2004. Seismic character of bottom simulating reflectors: examples from the mid-Norwegian margin. Marine and Petroleum Geology 21, 723-733.

Beszczynska-Möller, A., Fahrbach, E., Schauer, U., Hansen, E., 2012. Variability in Atlantic water temperature and transport at the entrance to the Arctic Ocean, 1997–2010. ICES Journal of Marine Science 69, 852-863.

Bourke, R.H., Weigel, A.M., Paquette, R.G., 1988. The westward turning branch of the West Spitsbergen Current. Journal of Geophysical Research 93, 14065-14077.

Bryn, P., Berg, K., Forsberg, C.F., Solheim, A., Kvalstad, T.J., 2005. Explaining the Storegga Slide. Marine and Petroleum Geology 22, 11-19.

Bünz, S., Polyanov, S., Vadakkepuliyambatta, S., Consolaro, C., Mienert, J., 2012. Active gas venting through hydrate-bearing sediments on the Vestnesa Ridge, offshore W-Svalbard. Marine Geology 332-334, 189-197.

Dumke, I., Burwicz, E.B., Berndt, C., Klaeschen, D., Feseker, T., Geissler, W.H., Sarkar, S., 2016. Gas hydrate distribution and hydrocarbon maturation north of the Knipovich Ridge, western Svalbard margin. Journal of Geophysical Research 121, doi: 10.1002/2015JB012083.

Elger, J., Berndt, C., Krastel, S., Piper, D.J.W., Gross, F., Spielhagen, R.F., Meyer, S., 2015. The Fram Slide off Svalbard: a submarine landslide on a low-sedimentation-rate glacial continental margin. Journal of the Geological Society 172, 153-156.

Engen, Ø., Eldholm, O., Bungum, H., 2003. The Arctic plate boundary. Journal of Geophysical Research 108, 2075, doi:10.1029/2002JB001809, B2.

Engen, Ø., Faleide, J.I., Dyreng, T.K., 2008. Opening of the Fram Strait gateway: A review of plate tectonic constraints. Tectonophysics 450, 51-69.

Gardner, J.V., Prior, D.B., Field, M.E., 1999. Humboldt Slide – a large shear-dominated retrogressive slope failure. Marine Geology 154, 323-338.

Gebhardt, A.C., Geissler, W.H., Matthiessen, J., Jokat, W., 2014. Changes in current patterns in the Fram Strait at the Pliocene/Pleistocene boundary. Quaternary Science Reviews 92, 179-189.

Haflidason, H., de Alvaro, M.M., Nygard, A., Sejrup, H.P., Laberg, J.S., 2007. Holocene sedimentary processes in the Andøya Canyon system, north Norway. Marine Geology 246, 86-104.

Haflidason, H., Sejrup, H.P., Nygård, A., Mienert, J., Bryn, P., Lien, R., Forsberg, C.F., Berg, K., Masson, D., 2004. The Storegga Slide: architecture, geometry and slide development. Marine Geology 213, 201-234.

Harding, I.C., Charles, A.J., Marshall, J.E.A., Pälike, H., Roberts, A.P., Wilson, P.A., Jarvis, E., Thorne, R., Morris, E., Moremon, R., Pearce, R.B., Akbari, S., 2011. Sea-level and salinity fluctuations during the Paleocene–Eocene thermal maximum in Arctic Spitsbergen. Earth and Planetary Science Letters 303, 97-107.

Henrich, R., 1998. Dynamics of Atlantic water advection to the Norwegian-Greenland Sea—a time-slice record of carbonate distribution in the last 300 ky. Marine Geology 145, 95-131.

Henrich, R., Baumann, K.-H., 1994. Evolution of the Norwegian Current and the Scandinavian Ice Sheets during the past 2.6 my: evidence from ODP Leg 104 biogenic carbonate and terrigenous records. Palaeogeography, Palaeoclimatology, Palaeoecology 108, 75-94.

Hjelstuen, B.O., Eldholm, O., Faleide, J.I., 2007. Recurrent Pleistocene mega-failures on the SW Barents Sea margin. Earth and Planetary Science Letters 258, 605-618.

Howe, J.A., Shimmield, T.M., Harland, R., 2008. Late quaternary contourites and glaciomarine sedimentation in the Fram Strait. Sedimentology 55, 179-200.

Hühnerbach, V., Masson, D.G., partners of the COSTA-Project, 2004. Landslides in the North Atlantic and its adjacent seas: an analysis of their morphology, setting and behavior. Marine Geology 213, 343-362.

Hunter, J.R., Church, J.A., White, N.J., Zhang, X., 2013. Towards a global regionally varying allowance for sea-level rise. Ocean Engineering 71, 17-27.

Hustoft, S., Bünz, S., Mienert, J., Chand, S., 2009. Gas hydrate reservoir and active methane-venting province in sediments on < 20 Ma young oceanic crust in the Fram Strait, offshore NW-Svalbard. Earth and Planetary Science Letters 284, 12-24.

Ingólfsson, Ó., Landvik, J.Y., 2013. The Svalbard–Barents Sea ice-sheet–Historical, current and future perspectives. Quaternary Science Reviews 64, 33-60.

Kretschmer, K., Biastoch, A., Rüpke, L., Burwicz, E., 2015. Modeling the fate of methane hydrates under global warming. Global Biogeochemical Cycles 29, 610-625.

Karstens, J., Berndt, C., 2015. Seismic chimneys in the Southern Viking Graben – Implications for palaeo fluid migration and overpressure evolution. Earth and Planetary Science Letters 412, 88-100.

Kvalstad, T.J., Andresen, L., Forsberg, C.F., Berg, K., Bryn, P., Wangen, M., 2005. The Storegga slide: evaluation of triggering sources and slide mechanics. Marine and Petroleum Geology 22, 245-256.

Laberg, J.S., Vorren, T.O., 2000. The Trænadjupet Slide, offshore Norway—morphology, evacuation and triggering mechanisms. Marine Geology 171, 95-114.

Leynaud, D., Mienert, J., Vanneste, M., 2009. Submarine mass movements on glaciated and non-glaciated European continental margins: a review of triggering mechanisms and preconditions to failure. Marine and Petroleum Geology 26, 618-632.

Lindberg, B., Laberg, J.S., Vorren, T.O., 2004. The Nyk Slide—morphology, progression, and age of a partly buried submarine slide offshore northern Norway. Marine Geology 213, 277-289.

Løseth, H., Gading, M., Wensaas, L., 2009. Hydrocarbon leakage interpreted on seismic data. Marine and Petroleum Geology 26, 1304 - 1319.

Manley, T.O., 1995. Branching of Atlantic Water within the Greenland-Spitsbergen Passage: An estimate of recirculation. Journal of Geophysical Research 100, 20627-20634.

Mattingsdal, R., Knies, J., Andreassen, K., Fabian, K., Husum, K., Grøsfjeld, K., de Schepper, S., 2014. A new 6 Myr stratigraphic framework for the Atlantic-Arctic Gateway. Quaternary Science Reviews 92, 170-178.

Mienert, J., Vanneste, M., Bünz, S., Andreassen, K., Haflidason, H., Sejrup, H.P., 2005. Ocean warming and gas hydrate stability on the mid-Norwegian margin at the Storegga Slide. Marine and Petroleum Geology 22, 233-244.

Mosher, D.C., Piper, D.J.W., Campbell, D.C., Jenner, K.A., 2004. Near-surface geology and sediment-failure geohazards of the central Scotian Slope. The American Association of Petroleum Geologists Bulletin 88, 703-723.

Petersen, C.J., Bünz, S., Hustoft, S., Mienert, J., Klaeschen, D., 2010. High-resolution P-Cable 3D seismic imaging of gas chimney structures in gas hydrated sediments of an Arctic sediment drift. Marine and Petroleum Geology 27, 1981-1994.

Piper, D.J.W., Deptuck, M.E., Mosher, D.C., Clarke, J.E.H., Migeon, S., 2012. Erosional and depositional features of glacial meltwater discharges on the eastern Canadian continental margin, in: Prather, B. (Eds.), Deptuck, D., Mohrig, D., van Hoorn, B., Wynn, R., Application of the Principles of Seismic Geomorphology to Continental Slope and Base-of-slope Systems: Case Studies from Seafloor and Near-Seafloor Analogues. SEPM Special Publication, 99, 61-80.

Plaza-Faverola, A., Bünz, S., Johnson, J.E., Chand, S., Knies, J., Mienert, J., Franek, P., 2015. Role of tectonic stress in seepage evolution along the gas hydrate-charged Vestnesa Ridge, Fram Strait. Geophysical Research Letters 42, 733-742.

Quadfasel, D., Gascard, J.-C., Koltermann, K.-P., 1987. Large-scale oceanography in Fram Strait during the 1984 Marginal Ice Zone Experiment. Journal of Geophysical Research 92, 6719-6728.

Reches, Z., 1987. Mechanical aspects of pull-apart basins and push-up swells with applications to the Dead Sea transform. Tectonophysics, 141, 75-88.

Rudels, B., Fahrbach, E., Meincke, J., Budéus, G., Eriksson, P., 2002. The East Greenland Current and its contribution to the Denmark Strait overflow. ICES Journal of Marine Science 59, 1133-1154.

Sarkar, S., Berndt, C., Minshull, T.A., Westbrook, G.K., Klaeschen, D., Masson, D.G., Chabert, A., Thatcher, K.E., 2012. Seismic evidence for shallow gas-escape features associated with a retreating gas hydrate zone offshore west Svalbard. Journal of Geophysical Research 117, B09102. doi:10.1029/2011JB009126.

Schauer, U., Fahrbach, E., Osterhus, S., Rohardt, G., 2004. Arctic warming through the Fram Strait: Oceanic heat transport from 3 years of measurements. Journal of Geophysical Research 109, C06026. doi:10.1029/2003JC001823.

Schwab, W.C., Danforth, W.W., Scanlon, K.M., Masson, D.G., 1991. A giant submarine slope failure on the northern insular slope of Puerto Rico. Marine Geology 96, 237-246.

Shedd, W., Godfriaux, P., Frye, M., Bowell, R., Hutchinsons, D., 2009. Occurrence and variety in seismic expression of the base of gas hydrate stability in the Gulf of Mexico, USA. DOE-NETL Fire in the Ice Newsletter, Winter 2009, 11-14.

Stigall, J., Dugan, B., 2010. Overpressure and earthquake initiated slope failures in the Ursa region, northern Gulf of Mexico. Journal of Geophysical Research 115, B04101. Doi:10.1029/2009JB006848.

Stocker, T.F., Qin, D., Plattner, G.-K., Tignor, M.M.B., Allen, S.K., Boschung, J., Nauels, A., Xia, Y., Bex, V., Midgley, P.M., 2013. The Physical Science Basis Working Group I Contribution to the Fifth Assessment Report of the Intergovernmental Panel on Climate Change. Cambridge University Press: Cambridge, UK and New York, NY.

Sultan, N., Cochonat, P., Foucher, J.-P., Mienert, J., 2004. Effect of gas hydrates melting on seafloor slope instability. Marine Geology 213, 379-401.

Talwani, M., Eldholm, O., 1977. Evolution of the Norwegian-Greenland Sea. Geological Society of America Bulletin 88, 969-999.

Thiede, J., Myhre, A.M., Firth, J.V. & Shipboard Scientific Party, 1995. Cenozoic Northern Hemisphere Polar and Subpolar Ocean Paleoenvironments (Summary of ODP Leg 151 Drilling Results), in: Myhre, A.M., Thiede, J., Firth, J.V., et al. (Eds.) Proceedings of the Ocean Drilling Program, Initial Reports, US College Station, Texas, 151, pp. 397–420.

Vanneste, M., Guidard, S., Mienert, J., 2005. Bottom-simulating reflections and geothermal gradients across the western Svalbard margin. Terra Nova 17, 510-516.

Vanneste, M., Mienert, J., Bünz, S., 2006. The Hinlopen Slide: A giant, submarine slope failure on the northern Svalbard margin, Arctic Ocean. Earth and Planetary Science Letters 245, 373 - 388.

Vanneste, M., Sultan, N., Garziglia, S., Forsberg, C.F., L'Heureux, J.-S., 2014. Seafloor instabilities and sediment deformation processes: The need for integrated, multi-disciplinary investigations. Marine Geology 352, 183-214.

Winkelmann, D., Stein, R., 2007. Triggering of the Hinlopen/Yermak Megaslide in relation to paleoceanography and climate history of the continental margin north of Spitsbergen. Geochemistry, Geophysics, Geosystems 8, Q06018. doi:10.1029/2006GC001485.

Winkler, A., Wolf-Welling, T., Stattegger, K., Thiede, J., 2002. Clay mineral sedimentation in high northern latitude deep-sea basins since the Middle Miocene (ODP Leg 151, NAAG). International Journal of Earth Sciences 91, 133-148.

Wolf, T.C.W., Thiede, J., 1991. History of terrigenous sedimentation during the past 10 My in the North Atlantic (ODP Legs 104 and 105 and DSDP Leg 81). Marine Geology 101, 83-102.

Zachos, J., Pagani, M., Sloan, L., Thomas, E., Billups, K., 2001. Trends, Rhythms, and Aberrations in Global Climate 65 Ma to Present. Science 292, 686-693.

Chapter 4

Pipe structure formation as a trigger for submarine slope failures

Judith Elger[1], Christian Berndt[2], Lars Rüpke[3], Sebastian Krastel[4], Felix Gross[5], Wolfram H. Geissler[6]

[1] GEOMAR Helmholtz Centre for Ocean Research Kiel, Germany, jelger@geomar.de

[2] GEOMAR Helmholtz Centre for Ocean Research Kiel, Germany, cberndt@geomar.de

[3] GEOMAR Helmholtz Centre for Ocean Research Kiel, Germany, lruepke@geomar.de

[4] Institut für Geowissenschaften, Christian-Albrechts-Universität zu Kiel, Germany, skrastel@geophysik.uni-kiel.de

[5] Institut für Geowissenschaften, Christian-Albrechts-Universität zu Kiel, Germany, fgross@geophysik.uni-kiel.de

6 Alfred-Wegener-Institut Helmholtz-Zentrum für Polar- und Meeresforschung, Bremerhaven, Germany, Wolfram.Geissler@awi.de

This manuscript that is submitted to the Journal *Geology*.

4.1 Abstract

Submarine slope failures are a hazard to coastal and seafloor environment. Many slides overlap spatially with the occurrence of gas hydrates. Previous studies concentrated on the impact of gas hydrate dissociation on slope stability without finding conclusive proof for an interrelation. Here, we argue that overpressure below the gas hydrate stability zone may initiate retrogressive submarine slope failure by creating hydrofractures that transfer overpressure to weak layers in the shallow subsurface. This process is a more likely trigger for slope failures in gas hydrate provinces than gas hydrate dissociation as it does not require any changes in the gas hydrate stability conditions. It is able to explain hydrate-related slope failure initiation at all water depths where hydrates sufficiently reduce the sediment permeability for free gas to accumulate below.

4.2 Introduction

Spatial correlation between numerous submarine landslides and the occurrence of gas hydrates suggests a causal relationship. The leading paradigm for more than a decade stated that the dissociation of gas hydrates destabilizes the slope because it removes the cementation by hydrate and reduces the shear strength while at the same time it increases overpressure due to gas expansion (Bugge et al., 1988; Kvenvolden, 1999; Sultan et al., 2004). Although there is circumstantial evidence that hydrates may have an effect on slope stability (Booth et al., 1994; Micallef et al., 2009), it was not possible to find unequivocal proof that any of the large submarine landslides were triggered by gas hydrate dissociation (Paull et al., 2007). The fact that many submarine landslides are retrogressive and originated at the middle or lower continental slope (Kvalstad et al., 2005; Vanneste et al., 2006; Sawyer et al., 2009) contradicts the hypothesis that hydrate dissolution triggers slope failure. Pressure and temperature variations cause hydrate dissociation typically on the upper slope (Kretschmer et al., 2015), in much greater water depth than the pinch out of the gas hydrate stability zone (GHSZ). Hence, gas hydrate dissociation is unlikely the trigger of retrogressive slope failure.

In this paper we investigate the feasibility of a new process that links gas hydrate systems and submarine mass wasting. The process combines various verified mechanisms that are put in a new context. Gas hydrates reduce the permeability of sediments (Berndt and Goswami, 2007; Konno et al., 2015) resulting in the accumulation of free gas and the buildup of overpressure

below the GHSZ (Flemings et al., 2003; Hornbach et al., 2004). Elevated pore pressure may cause hydrofractures in the sediments which in turn lead to pipe formation and transfer of overpressure to shallower coarse-grained sediments (Bünz et al., 2003) to trigger slope failure. This novel mechanism of submarine slope failure initiation does not require any changes in the gas hydrate stability conditions and is applicable at all water depth.

The objective of this paper is to constrain the environmental conditions under which this process is viable and to specify the required parameters for future tests of this hypothesis. We use seismic and hydroacoustic data from offshore N Svalbard showing a pipe structure reaching from the base of the GHSZ up to the base of a mass transport deposit in combination with theoretical, and numerical models of hydrofracture and overpressure generation to evaluate (1) the required gas column height underneath the bottom simulating reflection (BSR) to initiate hydrofracturing and pipe structure formation, (2) if it is feasible that a pipe may stop within the subsurface once it has started to propagate upwards, and (3) if overpressure may start to build up laterally within the subsurface to trigger a retrogressive submarine landslide.

4.3 Methods

The study bases on Kongsberg EM122 multibeam bathymetric data that cover the NE slope of the Hinlopen-Yermak Slide and a time-migrated ~22.6 km-long 2D high-resolution seismic profile (20130390) using a digital 80-channel Geometrics GeoEel streamer and a 1.7l GI air gun (Fig. 4.1) (Geissler et al., submitted). The calculation of critical pore pressure is based on the Mohr-Coulomb criterion for shear failure (Paterson and Wong, 2005) and the theoretical criterion for tensile failure of a fluid filled crack from Griffith's theory (Murrell, 1964). The methodology of inferring the failure mode induced by a localized fluid overpressure source under different initial stress states is taken from Rozhko et al. (2007). These equations lead to a definition of the critical pore-fluid overpressure for shear and tensile failure in different compressional and extensional regimes. More details are provided in the supplemental material.

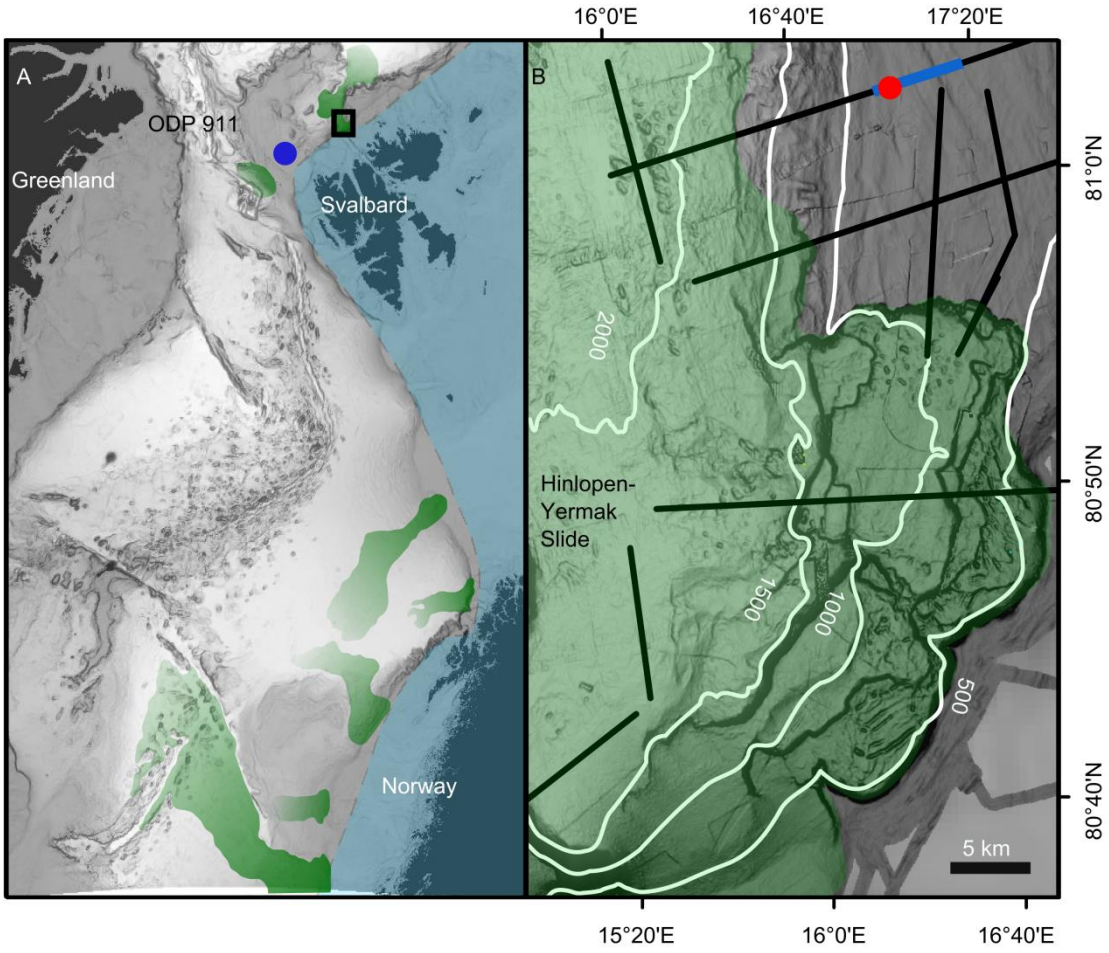

Figure 4.1. Location of the study area on the continental margin off Svalbard. (A) Overview map with with the maximum ice extent since 100 ka (blue area) (after Ingólfsson and Landvik, 2013), location of ODP Site 911 (blue dot) and the areas affected by the Storegga, Sklinnadjupet, Trænadjupet, Andøya, Bjørnøyrenna, Fram and Hinlopen-Yermak slides (green areas from south to north) (after Vanneste et al., 2006; Haflidason et al., 2007). (B) Local bathymetry with contour lines (white lines in meters), available 2D seismic profiles, location of the pipe structure (red dot) next to the Hinlopen-Yermak Slide (green area) and the location of the seismic profile shown in Fig. 4.2 (blue bold line).

4.4 Results

2D seismic data show parallel reflections that are upward-bended and interrupted by a vertical zone of amplitude blanking. This structure leads from an area of enhanced reflectivity to a body without visible internal structure (Fig. 4.2). We interpret it as a pipe structure of ~20 m diameter from the BSR up to the base of a mass transport deposit at ~40 mbsf (Fig. 4.2) in ~800 m water depth. The BSR marks the base of the gas hydrate stability zone and mimics the seafloor ~190 mbsf (assuming an interval velocity of 1500 m/s). The high-amplitude anomalies indicate a gas lens underneath the BSR of ~40 m height that might cause a pore overpressure of ~422 kPa (assuming interconnected gas pockets and a density contrast of ~1024 kg/m³ between water and gas). Considering a bulk density in the range of 1690-2140 kg/m³ (Shipboard Scientific Party, 1995) this pressure corresponds to 58-74 % of the overburden stress (Table 4.S1). The wavy reflections around the pipe structure (Fig. 4.2) indicate well stratified sediment waves of clay and silt grain sizes (Hernandez-Molina et al., 2009)

In order to test the feasibility of the new trigger process, we calculate the critical pore overpressure that initiates hydrofracturing or shear failure for a wide value range of Poisson ratios, cohesions, and bulk densities at the bottom and top of the pipe structure (Table 4.1 and Fig. 4.3). Figure 3 visualizes the strong dependence of the failure mode on cohesion and initial stress state. Unfortunately, cohesion of marine sediments is a poorly constrained parameter with estimates ranging between 0 and 2 MPa (e,g. Cook and Goldberg, 2005; Masui et al., 2005; Ghiassian and Grozic, 2013; Ikari and Kopf, 2015). We consider a value of 260 kPa to be reasonable for the base of the GHSZ as the presence of gas hydrates (Ghiassian and Grozic, 2013), over-consolidation (Ikari and Kopf, 2015), and an enhanced clay fraction (Ikari and Kopf, 2011; 2015) increase the stiffness and the shear strength of sediments. We assume that s_1 is vertical and that no significant tectonic forces are present. Only compaction without lateral strains occurs. The relationship $\sigma_{II} = \sigma_{III} = \frac{v}{(1-v)}\sigma_I$ results in a ratio of horizontal to vertical stress of ~0.4 for a Poisson ratio $v = 0.3$. In this case, our calculations indicate a critical pore overpressure at ~190 mbsf (Fig. 4.3) of ~800 kPa (701-1467 kPa for a range of Poisson ratios and bulk densities) to initiate tensile failure (Table 4.1). At the top of the pipe structure (~40 mbsf) we assume a negligible cohesion of normally consolidated marine sediments in the absence of gas hydrates (Ghiassian and Grozic, 2013) and calculate a critical pore overpressure for shear failure of 13-137 kPa for a range of Poisson ratios and friction angles (Table 4.1).

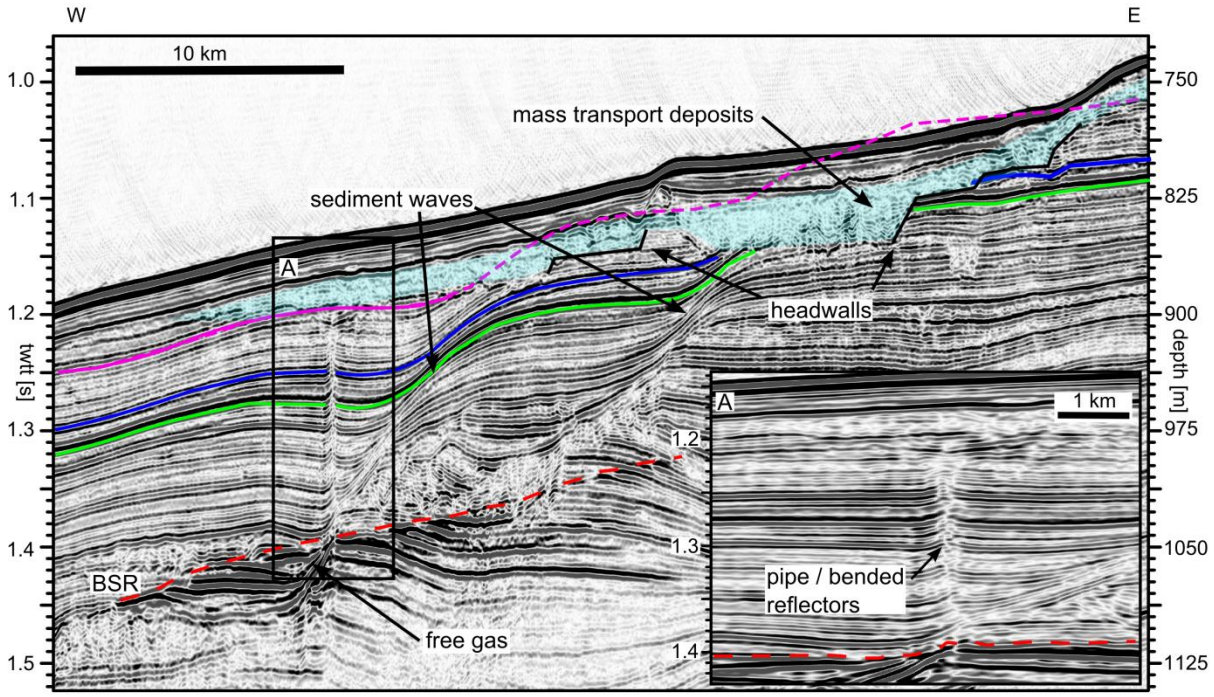

Figure 4.2. Reflection seismic profile 20130390 (location in Fig. 4.1) showing stratified layers, headwalls (black lines) and three highlighted color coded reflectors (green, blue and pink). (A) Zoom of the pipe structure reaching from the BSR (red dashed line) to the mass transport deposit (light blue area). The assumed sediment sound velocity for depth calculation is 1500 m/s.

TABLE 4.1. PARAMETERS AND RESULTS OF THE CALCULATION OF THE CRITICAL OVERPRESSURE AND GAS COLUMN

depth [mbsf]	failure mode	rho bulk [kg/m³]	Poisson ratio	friction angle [°]	cohesion [kPa]	critical over-pressure [kPa]	gas column⁺ [m]
190	tensile	1800	0.3	30	260	**811**	**~81**
190	tensile	1690*	0.3	30	260	**701**	**~70**
190	tensile	2140*	0.3	30	260	**973**	**~97**
190	tensile	2140*	0.37	30	260	**1467**	**~146**
40	shear	1690*	0.3	30	7	**66**	**~7**
40	shear	1690*	0.3	30	7	**137**	**~14**
40	shear	1690*	0.3	25	0	**13**	**~1**

* minimal/maximal bulk density from ODP 911A
⁺ gas column height supposing 100% replacement of water by gas

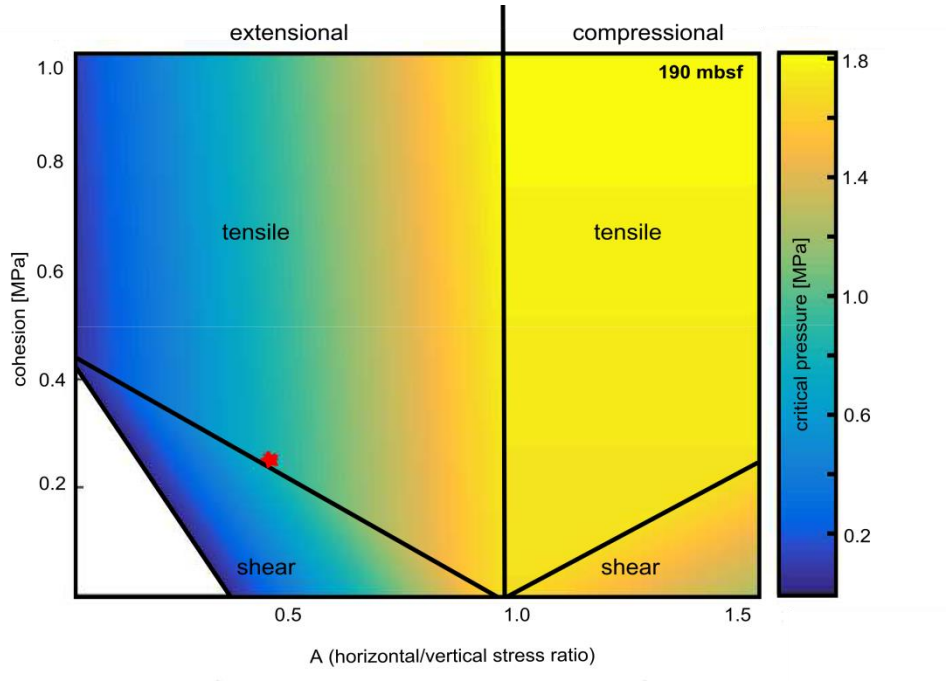

Figure 3. Critical pore overpressure as a function of horizontal/vertical stress ratio and cohesion at 190 mbsf that causes tensile or shear failure under extensional ($\sigma_h < \sigma_v$) or compressional ($\sigma_h > \sigma_v$) conditions. The red dot represents critical pore overpressure for tensile failure at the bottom of the GHSZ.

4.5 Pipe formation mechanisms and pore pressure evolution leading to slope failure

Previous studies of similar sedimentary environments showed that free gas can generate or reactivate fluid migration pathway within the GHSZ in critically pressured systems (Dugan and Flemings, 2000; Flemings et al., 2003; Hornbach et al., 2004). The estimated pore pressure/overburden stress ratio of 58-74 % (Table 4.S1) hints an active gas migration system at depth, which suggests that the imaged pipe structure developed under critically pressured conditions. A gas column height of ~80 m in 190 mbsf could cause the calculated critical overpressure (70-146 m for pressures of 701-1467 kPa and a density contrast of ~1024 kg/m³ between water and gas) to initiate tensile failure and form hydrofractures (Fig. 4.3, 4A, Table 4.1). Given that this height is based on the rather unrealistic assumption that overpressure originates solely from complete replacement of pore water by gas, a gas column in the order of 80-100 m is a conservative estimate. To assume gas lenses of bigger dimension would suggest that this process is unrealistic. However, several studies observed such pipe structures

in other study areas (Bünz et al., 2003; Plaza-Faverola et al., 2011; Gay et al., 2012; Karstens and Berndt, 2015), and showed that also compaction and gas migration are capable to generate significant additional overpressures (Crutchley et al., 2014), especially at the presence of gas hydrates in clayey sediments (Liu & Flemings, 2007). Numerical simulations of overpressure generation from mechanical compaction, loaded with the inferred sedimentation history of the Hinlopen area, predict pore overpressures of 30-380 kPa beneath the GHSZ for hydrate saturations of 20-60%. This reduces the critical gas column height by 3-38 m (further details in the supplemental material). We conclude that buoyancy is only one of the mechanisms that generated overpressure and that an additional source of pore pressure, e.g. mechanical compaction during sedimentation, assisted in the formation critical gas overpressure.

Once hydrofracturing occurs, a pipe structure may develop and transfer overpressure from the base of the GHSZ to layers in the shallow subsurface (Fig. 4.4A-B). Truncated reflections at the edge of the pipe structure (Fig. 4.2A) and parallel, upward-bended reflections indicate that the pipe structure developed rapidly (Plaza-Faverola et al., 2011). Within this fast forming conduit pore water, free gas, and dissolved gas may start to migrate upwards, maintaining the pressure of the overpressure reservoir as long as the reservoir is large compared to the fracture volume in the pipe structure. Free gas can migrate through the GHSZ without forming gas hydrate due to limited water supply (Clennell et al., 1999; Suess et al., 1999), shifting pressure-temperature conditions (Wood et al., 2002), capillary effects in fine-grained sediments (Clennell et al., 1999), high pore water salinity (Haeckel et al., 2004) or a combination of these (Liu and Flemings, 2006). Ample evidence for gas seepage through the GHSZ has been observed throughout the world (Greinert et al., 2006; Crutchley et al., 2010; Bünz et al., 2012). The precise mechanism for gas migration through the GHSZ is of secondary importance as long as hydrate formation does not close the conduit.

In order to transfer the pore pressure from the overpressure zone at the base of the GHSZ into the shallow subsurface, a developing pipe structure must not propagate to the sea floor but bleed of overpressure into a shallow sediment layer of enhanced permeability. This process is favored by heterogeneity and anisotropy of the penetrated material, e.g. discontinuities, stress barriers or layers of strongly contrasting Young's moduli (Gudmundsson and Brenner, 2001). Indications for such barrier are seismic stratification (Fig. 4.2) and local density differences of ~0.4 g/cm³ that are revealed in ODP bore hole 911A (Shipboard Scientific Party, 1995). Dense layers can function as stress barriers and encourage arrest of fractures (Gudmundsson

and Brenner, 2001) whereas layers with a high fraction of sand increase the permeability and facilitate horizontal fluid migration. Cohesion of normally consolidated shallow sediments is negligible (Ghiassian and Grozic, 2013) and forces failure to change from tensile to shear (Fig. 4.3). Seismic data (e.g. Karstens and Berndt, 2015) and experimentally sand box models (Gay et al., 2012) prove change from vertical to V-shaped migration. The calculated critical pore overpressure in ~40 mbsf in the order of ~66 kPa equals a gas column height of ~7 m (1-14 m for pressure of 13-137 kPa depending on the parameter range (Table 4.1)). We conclude that a pipe migrating through normally consolidated material favors to broaden in the upper part as resistance to sideway propagation diminishes (Fig. 4.4B).

Multiple headwalls and glide planes of the adjacent Hinlopen-Yermak Slide (Vanneste et al., 2006) indicate that the regional slope contains several weak layers and is overall prone to fail. Studies off mid-Norway show that contourite drifts are highly unstable because they contain weak layers (Berg et al., 2005). Seismic data reveal sediment waves (Fig. 4.2) that alter the layer thickness and build a potential barrier retaining the gas to migrate further upslope. Marine clays undergo strain softening and may be susceptible to slope failure even if the slope inclination is only ~ 0.6° (Kvalstad et al., 2005). Average slope angles of 1.5 to 3.2° at the top of the pipe structure (Fig. 4.2) and an inherently unstable slope with weak layers strongly suggest that the area may fail when the system is disturbed by pipe structures and changes in pore pressure. Once deformation takes place a shear band may propagate into the adjacent slope and could initiate retrogressive slope failure (Fig. 4.4C) (Puzrin et al., 2015) causing headwalls further upslope.

Considering the simplified approach we conclude that free gas at the base of the GHSZ causes excess fluid pressure and induces hydrofracturing. Pipe structures form a fluid pathway through the GHSZ and transfer overpressure from below the GHSZ to an inherently unstable slope with weak layers in the shallow subsurface. We show that this process is feasible to initiate a retrogressive submarine slope failure. To further test this hypothesis we suggest an integrated, multi-disciplinary investigation. 3D high-resolution seismic data from areas with pipe structures should be screened to identify possible pipes that are forming presently. In case such pipes can be found, drilling would provide the ambient pressure and geomechanical parameters to constrain the process. In the absence of such sites also a re-evaluation of existing bore holes such as ODP Site 1073 on the New Jersey continental slope (Dugan and Flemings, 2000) may provide further constraints on (1) effective cohesion of the sediments in

the GHSZ, (2) Poisson ratio, and (3) in situ stress in the different depth to parameterize further simulations.

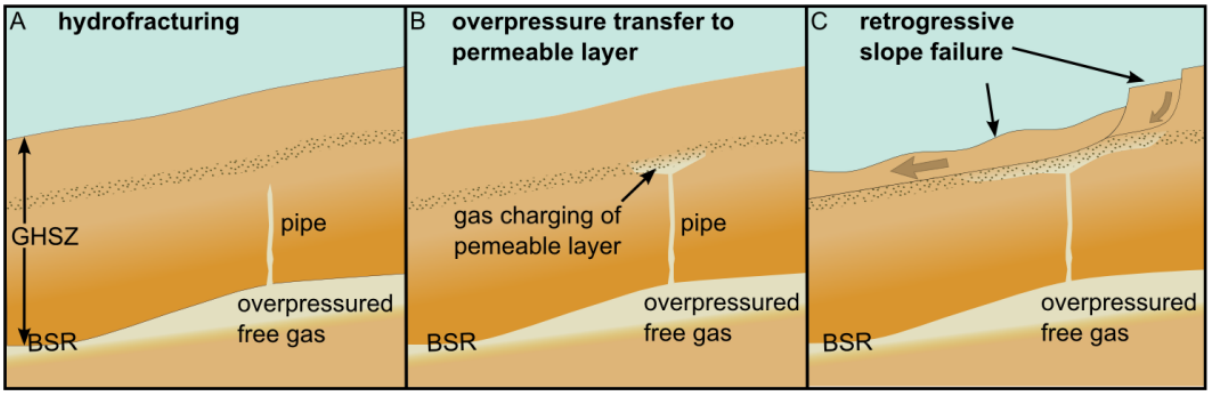

Figure 4. Schematic evolution of retrogressive slope failure due to overpressured gas below the BSR: (A) submarine slope with gas hydrate-bearing sediments (gradually decreasing saturation from the bottom of the GHSZ) and overpressured gas (bright area) at the bottom of the GHSZ induces pipe generation into the GHSZ, (B) the conduit encounters a permeable layer; gas enters and leads to overpressure transfer from the bottom of the GHSZ to the shallow subsurface, (C) overpessured gas causes shear banding in the weak layer and generates retrogressive slope failure.

4.6 Supplemental material

Geophysical data

2D high high-resolution seismic data were acquired using an 80-channel digital Geometrics GeoEel streamer with a total length of 125 m and group spacing of 1.5625 m. A SERCEL GI air gun with a volume of 1.7 l was shot in harmonic mode at 200 bar in ~2 m water depth. Seismic processing was carried out by using the commercial software Schlumberger Vista Seismic Processing 13®. Data were sampled at 0.5 ms and sorted into common midpoint (CMP) domain with a bin spacing twice the group spacing. Normal move out correction was obtained with a velocity of 1500 m/s and an Ormsby bandpass filter with corner frequencies at 10, 20, 200 and 400 Hz was applied. Due to the short length of the streamer system and relatively high water depths, the data were time migrated with water velocity, as the system is

not capable of a dedicated velocity analysis. The shooting intervals of 7 seconds at ~4.5 knots results in a shot point distance of 16 m. The entire water column was recorded during seismic acquisition. The seismic profile starts at 81°04.163'N/17°17.735'E and ends at 81°04.209'N/15°54.633'E.

Multibeam bathymetric data were recorded during MSM31 by the hull-mounted Kongsberg Simrad EM122 system with 191 beams per ping, an angular coverage of 150° and 12 kHz nominal frequency (Geissler et al., submitted). Bathymetric data were processed using the software CARIS HIPS & SIPS and gridded with GMT. The grid shown in Fig. 4.1 has a horizontal bin size of 50 m.

Overpressure calculation

Calculations of the critical overpressure are based on the Mohr Coulomb criterion for shear failure (Paterson and Wong, 2005):

$\tau - \sigma'_m \sin(\phi) = C \cos(\phi)$ (1)

and on the theoretical criterion for tensile failure of a fluid filled crack from the Griffith's theory (Murrell, 1964):

$\tau - \sigma'_m = \sigma_T$ (2)

where $\tau = \sqrt{(\sigma_{xx} - \sigma_{yy})^2/4 + {\sigma_{xy}}^2}$ is the stress deviator, $\sigma'_m = (\sigma_{xx} + \sigma_{yy})/2 - p$ is the mean effective stress, ϕ is the internal friction angle, C is the cohesion, $\sigma_T = C/10$ (Jaeger et al., 2009) is the tensile strength and p is the pore fluid overpressure. These criteria for shear (equation (1)) and tensile failure (equation (2)) are visualized in Fig. 4.S1A and B as lm and kl envelopes, respectively. The black Mohr circles represent an initial state of stress with zero fluid overpressure; σ'_m defines the center and τ the radius of the circle. If pore fluid pressure increases homogenously by the amount of p the radius of the circle does not change but shifts to the left until it touches the failure envelope. Depending on where it touches the failure envelope it causes shear bands or tensile fractures. As we aim to calculate the critical overpressure of a localized source to describe how seepage forces modify the local stress state we apply the expression for τ and σ'_m from Rozhko et al. (2007):

$\tau = \left|\frac{\sigma_V - \sigma_H}{2} - \beta_\tau p\right|$ (3)

$$\sigma'_m = \sigma_m - p = \frac{\sigma_V + \sigma_H}{2} - \beta_\sigma p \text{ . (4)}$$

This approach is based on a 2D porous medium embedded in a box of length L, height h ≪ L and source of pore fluid overpressure at its bottom of width w ≪ h (Fig. 4.S2). The initial horizontal stress σ_H is assumed to be proportional by the constant coefficient A to the vertical stress σ_V which is defined by the bulk density ρ, the gravitational acceleration g and depth –y:

$$\sigma_V = -\rho g y, \qquad \sigma_H = A\sigma_V \text{ . (5)}$$

As the pore fluid pressure increases locally, the two parameters β_σ and β_τ control the shift and change of the radius of the Mohr circle, respectively (Fig. 4.S1C and 1D). Rozhko et al. (2007) defined them as:

$$\beta_\sigma = 1 - \frac{\alpha}{2}\frac{1-2\nu}{1-\nu}\left(1 - \frac{1}{2}\frac{1}{ln\left(\frac{4h}{w}\right)}\right), \text{ (6)}$$

$$\beta_\tau = \frac{\alpha}{4}\frac{1-2\nu}{1-\nu}\frac{1}{ln\left(\frac{4h}{w}\right)} \text{ (7)}$$

with the Biot-Willis coupling constant α, the Poisson ratio ν and the model parameters h and w (Fig. 4.S2). After calculating the initial stresses σ_V and σ_H using equation (5) and substituting τ and σ'_m from equations (3) and (4) using equations (6) and (7) in the failure conditions (equations (1) and (2)) the critical pore fluid overpressure p_c is defined as

$$p_c = \frac{(\sigma_V - \sigma_H) + k_\tau + k_\sigma(\sigma_V + \sigma_H)}{k_f} \text{ . (8)}$$

This equation leads to 4 solutions considering the definitions of the coefficients k_τ, k_σ and k_f in Table 4.S1 for shear and tensile failure under extensional ($\sigma_V > \sigma_H$) and compressional ($\sigma_V < \sigma_H$) conditions. The resulting failure patterns are shown in Fig. 4.S3 and relate to the subdivision of the critical pore overpressure in 4 areas in Fig. 4.3.

The minimal value of p_c for pattern I-IV distinguishes the pore fluid overpressure at failure initiation and the pattern. The system is stable ff the local pore fluid overpressure is smaller than p_c.

To calculate the ratio of pore and lithostatic pressure we used bulk densities from ODP hole 911A (Shipboard Scientific Party, 1995) to calculate the lithostatic pressure and defined the pore pressure as the sum of hydrostatic pressure and overpressure.

TABLE 4.S1. COEFFICIENTS THAT SOLVE EQUATION (8) AND GENERATE FAILURE PATTERN I-IV THAT ARE SHOWN IN FIG. 4.S3.

failure pattern		k_f	k_τ	k_σ
shear	I*	$2(\beta_\tau + \sin(\varphi)\,\beta_\sigma)$	$2C\cos(\varphi)$	$\sin(\varphi)$
	II	$2(\beta_\tau - \sin(\varphi)\,\beta_\sigma)$	$-2C\cos(\varphi)$	$-\sin(\varphi)$
tensile	III*	$2(\beta_\tau + \beta_\sigma)$	$2\sigma_T$	1
	IV	$2(\beta_\tau - \beta_\sigma)$	$-2\sigma_T$	-1
*	compressional environment			

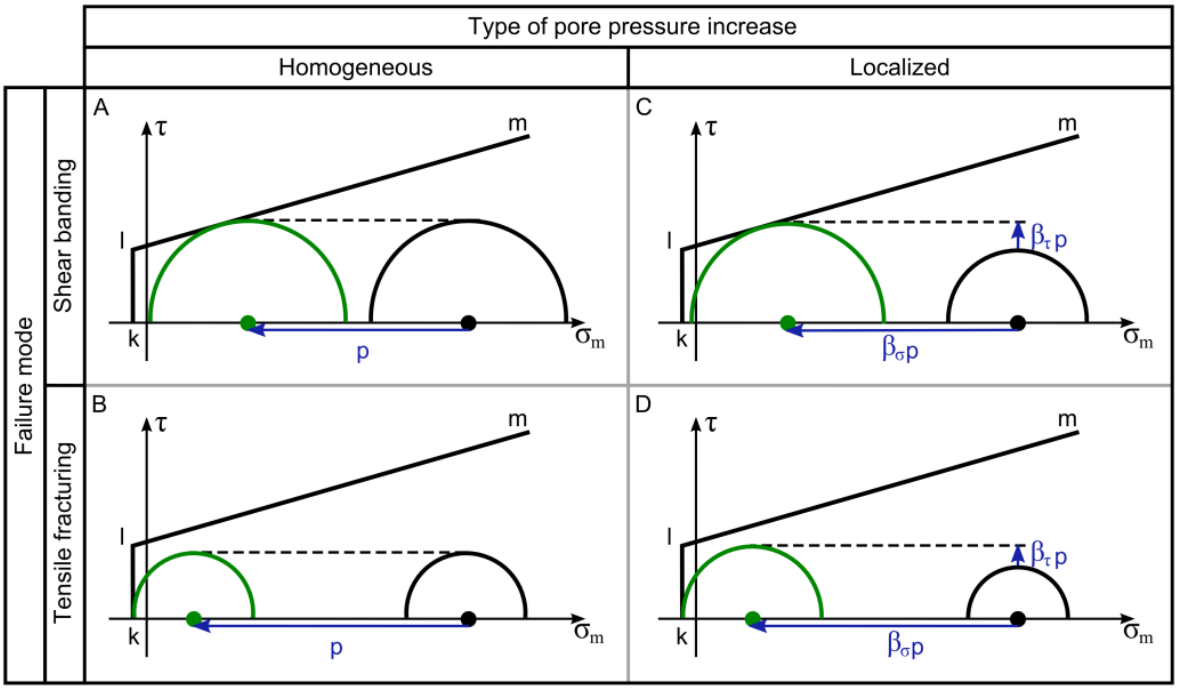

Figure S1. The impact of homogeneous (A, B) and localized increase of pore-fluid pressure on sediment stability. The lm envelope represents the Mohr-Coulomb failure criterion (equation (1)); the kl is the tensile cut-off boundary (equation (2)). The black circles describe the initial stress conditions. The green circles are shifted along the arrows due to a pore-fluid increase p to a condition at failure; shear banding when the circle meets the lm envelope (A, D) or tensile fracturing when they meet the kl envelope (B, D). Localized pore-fluid pressure increase changes the radius by the amount of $\beta_\tau p$ in addition to the displacement to the left of the amount of $\beta_\sigma p$. The two dimensionless parameters β_τ and β_σ are given in equations (6) and (7).

TABLE 4.S2. PRESSURE RATIO OF THE PORE PRESSURE (DEFINED AS THE SUM OF HYDROSTATIC PRESSURE AT 190 mbsf AND OVERPRESSURE GENERATED BY 42 m GAS COLUMN) AND THE LITHOSTATIC PRESSURE AT 190 FOR A MINAML AND MAXIMAL BULK DENSITY (Shipboard Scientific Party, 1995).

	min	max
rho bulk [kg/m³]	1690	2140
lithostatic pressure at 190 mbsf [kPa]	3149	3987
pore pressure* [kPa]	2332	2332
pressure ratio pore/lithostatic [%]	**58**	**74**

* hydrostatic plus overpressure

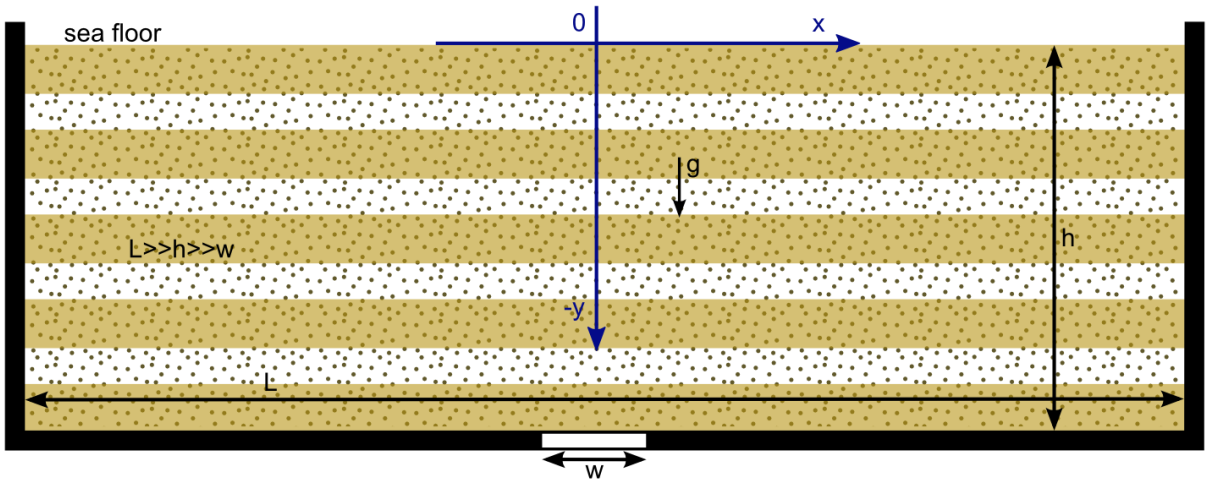

Figure S2. Geometry of the model that was used to calculate the critical pore overpressure (equation (8) with height h, width L and local fluid pressure source of diameter w.

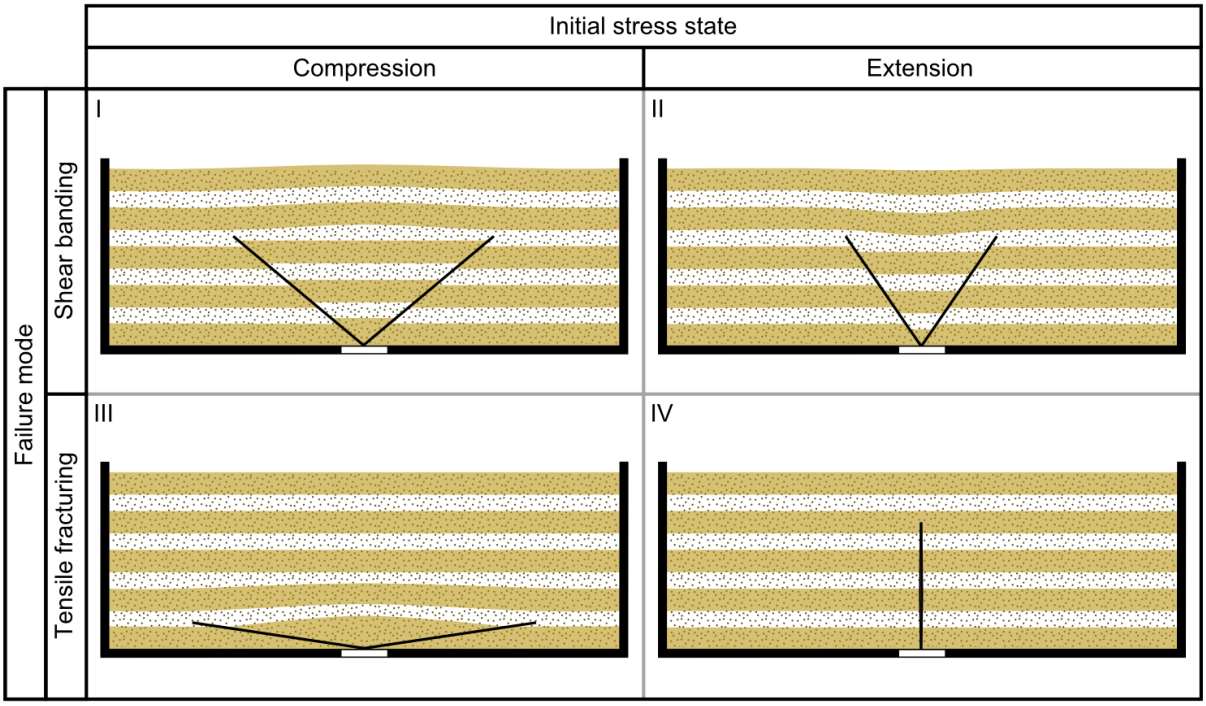

Figure S3. Possible failure patter that can develop due to locally increased pore-fluid pressure at depth. Under extensional ($\boldsymbol{\sigma_V > \sigma_H}$) or compressive ($\boldsymbol{\sigma_V < \sigma_H}$) conditions can occur either shear bands (I, II) or tensile failures (III, IV).

Overpressure from sediment compaction

In order to assess the critical gas column height necessary to initiate hydrofracturing, the background pressure state has to be known. Sediment compaction can raise the pore fluid pressure well above hydrostatic values. Here we investigate under-compaction and overpressure generation beneath the GHSZ. For this purpose we solve the pressure equation:

$$\frac{D\phi}{Dt} = -C\frac{D\sigma'_z}{Dt}$$

$$\sigma'_z = u_l - u = P_{litho} - P_{hydro} - u$$

$$\frac{C}{(1-\phi)}\frac{Du}{Dt} - \nabla\cdot\left(\frac{k}{\mu}\nabla u\right) = \frac{C}{(1-\phi)}\frac{Du_l}{Dt},$$

where u is the pore excess pressure (P - P_{hydro}), C=0.09613 x 10^{-6} Pa^{-1} is the Athy compaction constant, k is permeability, and μ is the temperature dependent viscosity. We use a porosity-dependent permeability function for shales (Hantschel and Kaueraff, 2009) and assume that

the permeability further changes with hydrate saturation within the GHSZ (Liu and Flemings, 2007):

$$k = k_0 \left[1 - S_h^2 + \frac{2(1-S_h)^2}{\log(S_h)} \right]$$

The above equations have been implemented in Matlab using a Lagrangian finite element method. The model is initialized to a 1140 m thick layer that is at hydrostatic conditions. 360 m of sediment are added in each simulation throughout the Quaternary at deposition rates inferred for the study area (Shipboard Scientific Party, 1995), so that the final sediment thickness is 1500 m. Figure S4-S6 show the results of three example calculations assuming 20, 50, and 60% hydrate saturation within the GHSZ (cf. Liu and Flemings, 2007). For these three model runs, overpressures of 30, 170, and 380 kPa are predicted at the base of the GHSZ, which reduces the critical gas column heights by 3-38 m.

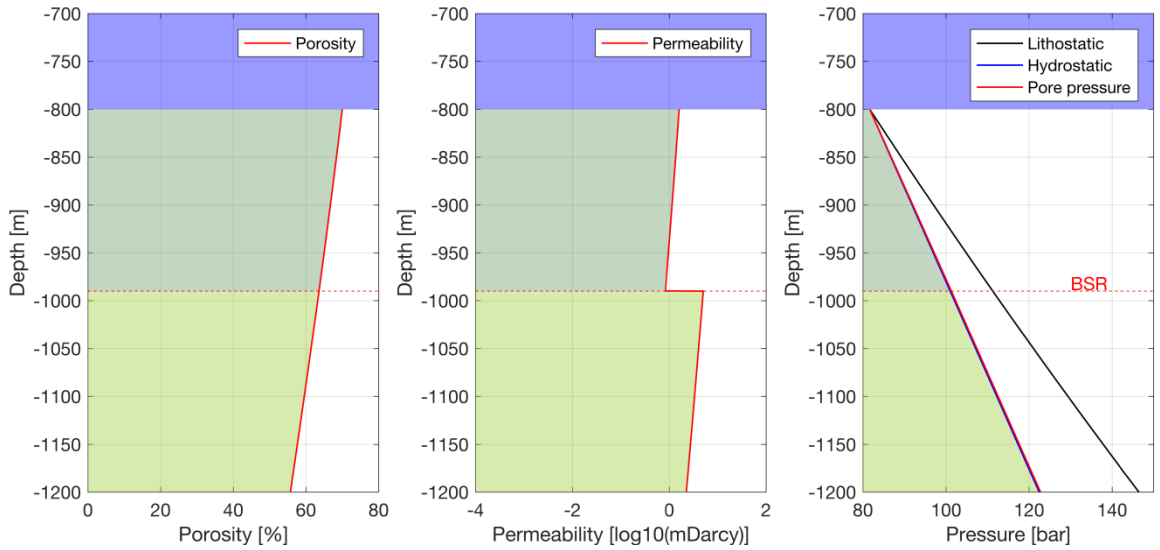

Figure S4. Calculated porosity, permeability and pressure depth-profile of sediments at 800 m water depth assuming a gas hydrate saturation of 20% above the BSR in the gas hydrate stability zone (dark green area). The presence of gas hydrates reduces the permeability (B) and changes pore pressure (C) during mechanical compaction. The hydrostatic pressure is elevated by 30 kPa overpressure and in total much smaller than the lithostatic pressure (red, blue and black line in C, respectively).

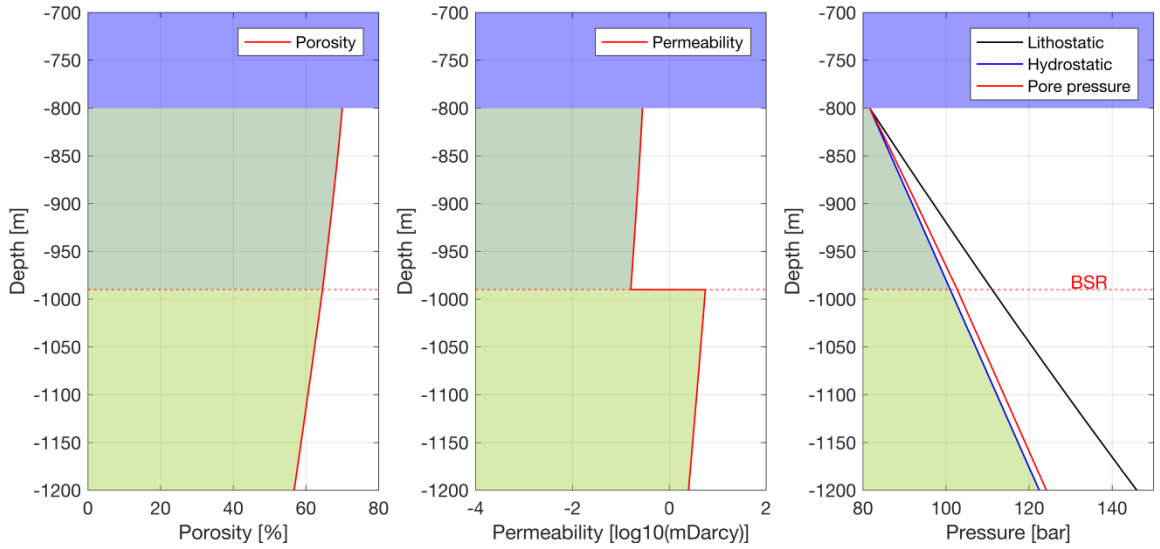

Figure S5. Calculated porosity, permeability and pressure depth-profile of sediments at 800 m water depth assuming a gas hydrate saturation of 50% above the BSR in the gas hydrate stability zone (dark green area). The presence of gas hydrates reduces the permeability (B) and changes pore pressure (C) during mechanical compaction. The hydrostatic pressure is elevated by 170 kPa overpressure and in total smaller than the lithostatic pressure (red, blue and black line in C, respectively).

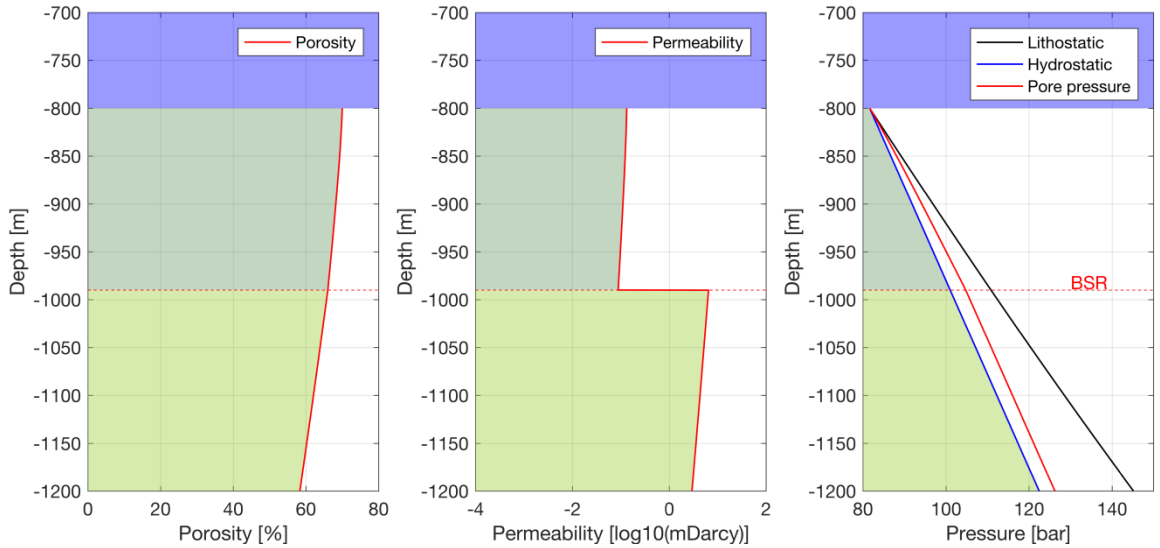

Figure S6. Calculated porosity, permeability and pressure depth-profile of sediments at 800 m water depth assuming a gas hydrate saturation of 60% above the BSR in the gas hydrate stability zone (dark green area). The presence of gas hydrates reduces the permeability (B) and changes pore pressure (C) during mechanical compaction. The hydrostatic pressure is elevated by 380 kPa overpressure and significantly reduces the offset to the lithostatic pressure (red, blue and black line in C, respectively).

Acknowledgments

We thank the captain of R.V. Maria S. Merian and his crew for their excellent support at sea. Ship time for cruise MSM31 was provided by the DFG Senatskomission für Ozeanographie. J.E. was financed by the Helmholtz graduate school HOSST.

References

Berg, K., Solheim, A., and Bryn, P., 2005, The Pleistocene to recent geological development of the Ormen Lange area: Marine and Petroleum Geology, v. 22, p. 45–56, doi:10.1016/j.marpetgeo.2004.10.009.

Berndt, C., and Goswami, B., 2007, Gas hydrate-related sedimentary pore pressure changes offshore Angola: Proceedings of the International Conference on Gas Hydrates: Energy, Climate and Environment, Taipei, Taiwan, p. 156–161.

Booth, J.S., Winters, W.J., and Dillon, W.P., 1994, Circumstantial evidence of gas hydrate and slope failure associations on the United States Atlantic continental margin: Annals of the New York Academy of Sciences, v. 714, p. 487–489, doi:10.1111/j.1749-6632.1994.tb38863.x.

Bugge, T., Belderson, R.H., and Kenyon, N.H., 1988, The Storegga Slide: Philosophical Transactions of the Royal Society of London, v. 325, p. 357–388, doi:10.1098/rsta.1988.0055.

Bünz, S., Mienert, J., and Berndt, C., 2003, Geological controls on the Storegga gas-hydrate system of the mid-Norwegian continental margin: Earth and Planetary Science Letters, v. 209, p. 291 – 307, doi:10.1016/S0012-821X(03)00097-9.

Bünz, S., Polyanov, S., Vadakkepuliyambatta, S., Consolaro, C., and Mienert, J., 2012, Active gas venting through hydrate-bearing sediments on the Vestnesa Ridge, offshore W-Svalbard: Marine Geology, v. 332-334, p. 189-197, doi:10.1016/j.margeo.2012.09.012.

Clennell, M.B., Hovland, M., Booth, J.S., Henry, P., and Winters, W.J., 1999, Formation of natural gas hydrates in marine sediments: 1. Conceptual model of gas hydrate growth conditioned by host sediment properties: Journal of Geophysical Research: Solid Earth, v. 104, p. 22985-23003, doi:10.1029/1999jb900175.

Cook, A.E., and Goldberg, D., 2005, Cohesive strength of gas-hydrate-bearing marine sediments: Abstract OS42A-07 presented at 2005 Fall Meeting, AGU, San Francisco, California, 5-9 December.

Crutchley, G.J., Klaeschen, D., Planert, L., Bialas, J., Berndt, C., Papenberg, C., Hensen, C., Hornbach, M.J., Krastel, S., and Brueckmann, W., 2014, The impact of fluid advection on gas hydrate stability: Investigations at sites of methane seepage offshore Costa Rica: Earth and Planetary Science Letters, v. 401, p. 95-109, doi:10.1016/j.epsl.2014.05.045.

Crutchley, G.J., Pecher, I.A., Gorman, A.R., Henrys, S.A., and Greinert, J., 2010, Seismic imaging of gas conduits beneath seafloor seep sites in a shallow marine gas hydrate province, Hikurangi Margin, New Zealand: Marine Geology, v. 272, p. 114-126, doi:10.1016/j.margeo.2009.03.007.

Dugan, B., and Flemings, P.B., 2000, Overpressure and fluid flow in the New Jersey continental slope: Implications for slope failure and cold seeps: Science, v. 289, p. 288-291, doi:10.1126/science.289.5477.288.

Flemings, P.B., Liu, X., and Winters, W.J., 2003, Critical pressure and multiphase flow in Blake Ridge gas hydrates: Geology, v. 31, p. 1057-1060, doi:10.1130/g19863.1.

Gay, A., Mourgues, R., Berndt, C., Bureau, D., Planke, S., Laurent, D., Gautier, S., Lauer, C., and Loggia, D., 2012, Anatomy of a fluid pipe in the Norway Basin: Initiation, propagation and 3D shape: Marine Geology, v. 332-334, p. 75-88, doi:10.1016/j.margeo.2012.08.010.

Geissler, W.H., Gebhardt, A.C., Gross, F., Wollenburg, J., Jensen, L., Schmidt-Aursch, M.C., Krastel, S., Elger, J., and Osti, G., submitted, Arctic megaslide at rest? Continental slope deformation in the vicinity of the Hinlopen/Yermak Slide Complex offshore North Svalbard: Scientific Reports.

Ghiassian, H., and Grozic, J.L.H, 2013, Strength behavior of methane hydrate bearing sand in undrained triaxial testing: Marine and Petroleum Geology, v. 43, p. 310-319, doi:10.1016/j.marpetgeo.2013.01.007.

Greinert, J., Artemov, Y., Egorov, V., De Batist, M., and McGinnis, D., 2006, 1300-m-high rising bubbles from mud volcanoes at 2080m in the Black Sea: Hydroacoustic characteristics and temporal variability: Earth and Planetary Science Letters, v. 244, p. 1-15, doi:10.1016/j.epsl.2006.02.011.

Gudmundsson, A., and Brenner, S.L., 2001, How hydrofractures become arrested: Terra Nova, v. 13, p. 456-462, doi:10.1046/j.1365-3121.2001.00380.x.

Haeckel, M., Suess, E., Wallmann, K., and Rickert, D., 2004, Rising methane gas bubbles form massive hydrate layers at the seafloor: Geochimica et Cosmochimica Acta, v. 68, p. 4335-4345, doi:10.1016/j.gca.2004.01.018.

Haflidason, H., de Alvaro, M.M., Nygard, A., Sejrup, H.P., and Laberg, J.S., 2007, Holocene sedimentary processes in the Andøya Canyon system, north Norway: Marine Geology, v. 246, p. 86-104, doi:10.1016/j.margeo.2007.06.005.

Hantschel, T., and Kauerauf, A.I., 2009, Fundamentals of basin and petroleum systems modeling – Springer-Verlag, Berlin Heidelberg.

Hernández-Molina, F.J., Paterlini, M., Violante, R., Marshall, P., de Isasi, M., Somoza, L., and Rebesco, M., 2009, Contourite depositional system on the Argentine Slope: An exceptional record of the influence of Antarctic water masses: Geology, v. 37, p. 507-510, doi:10.1130/g25578a.1.

Hornbach, M.J., Saffer, D.M., and Holbrook, W.S., 2004, Critically pressured free-gas reservoirs below gas-hydrate provinces: Nature, v. 427, p. 142-144, doi:10.1038/nature02172.

Ikari, M.J., and Kopf, A.J., 2011, Cohesive strength of clay-rich sediment: Geophysical Research Letters, v. 38, L16309, doi:10.1029/2011gl047918.

Ikari, M.J., and Kopf, A.J., 2015, The role of cohesion and overconsolidation in submarine slope failure: Marine Geology, v. 369, p. 153-161, doi:10.1016/j.margeo.2015.08.012.

Ingólfsson, Ó., and Landvik, J.Y., 2013, The Svalbard–Barents Sea ice-sheet – Historical, current and future perspectives: Quaternary Science Reviews, v. 64, p. 33-60, doi:10.1016/j.quascirev.2012.11.034.

Jaeger, J.C, Cook, N.G.W., and Zimmermann, R., 2009, Fundamentals of rock mechanics – John Wiley & Sons.

Karstens, J., and Berndt, C., 2015, Seismic chimneys in the Southern Viking Graben – Implications for palaeo fluid migration and overpressure evolution: Earth and Planetary Science Letters, v. 412, p. 88-100, doi:10.1016/j.epsl.2014.12.017.

Konno, Y., Yoneda, J., Egawa, K., Ito, T., Jin, Y., Kida, M., Suzuki, K., Fujii, T., and Nagao, J., 2015, Permeability of sediment cores from methane hydrate deposit in the Eastern Nankai Trough: Marine and Petroleum Geology, v. 66, p. 487-495, doi:10.1016/j.marpetgeo.2015.02.020.

Kretschmer, K., Biastoch, A., Rüpke, L., Burwicz, E., 2015, Modeling the fate of methane hydrates under global warming: Global Biogeochemical Cycles, v. 29, p. 610-625, doi:10.1002/2014GB005011.

Kvalstad, T.J., Andresen, L., Forsberg, C.F., Berg, K., Bryn, P., and Wangen, M., 2005, The Storegga slide: evaluation of triggering sources and slide mechanics: Marine and Petroleum Geology, v. 22, p. 245-256, doi:10.1016/j.marpetgeo.2004.10.019.

Kvenvolden, K.A., 1999, Potential effects of gas hydrate on human welfare: Proceedings of the National Academy of Sciences, v. 96, p. 3420-3426, doi:10.1073/pnas.96.7.3420.

Liu, X., and Flemings, P.B., 2006, Passing gas through the hydrate stability zone at southern Hydrate Ridge, offshore Oregon: Earth and Planetary Science Letters, v. 241, p. 211-226, doi:10.1016/j.epsl.2005.10.026.

Liu, X., and Flemings, P.B., 2007, Dynamic multiphase flow model of hydrate formation in marine sediments: Journal of Geophysical Research: Solid Earth, v. 112, B03101, doi:10.1029/2005JB004227.

Masui, A., Haneda, H., Ogata, Y., and Aoki, K., 2005, Effects of methane hydrate formation on shear strength of synthetic methane hydrate sediments: Proceedings of the 15th International Offshore and Polar Engineering Conference, Seoul, Korea, p. 364-369.

Micallef, A., Masson, D.G., Berndt, C., and Stow, D.A.V., 2009, Development and mass movement processes of the north-eastern Storegga Slide: Quaternary Science Reviews, v. 28, p. 433–448, doi:10.1016/j.quascirev.2008.09.026.

Murrell, S.A.F, 1964, The theory of the propagation of elliptical Griffith cracks under various conditions of plane strain or plane stress: parts II and III: British Journal of Applied Physics, v. 15, p. 1211-1223, doi:10.1088/0508-3443/15/10/309.

Paterson, M.S., and Wong, T.-F., 2005, Experimental Rock Deformation -The Brittle Field: Springer, Berlin, 346 p.

Paull, C.K., Ussler, W., and Holbrook, W.S., 2007, Assessing methane release from the colossal Storegga submarine landslide: Geophysical Research Letters, v. 34, L04601, doi:10.1029/2006gl028331.

Plaza-Faverola, A., Bünz, S., and Mienert, J., 2011, Repeated fluid expulsion through sub-seabed chimneys offshore Norway in response to glacial cycles: Earth and Planetary Science Letters, v. 305, p. 297-308, doi:10.1016/j.epsl.2011.03.001.

Puzrin, A.M., Gray, T.E., and Hill, A.J., 2015, Significance of the actual nonlinear slope geometry for catastrophic failure in submarine landslides: Proceedings of the Royal Society A: Mathematical, Physical and Engineering Sciences, v. 471, p. 20140772, doi:10.1098/rspa.2014.0772.

Rozhko, A.Y., Podladchikov, Y.Y., and Renard, F., 2007, Failure patterns caused by localized rise in pore-fluid overpressure and effective strength of rocks: Geophysical Research Letters, v. 34, L22305, doi:10.1029/2007gl031696.

Sawyer, D.E., Flemings, P.B., Dugan, B., and Germaine, J.T., 2009, Retrogressive failures recorded in mass transport deposits in the Ursa Basin, Northern Gulf of Mexico: Journal of Geophysical Research: Solid Earth, v. 114, B10102, doi:10.1029/2008jb006159.

Shipboard Scientific Party, 1995, Site 911, in Myhre, A.M., Thiede, J., Firth, J.V., et al., Proceedings of the Ocean Drilling Program, Initial reports, Volume 151: College Station, TX (Ocean Drilling Program), p. 271-318, doi:10.2973/odp.proc.ir.151.109.1995.

Suess, E., et al., 1999, Gas hydrate destabilization: enhanced dewatering, benthic material turnover and large methane plumes at the Cascadia convergent margin: Earth and Planetary Science Letters, v. 170, p. 1-15, doi:10.1016/s0012-821x(99)00092-8.

Sultan, N., Cochonat, P., Foucher, J.-P., and Mienert, J., 2004, Effect of gas hydrates melting on seafloor slope instability: Marine Geology, v. 213, p. 379-401, doi:10.1016/j.margeo.2004.10.015.

Vanneste, M., Mienert, J., and Bünz, S., 2006, The Hinlopen Slide: A giant, submarine slope failure on the northern Svalbard margin, Arctic Ocean: Earth and Planetary Science Letters, v. 245, p. 373-388, doi:10.1016/j.epsl.2006.02.045.

Wood, W.T., Gettrust, J.F., Chapman, N.R., Spence, G.D., and Hyndman, R.D., 2002, Decreased stability of methane hydrates in marine sediments owing to phase-boundary roughness: Nature, v. 420, p. 656-660, doi:10.1038/nature01263.

Chapter 5

Conclusions, implications and outlook

This thesis uses results from the investigation of the FSC to draw conclusions concerning its evolution, causal processes for slope failure and potential hazards. In combination with results from the feasibility study on a new preconditioning process, the conclusions correspond to the study objectives presented in Chapter 1. They can be applied to other potentially instable slopes, e.g. the Vestnesa area, and inspire future research on slope stability.

5.1 Conclusions

Evolution of the Fram Slide Complex

The FSC covers an area of ~5500 km² in 850 to 4200 m water depth NW off Svalbard. Repeated slope failures started in the entire FSC over 5 Ma ago without obvious limitation or concentration to a certain period. Recurrence frequencies and volume of past failures significantly differ within the FSC. One initial major slope failure occurred in the late Miocene and primarily shaped the northern part of the FSC. It evacuated ~1160 km³ of sediment and created a headwall of ~600 m height. The southern part experienced more frequent but smaller (2 to 62 km³ evacuated volume) slope failures between the late Miocene and late Pleistocene.

Causal processes of slope failure

Low sedimentation rates and its distal setting relative to proximal plume deposits rule out a causal relationship of the FSC to overpressure generation by rapidly deposited glacial sediments. Recurrence frequencies of slope failures vary spatially and demonstrate that local destabilizing preconditioning dominated slope stability as regional processes linked to tectonics, climate and oceanographic conditions could not explain the different local failure

patterns. It was not possible to establish a distinct reason for the late Miocene major slope failure in the northern part of the survey area. The combination of toe erosion and slope shape most likely caused repeated slope failure in the southern part. Rotational block movement along gravity-driven faults destabilized the slope at its toe and initiated retrogressive slope failure. Patchy sedimentation of weak contouritic material favored this process as it caused over-steepening and uneven sediment loading along the slope. Cementation removal due to hydrate dissolution was not relevant for the destabilization because the investigated slope was always within the hydrate stability zone. However, overpressure caused by free gas underneath the BSR may have influenced slope stability in the southern part of the FSC. High seismicity related to the system of ridges connected by transfer faults probably triggered slope failure within the FSC.

Numerical modelling suggests that there may be a previously unconsidered causal relationship between gas hydrates and slope failures. As overpressure below the gas hydrate stability zone increases due to the buoyancy of gas that is trapped, it causes hydrofracturing and forms pipe structures. Mechanical compaction of hydrate-bearing sediments may amplify pore pressure increase and cause critical overpressure. Resulting pipe structures provide fluid pathways through the GHSZ and transfer overpressure from below the GHSZ to inherently weak layers in the shallow subsurface. Overpressure could then start to build up laterally within the shallow subsurface and facilitate retrogressive submarine landslides.

Potential hazards of the Fram Slide Complex

Long periods of repeated failure within the FSC and very shallow mass transport deposits indicate that the investigated region is highly instable and might still be active. Regardless of the dimension of evacuated volume and water depth, these slope failures are a threat to offshore infrastructure. Because of the small volumes of recent slides (up to 62 km³) in water depth of up to 2700 m in the southern part of the FSC, the tsunami potential of the FSC is likely small. However, the major failure of ~1200 km^3 in the northern part of the FSC which is comparable to the Tampen, Trænadjupet, Møre and Bjørnøya slides clearly shows that future slope failures pose a serious hazard if they cut further back onto the Yermak Plateau or mobilize the slope over a long lateral distance. In this case, the system could generate sizeable destructive tsunamis (cp. Berndt et al., 2009).

5.2 Implications

The special location of the FSC illustrates that quickly accumulating glacial deposits are not a necessary prerequisite for the initiation of large submarine landslides on low gradient (2-6°) slopes on passive continental margins. Unlike other large-scale slope failures on the glaciated North Atlantic European margin, the FSC demonstrates that low-sedimentation rate slopes are also prone to slope failure of dimensions that could cause destructive tsunamis. This fact implies that hazard assessments for the glaciated NW European continental margins are much more complex than many studies of the major slope failures adjacent to trough mouth fans suggest (e.g. Laberg et al., 2000; Haflidason et al., 2004). The assessment of timing, recurrence frequencies and potentially threatened locations in the North Atlantic might be misled by the suggested relationship to cyclic sedimentation caused by glacial periods. The focusing on the glacial cycles and has to be reconsidered and expanded.

So far, low shear strength and vulnerability to liquefaction classified contourites as destabilizing factors for continental slopes, especially in combination with high sedimentation rates (Sultan et al., 2004). The comparisons of the different parts of the FSC and the Vestnesa area reveal slight variations of local slope geometry and sedimentation rate that might have caused the differences in slope stability. These observations emphasize that thick drift bodies formed by high sedimentation rates of contourites can smoothen seabed topography of tectonically controlled margin shape and reduce the chance of slope failures. Similarities of tectonic setting and seismic activity, and the small distance between the investigated areas suggest similar slope stability. Based on prior understanding of the preconditioning factors for slope stability, the drift body of the Vestnesa Ridge and its vicinity to the trough mouth fans of the Kongsfjorden and Isfjorden, in combination with the seismicity of the active system of ridges and transfer faults, would suggest that repeated slope failures during periods of post-glacial rebound should have occurred here (e.g. Bryn et al, 2005). But high-resolution seismic data with penetration depths of about 350 m area did not reveal any slope failure in the Vestnesa area. On the contrary, the FSC does not match the concept of a highly unstable area yet has a long history of repeated slope failure. The unexpected chronologies of the slope failures indicate that basic understanding on slope stability, preconditioning, and hazard assessment is still not fully developed and needs further investigation. The similar setting and geological factors controlling slope stability in both areas would suggest an increased probability of future slope failure at the intersection of the Knipovich Ridge with the Molløy Transfer Fault.

Numerous studies point to a spatial correlation of large-scale submarine landslides and gas hydrate systems (e.g. Booth et al., 2004; Mienert et al, 2005). Although results from laboratory and field studies on the effect of gas hydrates and free gas indicate a high impact on geomechanical properties (e.g. Cook and Goldberg, 2005; Ghiassian and Grozic, 2013), a causal relationship between gas hydrates and slope failure has not been proven till now (Paull et al., 2007). The numerical modeling approach presented in this thesis shows that the development of pipe structures may be feasible mechanism to initiate retrogressive submarine slope failure. This process more likely triggers slope failures in gas hydrate provinces than gas hydrate dissolution because it does not require any changes in the gas hydrate stability conditions. The tested process is able to explain hydrate-related slope failure initiation at all water depths where hydrates reduce the sediment permeability and cause fluid accumulation. This reconciles the observation of retrogressive slope failures starting at great water depth (e.g. Bryn et al., 2005) with gas hydrate models that suggest that mainly the upper part of the slope would be affected by climate induced hydrate dissociation.

5.3 Outlook

To further analyze the stability of slopes in the FSC and the Vestnesa area, future integrated and multi-disciplinary investigation of geophysical and geotechnical data should be considered (cf. Vanneste et al, 2014). A compilation of in situ and laboratory measurements and experiments, e.g. based on drilling and gravity cores of failed and intact sediments, could provide information on the detailed sediment composition, e.g. shear strength, environmental in situ stresses or pore pressure. Combined with 3D-information about the subsurface geometry in the Vestnesa area and FSC, slope stability could be calculated. A model could reveal the reason for the different slope failure histories and test the destabilization processes and scenarios that are discussed in Chapter 3. This approach could give insights about the suggested retrogressive failure dynamic. The relationship between hydrate saturation and pore pressure could be measured in situ to reveal possible differences and to model the resulting pore pressure. Such models should be able to provide the factor of safety of the Vestnesa area and verify the probability of a future slope failure in both areas.

An integrated, multi-disciplinary investigation could also further test the potential of pipe structures to trigger slope failure. 3D high-resolution seismic data from areas with pipe structures should be screened to identify possible pipes that are forming presently. In case

such pipes can be found, drilling with the necessary precautions would provide the ambient pressure and geomechanical parameters to constrain the process. In the absence of such sites a re-evaluation of existing bore holes such as ODP Site 1073 on the New Jersey continental slope (Dugan and Flemings, 2000) may provide further constraints on (1) effective cohesion of the sediments in the GHSZ, (2) Poisson ratio, and (3) in situ stress in the different depth to parameterize further simulations. The findings from this thesis contribute to a new assessment of slope stability in the North Atlantic. Such assessments require reliable dating of large-scale landslides, for example through dating of turbidite beds in the abyssal plains. Presently the UK-funded Arctic Research Programme attempts to do this based on gravity coring. A drilling campaign would reveal the age of slope failures that occurred during Miocene and Pleistocene. To date the most critical slide history during the Pleistocene and Holocene it would suffice to use smaller drilling gear, e.g. MeBo. Coring of the upper slopes would provide insight into the geomechanical properties of the layers within and adjacent to slope failures, e.g. shear strength, cohesion and sediment type and composition helping to identify weak layers. Other in situ measurements should be aimed at determining the saturation and distribution and emplacement style of gas hydrates and the in situ stress regime. Combined with 3D-information about the subsurface geometry the established destabilizing processes could be tested, including the new destabilization process related to gas hydrates that is presented in Chapter 4 of this thesis. The creation of a large data base on landslide-related parameters would be another viable approach to improve understanding processes and geomechanical properties that are important for slope stability. This data base should contain all available information on offshore areas, even if a causal relationship so slope stability is not obvious. Potential characteristics could be existence and chronology of slope failure, sediment type and geomechanical properties, sediment structure, sedimentation rates, environmental conditions as water temperature and stress, temporal variation of environmental conditions, flora, and fauna. Data mining could be used within the "knowledge discovery in databases" process to analysis these large quantities of data to extract previously unknown patterns that could indicate new causal relationships for slope stability. Geodetic monitoring of identified areas of incipient slope failure could provide information on ongoing deformation of the slope, while additional measurements of seismicity, temperature, and pressure changes may help to understand the underlying causes. Borehole measurement could report on in situ pressure, in situ stress, fluid flow and heat flow. These measurements would show how slope stability evolves, giving insight into the time scale of destabilization processes and their specific impact on slope stability.

References

Berndt, C., Brune, S., Nisbet, E., Zschau, J., Sobolev, S.V., 2009. Tsunami modeling of a submarine landslide in the Fram Strait. Geochemistry, Geophysics, Geosystems 10. doi:10.1029/2008GC002292

Booth, J.S., Winters, W.J., Dillon, W.P., 1994. Circumstantial evidence of gas hydrate and slope failure associations on the United States Atlantic continental margin. Annals of the New York Academy of Sciences 714, 487–489.

Bryn, P., Berg, K., Forsberg, C.F., Solheim, A., Kvalstad, T.J., 2005. Explaining the Storegga Slide. Marine and Petroleum Geology 22, 11 – 19.

Cook, A.E., and Goldberg, D., 2005, Cohesive strength of gas-hydrate-bearing marine sediments: Abstract OS42A-07 presented at 2005 Fall Meeting, AGU, San Francisco, California, 5-9 December.

Dugan, B., and Flemings, P.B., 2000, Overpressure and fluid flow in the New Jersey continental slope: Implications for slope failure and cold seeps: Science, v. 289, p. 288-291, doi:10.1126/science.289.5477.288.

Ghiassian, H., and Grozic, J.L.H, 2013, Strength behavior of methane hydrate bearing sand in undrained triaxial testing: Marine and Petroleum Geology, v. 43, p. 310-319, doi:10.1016/j.marpetgeo.2013.01.007.

Haflidason, H., Sejrup, H.P., Nygård, A., Mienert, J., Bryn, P., Lien, R., Forsberg, C.F., Berg, K., Masson, D., 2004. The Storegga Slide: architecture, geometry and slide development. Marine Geology 213, 201-234. doi:10.1016/j.margeo.2004.10.007

Laberg, J.S., Vorren, T.O., Dowdeswell, J.A., Kenyon, N.H., Taylor, J., 2000. The Andøya Slide and the Andøya Canyon, north-eastern Norwegian–Greenland Sea. Marine Geology 162, 259 – 275. doi:http://dx.doi.org/10.1016/S0025-3227(99)00087-0

Mienert, J., Vanneste, M., Bünz, S., Andreassen, K., Haflidason, H., Sejrup, H.P., 2005. Ocean warming and gas hydrate stability on the mid-Norwegian margin at the Storegga Slide. Marine and Petroleum Geology 22, 233–244. doi:10.1016/j.marpetgeo.2004.10.018

Acknowledgements

Many thanks to my first PhD supervisor Sebastian Krastel. Although I stayed most time at GEOMAR due to my HOSST fellowship, you always supported me, helped me and discussed my work with me during the past years. I always felt very welcome in my office at the university.

Many thanks to Christian Berndt, my second PhD supervisor, for the supervision, motivation, advice and guidance over the past years. I could always come by your office whenever I needed support or feedback. I really appreciate that you took the time to discuss my research, explain processes and thereby improved my scientific thinking, working and writing. Especially the discussion during the long-lasting preparation of the second paper encouraged me and let me leave your office much more positive then I entered it before. Thank you very much!

Many thanks to David Piper, my PhD co-supervisor through HOSST in Canada. You know that you often challenged me with your critical scientific discussions but I really appreciated your feedback and your opinion from a geological background. You encouraged me to question existing knowledge and to develop my own ideas and hypothesis. Thank you very much for inviting me to the Bedford Institute of Oceanography in Halifax.

Many thanks to the Transatlantic Research School HOSST for the financial support for this project, my extended stay in Canada and the summer schools in Canada, Kiel and on Cape Verde.

Many thanks to all colleagues that contributed to this work as through discussion, advice, data processing and help with software: Lars Rüpke, Robert Spielhagen, Felix Gross, Chrisoph Böttner, Jasper Hoffmann, Cord Papenberg, Jens Karstens, Ines Dumke, Morelia Urlaub and Felix Gross. Felix, special thanks go to you for your support during MSM31. Swaantje Bennecke, Felix Gross and Allanah Paul, I thank you so much for proof reading.

I would also like to thank everyone for the cheerful time we had during lunch, cake, ice cream, or sun breaks.

Many thanks go to the Baltic Sea for always cheering me up with some “real weather” on windy, stormy, rainy or sunny days during lunch breaks, sailing, walking at the beach, swimming or scuba diving.

Very special huge thanks go to my family for your endless support!!

Curriculum Vitae

Judith Elger

Date of birth:	19. April 1986
Place of birth:	Berlin
Citizenship:	German
Permanent address:	Adolfplatz 10
	24105 Kiel

Education

Since 11/2012	Doctorate funded by the Transatlantic Research School HOSST GEOMAR Helmholtz Centre for Ocean Research / Christian-Albrechts-Universität zu Kiel Supervisors: Prof. Dr. Sebastian Krastel-Gudegast Prof. Dr. Christian Berndt
08/2012	Master of Science
10/2009 - 08/2012	studies in Geotechnology at the Technical University Berlin, Germany
09/2009	Bachelor of Science
10/2006 - 09/2009	studies in Geotechnology at the Technical University Berlin, Germany
06/2005	Abitur
08/1998 - 06/2005	Gymnasium Katholische Schule Liebfrauen, Berlin